BI-METALLIC ZIF DERIVED ELECTROCATALYST FOR FUEL CELL

By

Saadia Hanif

(Registration No: NUST201590311PCES9215F)

Thesis Supervisor Assoc. Prof. Dr. Naseem Iqbal

US-Pakistan Center for Advanced Studies in Energy (USPCAS-E)

National University of Sciences and Technology (NUST)

Islamabad, Pakistan

(2020)

BI-METALLIC ZIF DERIVED ELECTROCATALYST FOR FUEL CELL

By

Saadia Hanif

(Registration No: NUST201590311PCES9215F)

A thesis submitted to the National University of Sciences and Technology, Islamabad,

in partial fulfillment of the requirements for the degree of

Doctor of Philosophy in

ENERGY SYSTEMS ENGINEERING

Thesis Supervisor Assoc. Prof. Dr. Naseem Iqbal

US-Pakistan Center for Advanced Studies in Energy (USPCAS-E)

National University of Sciences and Technology (NUST)

Islamabad, Pakistan

(2020)

Thesis Acceptance Certificate

Certified that final copy of PhD thesis written by Ms. Saadia Hanif, (Registration No. NUST201590311PCES9215F), of U.S Pakistan Center for Advanced Studies in Energy has been vetted by undersigned, found complete in all respects as per NUST Statues/Regulations, is within the similarity indices limit and is accepted as partial fulfillment for the award of PhD degree. It is further certified that necessary amendments as pointed out by GEC members of the scholar have also been incorporated in the said thesis.

Signature: _____

Name of Supervisor: Dr. Naseem Iqbal

Date: _____

Signature (HoD): _____

Date: _____

Signature (Dean/Principal): _____

Date: _____

Form PhD-7 (Revised)
DOCTORAL PROGRAMME
OF STUDY
(Must be type written)

National University of Sciences & Technology
REPORT OF DOCTORAL THESIS DEFENCE

Name: **Saadia Hanif** NUST Regn No: **NUST201590311PCES9215F**

Centre: U.S.-Pakistan Center for Advanced Studies in Energy, NUST, Islamabad, Pakistan

DOCTORAL DEFENCE COMMITTEE

Doctoral Defence held on 17th November 2020 at 14:00 hrs using "MS Teams" program

	QUALIFIED	NOT QUALIFIED	SIGNATURE
GEC Member-1: Dr. Zuhair S. Khan, USPCAS-E	✓		
GEC Member-2: Dr. Nadia Shehzad, USPCAS-E	✓		
GEC Member (External): Dr. Tayyaba Noor, SCME	✓		
Supervisor: Dr. Naseem Iqbal, USPCAS-E	✓		
Co Supervisor (if appointed):	✓		
External Evaluator-1: Dr. Abdullah Khan (Local Expert)	✓		
External Evaluator-2: Dr. Toheed Akhtar (Local Expert)	✓		
External Evaluator-3: Dr. Jawwad A. Darr (Foreign Expert)	✓		
External Evaluator-4: Dr. Tim-Patrick Fellinger (Foreign Expert)	✓		

FINAL RESULT OF THE DOCTORAL DEFENCE
(Appropriate box to be signed by HOD)

✓	PASS		FAIL

The student **Saadia Hanif** Regn # **NUST201590311PCES9215F** is accepted for Doctor of Philosophy Degree.

Dated: _____ Dean/Commandant/Principal/DG

Distribution:
1 x copy each for Registrar, Exam Branch, Dir R&D, Dir Acad Jat HQ NUST, HoD, Supervisor, Co-Supervisor (if appointed), one for student's dossier at the School/College/Centre and copy each for members of GEC.

Note:* Decision of External Evaluators (Foreign Experts) will be sought through video conference, if possible, on the same date and their decision will be intimated (on paper) to HQ NUST at a later date.

Certificate of Approval

This is to certify that the research work presented in this thesis, entitled "Bi-Metallic Zif Derived Electrocatalyst For Fuel Cell" was conducted by **Ms. Saadia Hanif** under the supervision of **Dr. Naseem Iqbal.**

No part of this thesis has been submitted anywhere else for any other degree. This thesis is submitted to the US-Pakistan Center for Advanced Studies in Energy (USPCAS-E) in partial fulfillment of the requirements for the degree of Doctor of Philosophy in the Field of Energy Systems Engineering at USPCAS-E, National University of Sciences and Technology, H-12, Islamabad, Pakistan.

Student Name: Saadia Hanif Signature: _____

Examination Committee:

a) External Examiner 1: Dr Jawwad A. Darr Signature: Jawwad Darr

b) External Examiner 2: Dr Tim-Patrick Fellinger Signature: _____

c) Internal Examiner: Dr Nadia Shehzad Signature: _____
Assistant Professor, USPCAS-E, NUST

Dr Naseem Iqbal, Supervisor: Signature: _____

Dr Naseem Iqbal, HoD: Signature: _____

Dr Adeel Waqas Principal/ Dean: Signature: _____

Plagiarism Undertaking

I solemnly declare that research work presented on the thesis titled **Bi-Metallic Zif Derived Electrocatalyst For Fuel Cell** is solely my research work with no significant contribution from any other person. Small contribution/help wherever taken has been duly acknowledged and that complete thesis has been written by me.

I understand the zero-tolerance policy of the HEC and National University of Sciences and Technology towards plagiarism. Therefore, I as an Author of the above titled thesis declare that no portion of my thesis has been plagiarized and any material used as reference is properly referred/cited.

I undertake that if I am found guilty of any formal plagiarism in the above title thesis even after award of PhD degree, the University reserves the rights to withdraw/revoke my PhD degree and that HEC and the University has the right to publish my name of the HEC/University Website on which names of students are placed who submitted plagiarized thesis.

Student/Author Signature: _____

Name: Saadia Hanif

Author's Declaration

I **Ms. Saadia Hanif** hereby state that my PhD thesis titled **Bi-Metallic Zif Derived Electrocatalyst For Fuel Cell** is my own work and has not been submitted previously by me for taking any degree from this University i.e. National University of Sciences and Technology or anywhere else in the country/world.

At any time if my statement is found to be incorrect even after my Graduate the University has the right to withdraw my PhD degree.

Name of Student: Saadia Hanif

Date: _____

Acknowledgements

All praise to the great **Allah Almighty** who has bestowed me with the opportunity to seek knowledge and enabled me to fulfill the obligation to explore the world of science up to my maximum limits.

I would like to express my sincere gratitude to my **research supervisor Dr. Naseem Iqbal** for his motivation, continuous support, patience and immense knowledge. He has guided me completely through-out my research work. Working under his supervision has indeed broadened my vision.

I am thankful to my GEC members, Dr. Zuhair S. Khan, Dr. Nadia Shahzad, and Dr. Tayyaba Noor for sparing precious time from their busy schedules, for suggestions as well as moral support. I would also like to thank the USPCASE faculty for being extremely cooperative.

I would also like to extend my gratitude to Professor Dr. AM Kannan for his guidance and supervision during my eight months visit to his **Batteries and Fuel cells** lab at Arizona State University, Arizona, USA. I did part of my research work in his lab where I carried out the advanced characterization including TEM, ICP-MS and XPS and electrochemical testing of the prepared samples on a fuel cell test station. Many thanks to Xuan Shi, a fellow PhD candidate in the Batteries and Fuel cells lab for guiding me about the electrochemical testing facility.

A special thanks to lab engineers at Synthesis lab, AEMS lab and Combined lab **Muhammad Naveed Ahmad, Asghar Ali, Aamir Satti, and Qamar-ud-Din** who helped me a lot in the experimental work and testing.

Last but not the least, I would pay my regards to my family for their un-parallel love, support and encouragement throughout my research work and my friends and lab fellows Aisha Asghar, Azra Nawar, Rabia Ahmad, Syed Aun Rizvi and Muhammad Daarain Haider to accompany me in this journey.

Saadia Hanif

Table of Contents

Acknowledgements **VIII**

Table of Contents **IX**

List of figures **XIII**

List of tables **XVI**

List of Research Papers **XVII**

List of Abbreviations **XVIII**

Abstract **XIX**

1. Introduction **21**

1.1 Global Energy Crisis 21

1.2 Alternative Energy resources: 22

1.3 Fuel cells 22

1.4 Types of fuel cells 24

1.4.1 Alkaline Fuel cells 25

1.4.2 Phosphoric acid fuel cell 26

1.4.3 Proton Exchange Membrane Fuel Cells 27

1.4.4 Molten Carbonate fuel cell 29

1.4.5 Solid oxide fuel cell 30

1.5 Hurdles in Commercialization of PEMFC and AFC 31

1.5.1 Economics 31

1.5.2 Durability Issues 32

1.6 Significance of research topic 33

1.7 Research Objectives 33

2. Literature Review **35**

2.1. PEMFC and AFC Catalyst Layers 35
2.1.1 Anode catalyst layers 36
2.1.2 Anode catalyst layer degradation 39
2.1.3 CO contamination 41
2.1.4 Oxygen Reduction Reaction (ORR) 42
2.1.5 Cathode catalyst layers 43
2.1.6 PGM- metal alloys catalysts 44
2.1.7 PGM-metal oxides catalysts 46
2.1.8 PGM-metal nanoparticles alloy catalyst 46
2.1.9 Cathode catalyst degradation 47
2.1.10 Pt nanoparticles migration 47
2.1.11 Pt dissolution: 48
2.1.12 Carbon corrosion: 48
2.1.13 Alternatives to Pt catalyst 50
2.1.14 Metal Organic Frameworks (MOF) 51
2.1.15 Catalytic activity of MOFs 51
2.1.16 Methods for enhancing current density 51
2.1.17 Nickel-Cobalt based Metal Organic Framework (Ni/Co-ZIF): 53
3. Characterization, Methodology and Experimentation 54
3.1 Physical Characterization 54
3.1.1 Scanning Electron Microscopy (SEM)/ Energy Dispersion Spectroscopy (EDS) 54
3.1.2 Thermal gravimetric analysis (TGA) 55
3.1.3 X-Ray Diffraction XRD 56
3.1.4 Transmission Electron Microscopy (TEM) 58

3.1.5 X-ray photoelectron spectroscopy (XPS) 59
3.2 Synthesis of ZIF-67 60
3.2.1 Solution Preparation 60
3.3 Synthesis of NiCo-ZIF 61
3.3.1 Solution preparation for NiCo-ZIF 61
3.3.2 Synthesis of PtNiCo/NC 62
3.3.3 Synthesis of NiCo NCNTs 62
3.3.4 Synthesis of Ni-MOF 63
3.3.5 Synthesis of activated carbon 63
3.3.6 Synthesis of Ni-MOF @ AC composites 63
3.4 Electrochemical Setup 64
3.4.1 Electrode fabrication for Electrochemical Evaluation in Acidic Medium 65
3.4.2 Electrochemical Evaluation on Rotating Disk Electrode in Acidic Medium 66
3.4.3 Electrode fabrication for Electrochemical Evaluation in Alkaline Medium 66
3.4.4 Electrochemical Evaluation on Rotating Disk Electrode in Alkaline Medium. 66
3.5 Fuel Cell Testing 67
3.5.1 Catalyst Coated Membranes for PEMFC Testing 67
3.5.2 Gas diffusion layer for PEMFC Testing 67
3.5.3 Membrane Electrode Assembly Fabrication for PEMFC Testing 67
3.5.4 Catalyst Coated Membranes for AFC Testing 68
3.5.5 Gas diffusion layer for AFC Testing 68
3.5.6 Membrane electrode assembly (MEA) for AFC Testing 69
4. Chapter 4 Results and Discussion 70
4.1 Electro-catalyst for Proton exchange membrane fuel cell (PEMFC) 70
4.1.1 Crystal Structure and phase purity 70

4.1.2 Microporous structures and elemental analysis 72
4.1.3 XPS Analysis 75
4.1.4 Electrochemical Characterization 78
4.1.5 Electrochemical Evaluation on Rotating Disk Electrode 78
4.1.6 Membrane Electrode Assembly and Fuel Cell Performance Evaluation 81
4.1.7 PEM Fuel Cell Evaluation 81
4.2 Electrocatalyst for alkaline fuel cell (AFC) 83
4.2.1 Crystal Structure and phase purity 83
4.2.2 Microporous structures and elemental analysis 85
4.2.3 XPS of NiCo/NCNTs electrocatalyst 86
4.2.4 Electrocatalytic performance of NiCo/NCNTs 87
4.2.5 CV and LSV 87
4.2.6 Electrode Fabrication and Alkaline Fuel Cell Performance 91
4.2.7 Single Fuel Cell Performance 91
5. Conclusions and recommendations 93
5.1 Conclusions 93
5.2 Future Recommendations 94

List of figures

Figure 1.1 Total energy supplies in 2018. This figure was taken and used without any modification from reference [3] 22
Figure 1.2 Alkaline fuel cell schematic diagram. This figure was taken and used without any modification from reference [11] 25
Figure 1.3 Schematic diagram of Phosphoric acid fuel cells. This figure was taken and used without any modification from reference [12] 27
Figure 1.4 Single typical proton exchange membrane fuel cell. This figure was taken and used without any modification from reference [14] 29
Figure 1.5 Schematic diagram of Molten carbonate fuel cell. This figure was taken and used without any modification from reference [15] 30
Figure 1.6 Schematic diagram of Solid oxide fuel cell. This figure was taken and used without any modification from reference[16] 31
Figure 1.7 Modeled cost frame of 80-kWnet fuel cell by DOE. This figure was taken and used without any modification from reference [20] 32
Figure 2.1 Volcano plot of log j_0 vs metal-hydrogen bond energy for different catalysts. This figure was taken and used without any modification from reference [34] 38
Figure 2.2 Voltage reversal experiment on anode & cathode w.r.t time variation. This figure was taken and used without any modification from reference [41] 40
Figure 2.3 (a) Reaction pathways of ORR in acidic media. (b) Modes of O_2 adsorption on catalyst surface. This figure was taken and used without any modification from reference [52] 43
Figure 2.4 Activity of the transition metals as function of oxygen binding energy. This figure was taken and used without any modification from reference [53] 44
Figure 2.5 Trends in oxygen reduction activity plotted as function of oxygen binding energy. This figure was taken and used without any modification from reference [52] 45
Figure 2.6 Overall lifetime cell voltage of automotive fuel cell w.r.t time. This figure was taken and used without any modification from reference [89] 49

Figure 2.7 Overall sequence of startup/shutdown and electrochemical reactions in PEMFC. This figure was taken and used without any modification from reference [97] 50
Figure 3.1 Schematic representation of basic SEM components 55
Figure 3.2 The basic design and working of a Thermogravimetric analyzer (TGA). This figure was taken and used without any modification from reference [134]. 56
Figure 3.3 A schematic of how XRD works. This figure was taken and used without any modification from reference [132] 57
Figure 3.4 A view of X-ray incident and diffraction through a material of spacing (d). This figure was taken and used without any modification from reference [133] 58
Figure 3.5 Functional diagram of TEM 59
Figure 3.6 Synthesis scheme (our own work) for Co-ZIF 61
Figure 3.7 Synthesis scheme (our own work) for NiCo-ZIF. 62
Figure 3.8 Three Electrode System 65
Figure 4.1 (a)XRD pattern of Co ZIF and NiCo ZIF with simulated pattern of Co ZIF (b) NiCo/NC and PtNiCo/NC, and (c) Pt, Ni, Co (111) regions with high resolution ... 71
Figure 4.2 FESEM of (a) Co ZIF (ZIF-67) , (b) NiCo-ZIF crystals, (c) NiCo/NC, (d) PtNiCo/NC 73
Figure 4.3 (a) The HAADF image of NiCo-ZIF, (b) EDS mapping of NiCo-ZIF (a), TEM (c), (d) STEM image of PtNiCo at different magnification 75
Figure 4.4 (a) XPS spectra of PtNiCo/NC (b)C1s, (c)N1s, (d) O1s, (e) Co2p and (f) Pt4f 76
Figure 4.5 Pt4f XPS comparison of PtNiCo/NC and Pt/C 78
Figure 4.6 Electrochemical oxygen reduction on PtNiCo/NC (a) CV profiles (red and black curves indicate CV curves recorded in N_2 and O_2 saturated 0.1M $HClO_4$ solution, respectively). (b) LSV curves of different samples at O_2-saturated 0.1M $HClO_4$ solution at 1600 rpm. Insert, The comparison of MAs at 0.85 V versus RHE (c) LSV curves at different rotation rates (rpm) for PtNiCo/NC (d) Charge transfer number (n). Insert, K–L plots, ω is the angular rotation speed. (e) Durability Test: ORR polarization curves (1600 rpm) of PtNiCo/NC before and after 5000 cycles. (f) Durability Test: ORR polarization curves (1600 rpm) of Pt/C before and after 5000 cycles. 79

Figure 4.7 The acidic fuel cell activity of (a) effect of Nafion:catalyst ratio on PtNiCo/NC performance, (b) Fuel cell performamnce with PtNiCo/NC, NiCo/NC and Pt/C with and without back pressure, (c) 100 h stability test for PtNiCo/NC catalyst at ambient pressure. (Measurements were taken at 70°C, 100% relative humidity with H_2 and O_2 at 0.2 and 0.3 NLPM with Nafion212 membrane) 83
Figure 4.8 XRD pattern of (a) Co ZIF, NiCo ZIF and simulated Co ZIF, (b) Co/NCNT, NiCo/NCNT (1:1), NiCo/NCNT (1:4), and NiCo/NCNT (4:1) 84
Figure 4.9 Morphology and structural analysis by a-c) FESEM. a) NiCo-ZIF, b,c) NiCo/NCNTs, d-f) HRTEM 86
Figure 4.10 (a) The XPS survey scan and the deconvoluted HR XPS scan of (b)C1s, (c)N1s and (d) Co2p..... 87
Figure 4.11 Electrochemical oxygen reduction on NiCo/NCNTs a, LSV curves of different samples at O2-saturated 0.1M KOH solution at 1600 rpm. b, LSV curves at different rotation rates (rpm) for NiCo/NCNT (1:1). c, K–L plots, ω is the angular rotation speed. d, Charge transfer number (n) 89
Figure 4.12 a, Tafel plots of Pt/C and NiCo/NCNTs derived from Figure 3a. b, Durability Test: ORR polarization curves (1600 rpm) of NiCo/NCNTs (1:1) before and after 5000 cycles. c, Durability Test: ORR polarization curves (1600 rpm) of Pt/C before and after 5000 cycles. d, Chronoamperometric response at 0.6V 90
Figure 4.13 The electrochemical performance evaluations in fuel cell. a, The voltages and power densities of H_2/O_2 fuel cells with NiCo/NCNTs as cathode (4 mg cm-2) at different temperatures. b, Comparison of NiCo/NCNTs, CoNCNTs and commercial Pt/C as cathode (0.12 mg_{Pt} cm^{-2}) (membrane: FAA-3-50, anode: 0.12 mg_{Pt} cm^{-2} back pressure: 0 atm, 50^{o}C) fuel cells with H_2 and O_2 in 100% RH..... 92

List of tables

Table 1.1 Major types of fuel cells 24
Table 4.1 The diffraction peaks position, lattice spacing, Pt:(Ni/Co) ratio and FWHM analysis of of Pt, Co, Ni, PtCo and PtNiCo 72
Table 4.2 Composition of elements in the PtNiCo/NC..... 77
Table 4.3 Performance comparison of different prepared catalyst with commercial Pt/C 80
Table 4.4 Performance comparison of different Pt based catalysts for ORR in acidic media (ORR test conditions: 1600 rpm and 0.1M $HClO_4$)..... 81
Table 4.5 The diffraction peaks position, lattice spacing, (Ni/Co) ratio and FWHM analysis of Ni/Co..... 84
Table 4.6 Performance comparison of reported ZIF based catalysts for ORR in alkaline media (ORR test conditions: 1600 RPM, 0.1M KOH). 91

List of Research Papers

Published

Saadia Hanif, Xuan Shi, Naseem Iqbal, Tayyaba Noor, Rehan Anwar, A.M. Kannan, ZIF derived PtNiCo/NC cathode catalyst for proton exchange membrane fuel cell, Applied Catalysis B: Environmental, Volume 258, 2019, 117947, ISSN 0926-3373, https://doi.org/10.1016/j.apcatb.2019.117947. **Impact Factor [16.683]**

Saadia Hanif, Naseem Iqbal, Xuan Shi, Tayyaba Noor, Ghulam Ali, A.M. Kannan, NiCo–N-doped carbon nanotubes-based cathode catalyst for alkaline membrane fuel cell, Renewable Energy, Volume 154, 2020, Pages 508-516, ISSN 0960-1481, https://doi.org/10.1016/j.renene.2020.03.060. **Impact Factor [6.274]**

Under Review:

Electro catalytic study of Ni-MOF with activated carbon composites for methanol oxidation reaction. Saadia Hanif, Naseem Iqbal, Aun M Rizvi, M Daarain Haider, Usman Ali Khan, Tayyaba Noor.

List of Abbreviations

AFC Alkaline fuel cell

AJK Azad Jammu and Kashmir

BET Brunauer Emmett Teller

BTC Benzene tricarboxylic

CA Chronoamperometry

CB Carbon Black

CE Counter Electrode

CHP Combined Heat and Power Efficiency

CNT's Carbon Nanotubes

CP Controlled potential

CV Cyclic Voltammetry

DC Direct Current

DI Di-Ionized Water

DMFC Direct Methanol Fuel Cell

DOE Department of Energy

EDS Energy Dispersive Spectroscopy

EIS Electrochemical Impedance Spectroscopy

FC Fuel cell

FTIR Fourier Transform Infrared Spectroscopy

GCE Glassy Carbon Electrode

GDL Gas Diffusion Layer

HOR Hydrogen Oxidation Reaction

HUPD Hydrogen under potential desorption

ICT Internal Combustion Engine

KPK Khyber Pakhtoon Khawa

Abstract

Fuel cells are the emerging energy conversion devices owing to their dynamic qualities. The low temperature fuel cells such as proton exchange membrane fuel cell (PEMFC) and alkaline membrane fuel cell (AMFC) are a promising alternative to fossil fuels for powering future vehicles. Oxygen electrochemistry involves oxygen reduction (ORR) and evolution reactions. For ORR development of highly efficient non-noble metal catalysts to improve the sluggish reaction kinetics is of high significance. In this work Zeolitic Imidazolate Framework (ZIF) derived catalyst which can provide hollow framework of nitrogen doped nano porous carbon with promising ORR activity have been developed for both PEMFC and AMFC. High performance electrocatalysts for oxygen reduction reaction (ORR) in fuel cells with low Pt consumption are significant for the commercial application of PEMFCs. The current study Zeolitic Imidazolate Framework (ZIF), which can provide hollow framework of nitrogen doped nano porous carbon with promising ORR activity. In this study, we report a bimetallic pyrolyzed NiCo-ZIF supported fine Pt/Pt alloy electrocatalyst for ORR. After pyrolysis, nano-porous carbon is obtained with well dispersed Pt/Pt alloy nanoparticles (~ 3nm). This catalyst shows superior catalytic activity and stability in acid than the commercial Pt/C catalyst. As a cathode in single cell PEMFC, it gives high peak power density of 1070 mW. cm^{-2} at 70 ^{o}C with a low cathode platinum loading of 0.12 mg cm^{-2}. The enhanced activity and durability can be attributed to the synergistic effect from the nitrogen doped nano-porous carbon derived from NiCo-ZIF and the defect rich carbon support to anchor Pt/Pt alloy nanoparticles. For alkaline membrane fuel cell, synthesis of nitrogen doped carbon

nanotubes (NCNTs) derived from Zeolitic Imidazolate Frameworks (ZIFs) and their activity towards (ORR) in alkaline medium are studied. The NCNTs showed excellent ORR performance in KOH with onset potential of 0.92 V and current density of -5.6 $mA.cm^{-2}$. The enhanced electrochemical activity and stability is attributed to the synergetic effect of the nitrogen doped carbon nanotubes and the Ni/Co active sites. The alkaline fuel cell performance of the membrane electrode assembly (MEA) prepared with NCNTs as cathode was 65 $mWcm^{-2}$, which was higher than the MEA prepared with Pt/C as cathode (60 $mWcm^{-2}$). These results indicate that NCNTs are highly efficient and durable as electrocatalysts for ORR in alkaline fuel cell. The exceptional electrocatalytic activity might be mainly attributed to the chemical composition and structure of the crystalline NCNTs formed, as well as their robust overall framework structure. This study opens up a new avenue for developing highly active MOF-derived electrocatalysts for different fuel cell applications and paving the way for their commercialization.

1. Introduction

1.1 Global Energy Crisis

Energy has a significant contribution in the prosperity and sustainable economic growth of a country. Energy is the major factor for running all manufacturing activities and acts as a backbone for the development of a country. The diversity in energy sources and their availability with respect to the economic development levels and strategies also differ from region to region [1]. Today, energy and transport sectors are driven by fossil fuel energy carriers which are depleting and are unsustainable source for energy production. World population is increasing at an alarming rate which is also resulting in increased energy demand and a burden on existing non-renewable energy sources which are depleting with increment in usage [2]. To meet the energy needs, 87% energy was produced by the fossil fuels including coal, oil and gas, 9% from the renewable sources and 4% from nuclear energy sources.

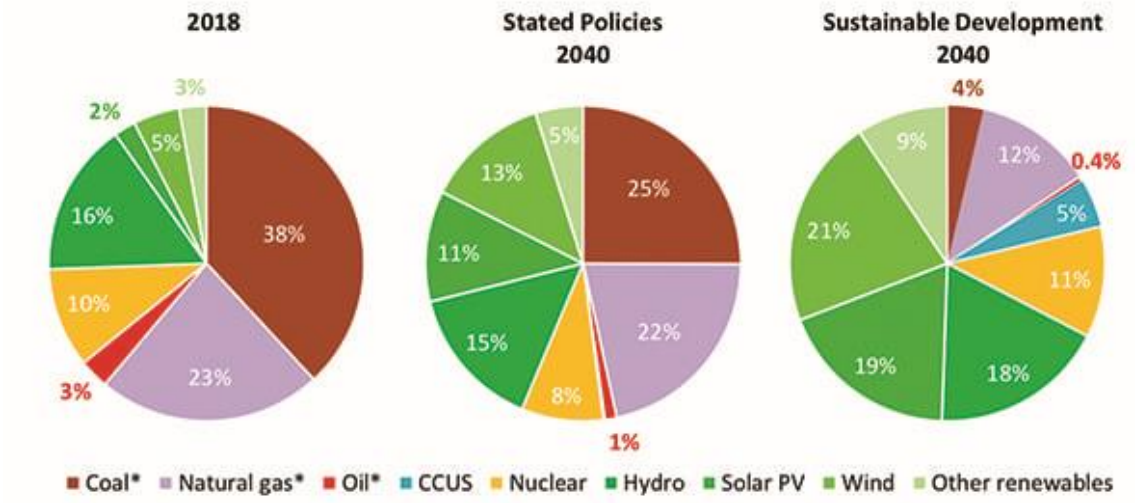

Figure 1.1 **Total energy supplies in 2018. This figure was taken and used without any modification from reference [3]**

Global warming, smog, acid rains and many other environmental concerns have forced the world for looking into the alternative environment friendly options which includes renewable energies like hydro power, solar technology, nuclear energy and wind

energy. With upcoming advancements in the technology and the improvements in the performances for new technologies, the world is seeing a brand new era with lower carbon emissions and sustainable developments [3].

1.2 Alternative Energy resources:

Pakistan being a developing country is undergoing immense challenges to meet its energy demands with limited energy resources. The energy crisis is widening because of the population bloom in country resulting in more than 7000MW shortage in electricity supply and demand [4]. The main energy source for the power production is fossil fuel which results in environmental issues [5]. With very little investments and few efforts, there is very little contribution of renewable energies in total percentage in energy supply scenario of the country. Our country is suffering from gas and electricity load shedding for about 8-10 hours daily [6].

Keeping these situations in view, there is a need to build and enhance alternative energy sources which are more reliable and environment friendly. Fuel cells are a promising alternative energy source with good performance for higher energy outputs as well as the clean and promising future.

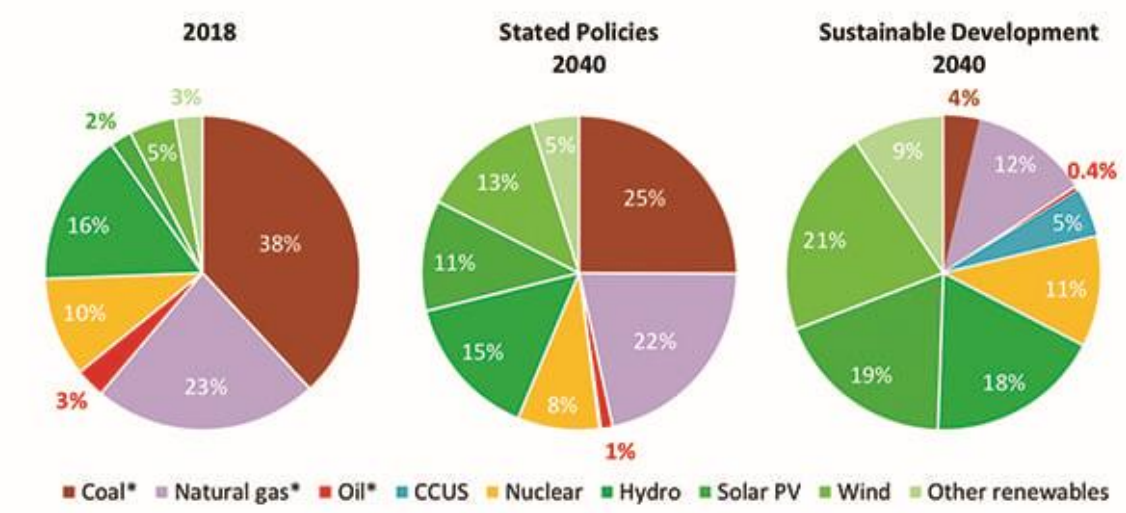

Figure 1.1 Total energy supplies in 2018. This figure was taken and used without any modification from reference [3]

1.3 Fuel cells

Fuel cells are the devices that convert the chemical energy present in the bonds of fuel into electrical energy directly. The single step process is comparable to the multistage processing of conversion of a fuel into electrical energy (i.e. chemical - thermal energy - mechanical energy - electrical energy), as it lacks the moving parts that are used in other combustion based systems[7].

Fuel cell was founded by German-Swiss scientists in 1839 while working on the electrolysis of the different metals. Later on, it was proved by Welsh Chemist Robert Grove through a gas voltaic battery that reaction between Oxygen and Hydrogen produces electric current. By following this idea, British chemist Ludwig Mond and Charles Langer used coal as the source fuel and obtained about $20Am^{-2}$ at 0.73V. Following their efficiency and energy outputs, alkaline fuel cell was used in Apollo space craft [8]. After that, depending on their power range and temperature variability, fuel cells began for their usage in public transport, heavy power loads and portable applications [9].

Fuel cells are considered more efficient when compared to other market technologies. The energy efficiency among photovoltaic devices, thermal solar technologies, waste incineration technology, gas powered turbines and nuclear power plants are much lower than fuel cell when it comes to portable, transportation and stationary applications. They don’t emit any hazardous waste neither release any waste gases that are responsible for global warming and other environmental aspects. With having advantage in both gravimetric as well as volumetric energy densities, fuel cells are used in priority for the portable applications. Their higher capacitive factors have urged their use in stationary sector as well [10].

When compared to batteries, fuel cell are quite similar as they both have same working principle i.e. two electrodes and working electrolyte that is sandwiched between two electrodes. They both involve the internal oxidation-reduction reactions undergoing. The difference comes in the composition of the electrodes and output current content and type. Fuel cells have proton conducting media electrodes whereas the batteries have metal electrodes. The major difference is the energy storage among them, batteries store the energy and discharge the current as

a capacitor whereas fuel cells just act as a continuous process i.e. take in the fuel and produce the current continuously [7].

1.4 Types of fuel cells

Fuel cells are first categorized on basis of the electrolyte used. Second grouping is done on base of the operating temperatures and the fuel used Table 1.1. Thus, there are two classes of fuel cells, high and low temperature fuel cells. Low temperature fuel cells have working temperature of 70-90°C, they include Proton exchange membrane fuel cells (also known as polymer electrolyte fuel cells) and alkaline fuel cells. Certain variants also come with different fuels sources including hydrocarbons for example methanol, ethanol and formic acid which can be used in direct methanol fuel cells (DMFC), direct ethanol fuel cells (DEFC), and direct formic acid fuel cell (DFAFC). Whereas, high temperature fuel cells operate at 500-1000°C including Molten carbonate fuel cells and Solid oxide fuel cells.

Table 1.1 Major types of fuel cells

Fuel Cell	**Fuel**	**Electrolyte Charge carriers**	**Operating Temperature (°C)**
Alkaline fuel cells (AFC)	Hydrogen	KOH solution OH^-	<80°C
Polymer electrolyte membrane fuel cell (PEMFC)	Hydrogen/ hydrocarbons	Polymer membrane H^+	<150°C
Phosphoric acid fuel cell (PAFC)	Hydrogen	Phosphoric acid	200°C
Molten carbonate fuel cell	Hydrocarbons	Molten carbonate CO_3^{2-}	650-800°C
Solid oxide fuel cell (SOFC)	Hydrocarbons	Ceramic O_2^-	500-1000°C

1.4.1 Alkaline Fuel cells

Alkaline fuel cell are low temperature operating fuel cells with highest efficiencies of all fuel cells. It only works with the pure gases which makes it low viable option to be used commercially. Yet, on basis of 30-40% KOH electrolyte, they have a plus point against the acidic fuel cells because of the fact that oxygen reduction reactions take place more actively in basic electrolyte medium than in acidic electrolyte medium. The optimal temperature for AFCs is considered to be 100°C. few experiments had previously been conducted by increasing the operating temperature to 200°C but that didn't proved any positive effects on the performance of the system [11]. The schematic diagram is shown in Figure 1.1.

The reactions taking place in AFCs are as follows:

At anode:

$$H_2 + 2OH^- \rightarrow 2H_2O + 2e^- \qquad (1.1)$$

At Cathode:

$$1/2O_2 + H_2O + 2e^- \rightarrow 2OH^- \qquad (1.2)$$

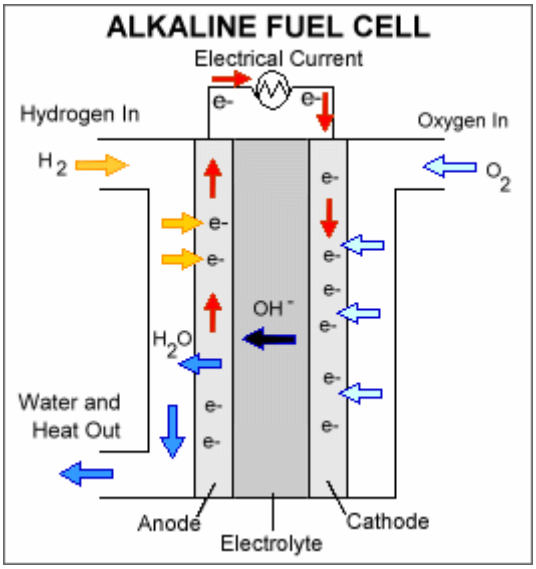

Figure 1.2 Alkaline fuel cell schematic diagram. This figure was taken and used without any modification from reference [11]

1.4.2 Phosphoric acid fuel cell

Phosphoric acid fuel cells require phosphoric acid as working electrolyte for conversion of chemical energy into electrical energy. The anode and cathode of the cell are prepared by finely distributed platinum on carbon and silicon carbide framework, holding phosphoric acid as electrolyte. They have lower energy tendency but have higher resistance against carbon poisoning. They have operating temperature of around 180C. The efficiency of the overall system can be increased up to 80% if the cogeneration system is used. They were commercialized in 1970s [12].

The overall reactions are:

At anode:

$$H_2 \rightarrow 2H^+ + 2e^- \qquad (1.3)$$

At Cathode:

$$\frac{1}{2}O_2 + 2H^+ + 2e^- \rightarrow H_2O \qquad (1.4)$$

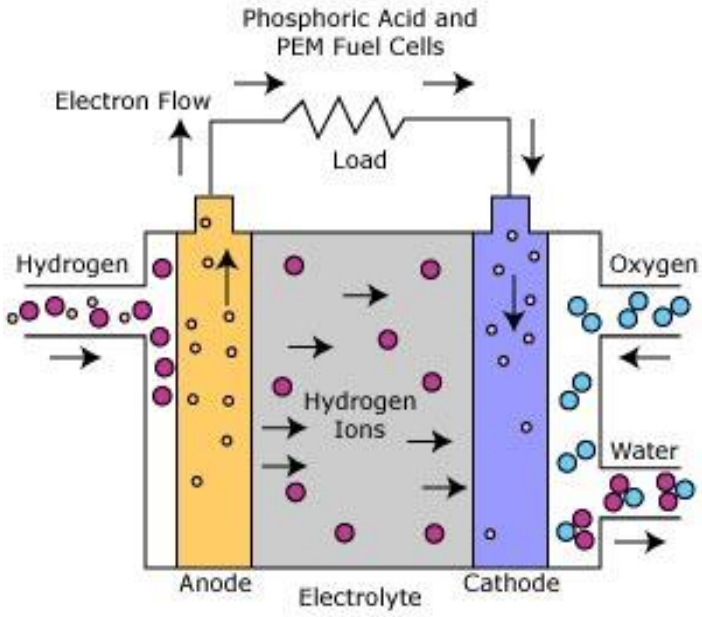

Figure 1.3 Schematic diagram of Phosphoric acid fuel cells. This figure was taken and used without any modification from reference [12]

1.4.3 Proton Exchange Membrane Fuel Cells

PEMFC are known as the devices which converts the hydrogen and oxygen fuel through electrochemical reaction that takes place through a polymeric membrane used as an electrolyte. They have an operating temperature of around 85-105°C. Due to their low temperature operations they are highly studied for many applications. They were first used in the Gemini program spaceship where they not just powered up the ship but also provided the pure drinking water for the astronauts which is obtained as a byproduct of the electrochemical reaction of the cell. At first the membrane used was Polystyrene sulfonate (PSS) which was highly unstable now they are replaced by the Nafion membranes (DuPont) with higher acidity and better conductivity with very efficient stability then the previous PSS membranes[7], [13].

The cell consists of a polymeric membrane as its electrolyte, which creates a separation between cathode and anode sids as illustrated in Figure 1.4. The membrane, the gas diffusion layer (GDL) and the catalyst layers are collectively called membrane electrode assembly (MEA).

Following reactions take place in the PEMFC:

At Anode, hydrogen is oxidized electrochemically into protons and electrons. This reaction is known as hydrogen oxidation reaction (HOR):

$$H_2 \rightarrow 2H^+_{(aq)} + 2e^- \qquad E= 0V \qquad (1.5)$$

The protons are then transported to cathode though membrane while electrons travel through external circuit to cathode due to the fact that electrolyte i.e. membrane is insulating material.

At Cathode side, the electrons are reacted with oxygen. The reactions is known as oxygen reduction reaction (ORR):

$$\frac{1}{2}O_2 + 2H^+ + 2e^- \rightarrow H_2O \qquad E°= 1.23V \qquad (1.6)$$

The overall reaction results in water and heat as by-product:

$$H_2 + \frac{1}{2}O_2 \rightarrow H_2O \qquad E°_{cell} = 1.23V \qquad (1.7)$$

Proton exchange is the core important factor in the PEM technology. Still there is a work done on the better membranes for easy proton transfer and stable conductivity.

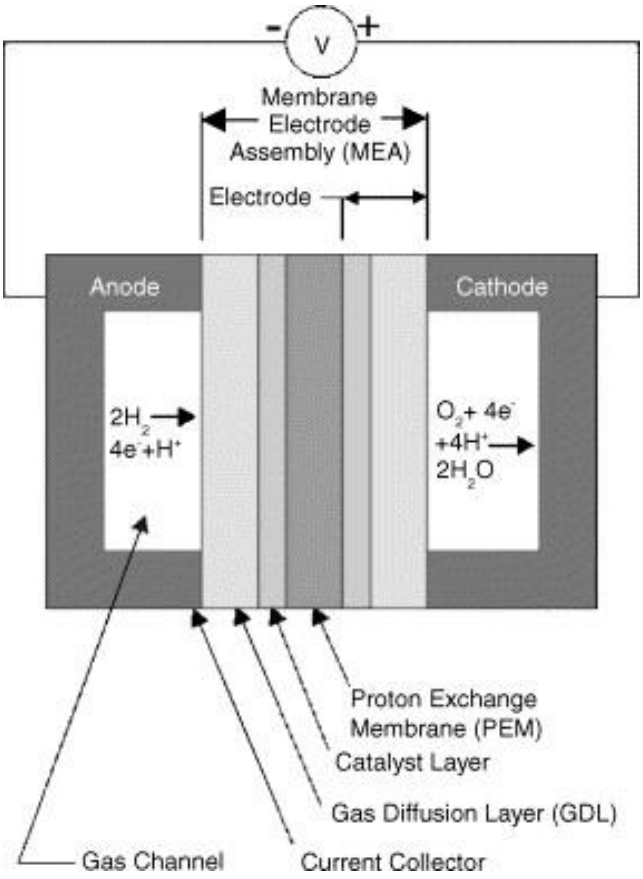

Figure 1.4 Single typical proton exchange membrane fuel cell. This figure was taken and used without any modification from reference [14]

1.4.4 Molten Carbonate fuel cell

The working mechanism of this fuel cell is same as the others, but it differs in terms of electrolyte i.e. carbonate compounds as the electrolyte, shown in figure 1.5. They use molten carbonate salts which are suspended in ceramic matrix as electrolyte. Commonly used salts are lithium carbonate, sodium carbonate and potassium carbonate. They usually operate on higher temperatures, 650°C. The higher temperature has many advantages including higher reaction kinetics, low carbon poisoning. They don't need noble metals for their operations therefore, they can rely on number of fuels including fuel gases, methane or natural gas. There are several disadvantages too related to the higher temperature of the cell as it may lead to the corrosion because of the corrosive electrolyte as well as higher temperature. MCFCs are majorly used in coal and natural gas based power plants for industrials operations i.e. electric utilities and for military applications [14].

In MCFC, following reactions takes place:

At anode:

$$H_2 + CO^{2-}_3 \rightarrow H_2O + CO_2 + 2e^- \qquad (1.8)$$

At Cathode:

$$\frac{1}{2}O_2 + CO_2 + 2e^- \rightarrow CO^{2-}_3 \qquad (1.9)$$

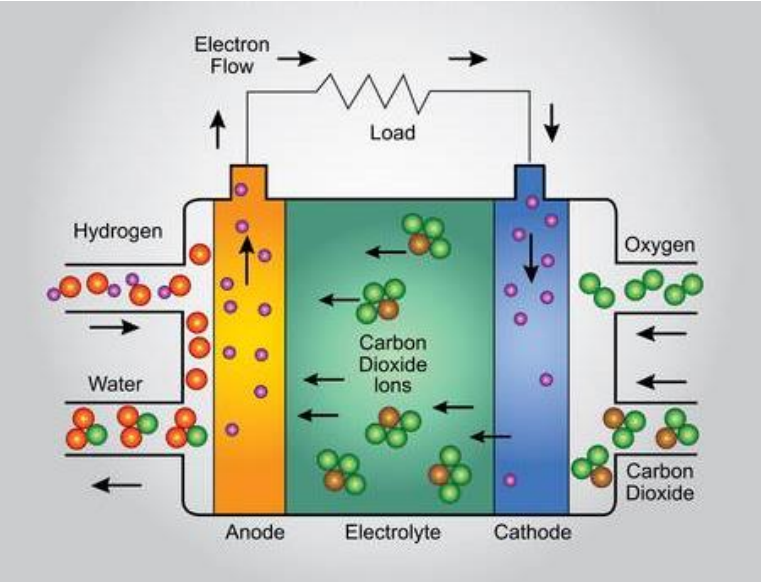

Figure 1.5 Schematic diagram of Molten carbonate fuel cell. This figure was taken and used without any modification from reference [15]

1.4.5 Solid oxide fuel cell

Solid oxide fuel cells are known for their high temperature activity. They usually work around 800-1000^{o}C. With an overall efficiency of 60%, if their produced heat is harnessed, the efficiency can be increased to 80%. They use solid ceramic electrolytes. Instead of using a liquid or a membrane, commonly used electrolytes are zirconium oxide which is stabilized with yttrium oxide. Due to their increased temperature, they have higher reaction kinetics and are prone to carbon poisoning. They can operate on number of fuels directly as they don't require any reforming of the fuels prior to use. They have limitations for their startups because they need time to reach the higher temperature and start the operation. They are

used in electricity utilities in industry either for large power generation or small scale [15], [16].

The overall reactions taking place in the cell are:

At anode:

$$H_2 + O^{2-} \rightarrow H_2O + 2e^- \qquad (1.10)$$

At cathode:

$$\frac{1}{2}O_2 + 2e^- \rightarrow O^{2-} \qquad (1.11)$$

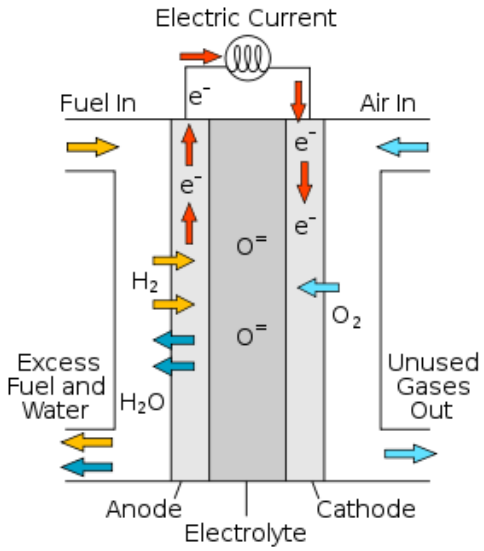

Figure 1.6 Schematic diagram of Solid oxide fuel cell. This figure was taken and used without any modification from reference[16]

1.5 Hurdles in Commercialization of PEMFC and AFC

Several challenges have been faced by the fuel cells and in order to mitigate them, DOE is funding the research to evaluate the improvements.

1.5.1 Economics

In order to compete with commercially available power sources, fuel cells have to be that efficient and cost competitive to outcome those sources. As per DOE studies, there are four ways to increase the fuel cell performance and decrease the

cost: 1) lowering the amount of Pt used as catalyst and replacing it with more durable catalyst, 2) increasing the activity by Pt to decrease PGM content, 3) developing non noble and non-platinum group metal electrocatalysts that can give the stable and durable activity as compared to Pt, 4) using advanced support materials that can reduce corrosion effects and increase durability in PEM fuel cell[17], [18]. As stated by the DOE cost breakdown reports of the fuel cell, catalyst is the main contributor to the PEMFC cost as shown in Figure 1.7. Pt catalyst that is used as primary catalyst for the cell, is very expensive and a not very abundant in earth's crust. Further cost comes from the manufacturing which are volume sensitive. The ICE vehicles use PGM metals as a catalyst in their catalytic converters. Therefore, to reduce the cost, Pt loading has been decreased to $0.125 mg_{pgm}/cm^2$ and the trend is still decreasing up to 2020 [19].

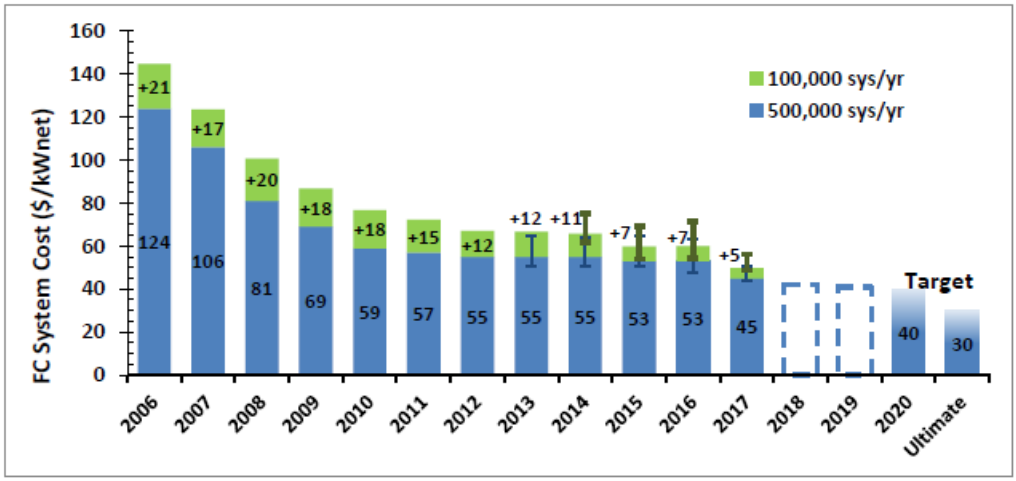

Figure 1.7 Modeled cost frame of 80-kWnet fuel cell by DOE. This figure was taken and used without any modification from reference [20]

1.5.2 Durability Issues

Continuous efforts and research techniques have shown that membrane, stack and fuel cell performance is 50% increased. Studies have shown decrement of voltage by 10% over the lifespan of fuel cell stack. Still, the life span has been increased to about 1900 hours.

For further improvements, DOE is focusing on the system components including catalyst degradation with time which is a big challenge to mitigate the lowering voltage form the stack. Catalyst poisoning, dissolution, particle growth and carbon corrosion are major factors for the performance degradation. As a solution, Pt alloys are seen as best remedy for these problems. With the advancements, Pt loading has been decreased to 0.2mg/cm^2[17].

1.6 Significance of research topic

The worldwide energy production has been dominated by fossil fuels since a very long time. The efforts are underway to eradicate the problems caused by fossil fuels for as soon as possible by moving towards alternative energy trends and more favorable sources. Since it is very difficult to totally move on from the fossil fuels as a primary fuel very soon owing to high energy efficiency and high yields. Considering fuel cells as alternative power sources have several barriers including the high maintenance cost and catalyst availability. For mitigating these barriers, a new catalyst system is proposed with higher stability and output reforms for better performance and stable outputs.

In this study, development of alternate catalyst material is focused for PEMFC and AFC with aims to reduce catalyst cost and improving the durability of the system.

1.7 Research Objectives

This project is based on following main objectives:

1. To synthesize series of BM-ZIF derived electro-catalysts and study the effect of transition metals on the activity of fuel cell.
2. To optimize the ratio of two metals (Ni, Co) in the synthesis of ZIF derived electro-catalyst and study their effect on fuel cell activity.
3. To study the effect of synthesis techniques on the activity of BM-ZIF derived electro-catalyst at different pyrolysis temperatures.
4. To study the effect of platinum loading on the activity of BM-ZIF derived electro-catalysts.

5. To carry out both *ex-situ* and *in-situ* electrochemical measurements to evaluate the performance of these electro-catalysts.

2. Literature Review

2.1. PEMFC and AFC Catalyst Layers

Since the development of PEMFC, Pt has been successfully used as deposited catalyst on the cell. A lot of research is under way to replace this expensive catalyst without effecting the performance of the system [20]. The early used PEMFCs utilized the fine powdered Pt black. For achieving a better performance rate, the material had a particle size of 50-100nm with physical surface area of about $10m^2g^{-1}$, requiring a loading of about $4mg.cm^{-2}$. After some time, carbon based electro catalysts were introduced [21]. They had an advantage over other catalysts as they had very low corrosion and deformation rate as compared to the previously used catalysts [22]. Later on, developments regarding metal organic frameworks (MOF) also revealed excellent characteristics of the materials. The materials have metallic and organic structure linked structures giving them more flexibility in structure as well as stability towards the reactions [23]. The structural tailoring is a plus point for these materials as there is a wide range of techniques to augment their performance and stability as required per application [24] [25].

Various electrocatalyst for PEMFC are developed to overcome the lag in oxidation reduction reaction at the cathode. The catalysts developed consist of Pt loading which is targeted to decrease by 2020 by 0.125 mg PGM/cm^2[19]. Pt is used on both the anode and cathode of the cell. Both the HOR at anode and ORR reactions at cathode require higher activation energy that can be provided by a catalyst having delicate properties. Pt adopts the form of small particles on the surface of the carbon particles supporting the ongoing reaction [18].

In the recent years, metal organic frameworks have acted as an active alternate for the application. The presence of non-precious metal electrocatalyst is considered an ideal solution for the replacement of Pt catalyst.

This chapter discusses in summary of the developments in the electrocatalyst for fuel cell cathode reactions (ORR). Major durability issues regarding the issue are also presented and approaches helpful to address them.

2.1.1 Anode catalyst layers

In the recent years, a lot of work is being conducted on PEMFC cathode to cater the slow reaction kinetics of the ORR. However, HOR is also considered to contribute activation over potential if there are any impurities in the fuel supplied. The reaction is 2 times more sluggish when it comes for basic media as compared to acid [26]. To overcome the slow nature of the reaction, it's ascribed to use a catalyst that can create bonding with adsorbed hydrogen either its basic media or acidic electrolytes [27].

In HOR, following reaction mechanism is followed:

Overall reaction in acidic media:

$$H_2 \leftrightarrows 2\ H^+ + 2\ e^- \qquad (2.1)$$

Overall reaction in alkaline media:

$$H_2 + 2\ OH^- \leftrightarrows 2\ H_2O + 2\ e^- \qquad (2.2)$$

In acid, reaction is comprised of two out of three microscopic steps (Tafel/Volmer or Heyrovsky/Volmer):

Tafel step:

$$H_2 \leftrightarrows 2\ H_{ad} \qquad (2.3)$$

Heyrovsky step:

$$H_2 \leftrightarrows H_{ad} + e- + H+ \qquad (2.4)$$

Volmer step:

$$H_{ad} \leftrightarrows H+ + e- \qquad (2.5)$$

In base, the Heyrovsky and the Volmer steps have traditionally been written with hydroxides rather than protons as reactants:

Heyrovsky step:

$$H_2 + OH- \leftrightarrows H_{ad} + e- + H_2O \qquad (2.6)$$

Volmer step:

$$H_{ad} + OH- \leftrightarrows H_2O + e- \qquad (2.7)$$

Since Pt is considered as most active and stable catalyst for the HOR, it proposed by the authors to combine Pt with more oxophilic materials i.e. Ru/Ni to enhance the interaction of H_2O/OH^- for yielding more HOR/HER activities in basic media [28], [29]. Studies have also revealed that with reducing the amount of Pt on anode, the voltage obtained from the RDE experiments is not affected [30], [31].

As previously discussed, Pt catalyst loading is required to be decreased for the commercialization of the PEMFC. In Figure 2.1, Pt and PGM are situated at the top of the plot depicting the highest hydrogen bonging energy of the catalysts [32]. This plot is a very useful tool for understanding the prediction and establishing of the energy and reactivity trends for the exchange current densities w.r.t hydrogen enthalpy or oxygen adsorption [33]. The plot explains that a heterogeneous catalyst must have enough strength to bind reaction intermediates for better electron transfer, but it should be weak enough to allow the desorption of the resultant product from the surface of the catalyst and free-up active reaction sites for further reactions. Pt and PGM are in the zone with intermediate energy values for hydrogen adsorption and that is why they are the best efficient catalysts considered for HOR among transition metals [34].

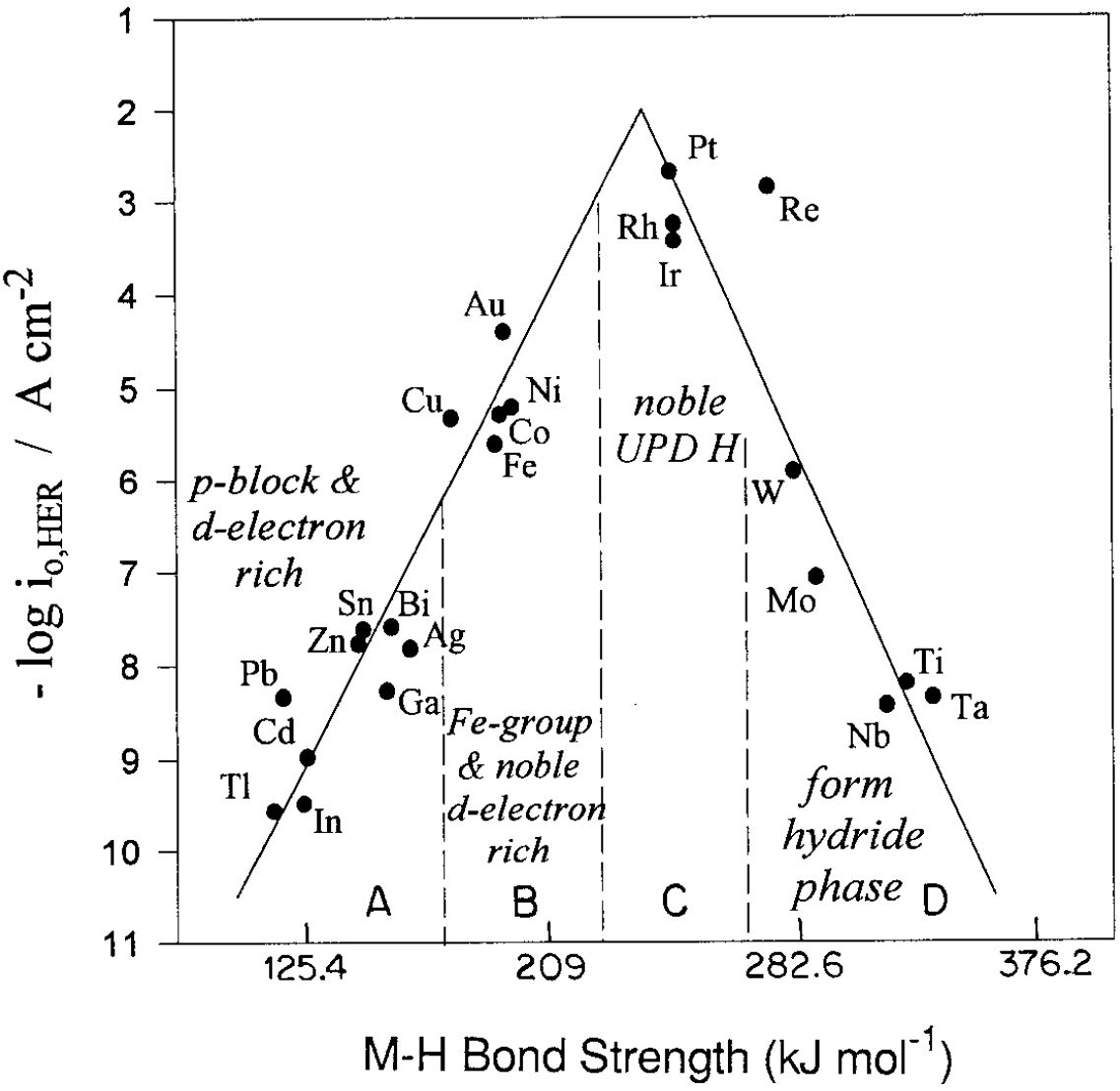

Figure 2.1 Volcano plot of log j_0 vs metal-hydrogen bond energy for different catalysts. This figure was taken and used without any modification from reference [34]

To explain the reactivity of the metals being used for the purpose, their reactivity is predicted by a useful theory for the transition metals developed by the Hammer and Norskov [35]. The theory explains the availability of the energy levels which is responsible for the metal to form bonds with other species[36]. A transition metal has different energy levels with electron filled in each level. The energy level decreases from the mid to outermost shell. The outermost shell has two further categories i.e. *s* and *d* states [37]. When an electron approaches the metal, *s* state is first attracted leading to the broadening and shift of the energy state, after that *d*-state is approached [38].

On basis of this theory, there's possibility to tune the *d*-band center of a metal by alloying it other metals. It is evident from the Figure 2.2, that Pt, Ir have higher energies which makes them as strong candidate for the purpose. Instead of using Pt for making alloys, Pd is alloyed with the Ir which makes it best catalyst for the HOR with comparable activity to that of Pt. we can say that HOR depends on the strength of the PdIr-H bonding [39]. When bonding was strong enough, the activity started to decrease because of the large *d*- band vacancy. With the variation in the Pd-Ir ratio, the increment in the tafel and exchange densities also increased explaining the role of electronic structure in the electrolytic reaction [40].

2.1.2 Anode catalyst layer degradation

In fuel cells operations, there may be chance of failure of one or more cells in the stack. These failed cells cannot produce any current but the overall voltage that is produced by the other cells in the stack is imposed on these failed cells [41]. This phenomena results in *voltage reversal* and is supposed to reduce the power output of the system and can permanently damage the MEAs, stack hardware and flow plates or any electrical contact with the plates [42]. This hazardous phenomena is observed in both the parallel and series cells which cause a major threat to the durability of the cell [43].

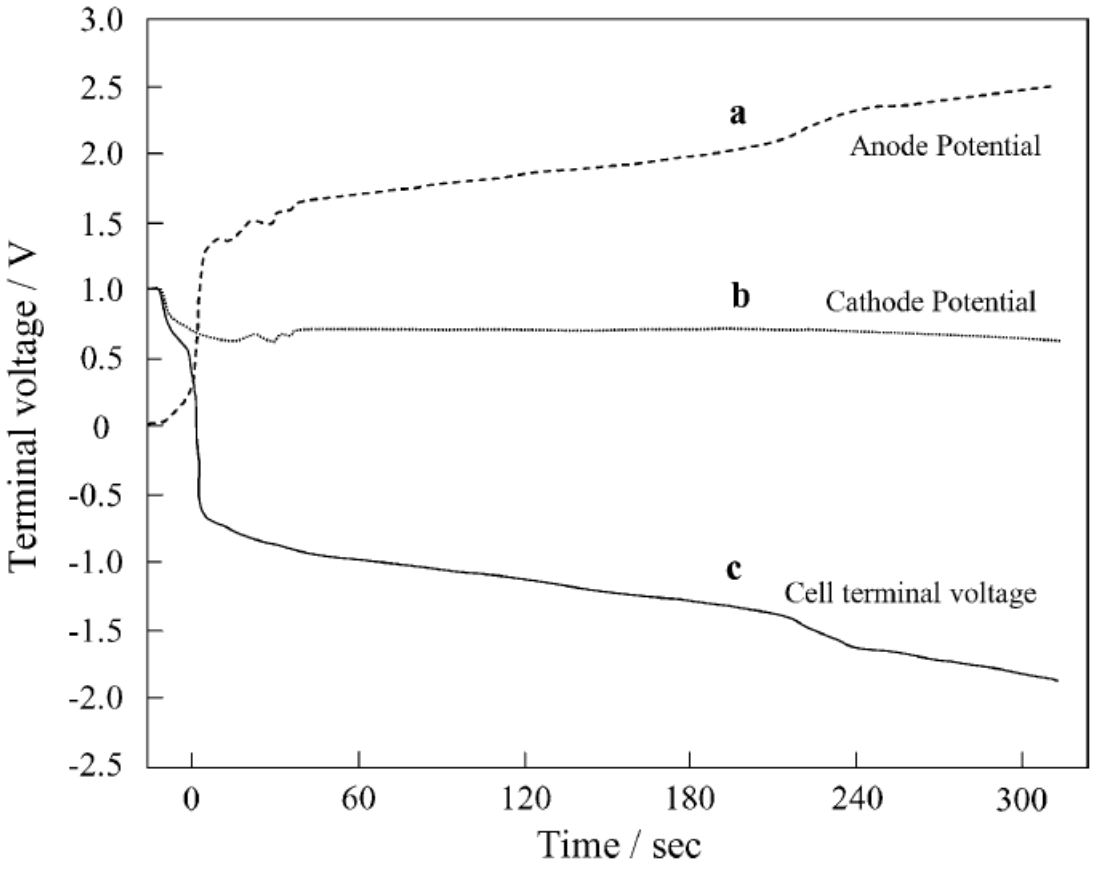

Figure 2.2 Voltage reversal experiment on anode & cathode w.r.t time variation. This figure was taken and used without any modification from reference [41]

Fuel starvation is one of the effects caused by the phenomena occurring at the anode. This happens when fuel supply is suddenly changed at pressure drop changes between cells, start/stop of the system and poor water management.Figure 2.2 shows the variation of the anode and cathode potentials when voltage reversal experiment was conducted. It indicates that when fuel is insufficiently supplied to the anode, the voltage line (ascribed as **line a**) rose to sustain the stack current with cell voltage dropping sharply. These high potentials when applied to anode, causing the carbon corrosion and leads to the dissolution of the metal which causes the anode catalyst layer to degrade. Catalytic activity is also reduced when this reduced metal is transferred through membrane from anode to cathode causing the catalyst contamination.

Voltage reversal can be controlled by several advanced techniques, but the main causes are imperfect system control that leads to the immense damage on the anode catalyst layers. One of the basic technique is to use corrosion resistive materials and by using the oxygen evolution catalyst to mitigate the problem [44].

2.1.3 CO contamination

Being an expensive fuel, hydrogen alone cannot be used in the PEMFC, at least not for short terms. It is therefore, a reformate gas with hydrogen is proposed to be a practical alternative fuel for the cell [45]. Reformate gas contains 1-2% of CO which is removed before entering the cell. But problems still arise because of trace amounts of CO present in the mixture, posing a threat to the catalyst as well as the performance of the system.

The catalyst poisoning is one of the major factors for the system failure. It occurs when CO is strongly adsorbed on the surface of the Pt which in return blocks the active sites of the catalyst hindering the performance and activity of the catalyst. The reaction is also feasible for the CO because the cell is operating under 100°C [46], [47].

Keeping in view the hazard, certain measures are proposed to eradicate the problem:

- One must install advanced reformer design to improve the capability of the system to remove the unwanted gases completely
- Utilization of CO tolerant catalysts
- Preparation of anode with composite materials that have active sites for CO making it to react with the first layer and then the Co free gas would react with second layer of Pt-catalyst
- Oxidant seeping into the fuel feed to convert CO into CO_2
- Using high activity membranes that can easily separate out the CO
- Using special membranes to separate hydrogen impurities.
- Supplying the pulse current or voltage to the cell for removal of CO from the catalyst surface

Out of the above proposed methods, layered anode preparation is considered to be the most promising of all for solving the CO poisoning problems. It has the benefit that it is not much complex as compared to the other methods and is much more economical way to mitigate the problem. The technique is to use Pt with a second metal with high CO activity forming an alloy with Pt [48]. The metals include Ru, Sn, Rh, Mo, Fe, Ni and Pd [49]. Among these metals, PtRu alloy is considered to be the most effective one with highest activity towards the CO tolerance [50], [51].

2.1.4 Oxygen Reduction Reaction (ORR)

Understanding the ORR mechanism is very important for the development of an efficient catalyst. Despite the long debates, Oxidation reduction reaction is more complex reaction when compared to HOR as it gives 4 electrons and a number of elementary steps with strongly associated reaction products which results in one magnitude lower exchange current density than HOR.

It is considered that ORR depends on the nature of electrode material, catalyst and electrolyte, but exact mechanism of the reaction is not well known yet. The ORR may occur in two pathways when observed in aqueous acidic media:

1. The overall reaction from O_2 to H_2O (4-electrons reduction):

$$O_2 + 4H^+ + 4e^- \rightarrow 2H_2O \qquad E = 1.29\ V \qquad (2.8)$$

2. 2 steps conversion of O_2 to H_2O (2-electron reduction):

$$O_2 + 2H^+ + 2e^- \rightarrow H_2O_2 \qquad E = 0.70\ V \qquad (2.9)$$

$$H_2O_2 + 2H^+ + 2e^- \rightarrow 2H_2O \qquad E = 1.76\ V \qquad (2.10)$$

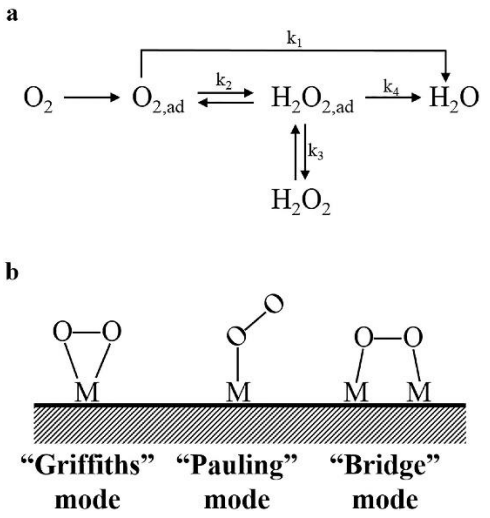

Figure 2.3 (a) Reaction pathways of ORR in acidic media. (b) Modes of O_2 adsorption on catalyst surface. This figure was taken and used without any modification from reference [52]

The ORR starts with the adsorption of the O_2 on the catalyst surface, it determines the electron mechanism of the ORR. The three adsorption modes on the catalyst are considered. The Griffiths model (one site), Bridge model (two sites) are suggested for the 4-electron reactions and the Pauling model (one site) is suggested for the 2- electron reactions Figure 2.3b). In fuel cells, peroxides accumulate in the electrolyte which are not desirable, therefore 4-electron reduction is preferred. Still, it comprises several reactions where O_2 is dissociated at the surface and for formation of H_2O, it recombines again with H_2. As a result, the reaction is of slow kinetics and active catalyst is needed.

2.1.5 Cathode catalyst layers

Considering the requirements, platinum supported on high surface carbon is the highly efficient and state of the art catalyst for the system. Keeping in view the activity of the different transition metals, 'volcano plot' defines the activity of the metals according to their binding energy Figure 2.4. Pt has specifically the highest activity for the oxygen with a binding energy of around $\Delta E_{0\,(Pt)} = +1.57\ eV$. There is a lot of room for the development of the more active and economical catalyst for the cell because when we consider density functional theory (DFT) calculations for the catalysts activity, the most favorable binding energy for the ORR is found to be around +1.8 to +2.0eV [52].

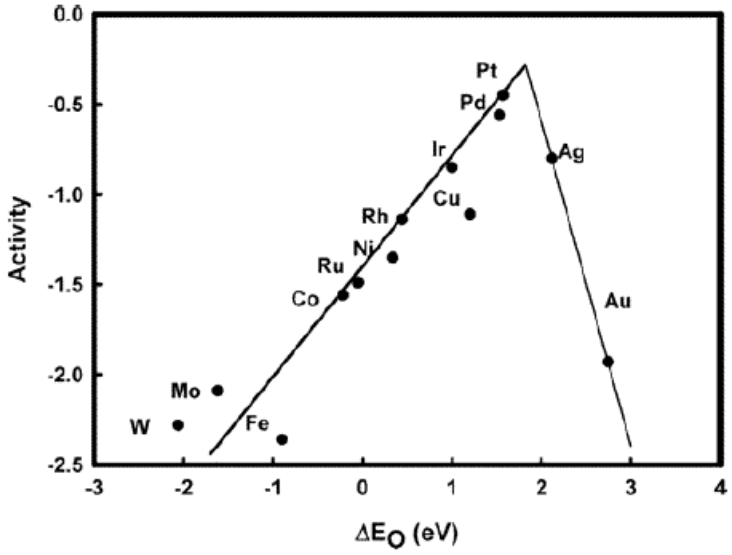

Figure 2.4 Activity of the transition metals as function of oxygen binding energy. This figure was taken and used without any modification from reference [53]

Due to problems with availability and expensive nature of the Pt metal, several techniques are used to reduce usage of Pt as catalyst as discussed earlier. A main strategy used for the purpose is to make alloys of other metals with platinum [53].

2.1.6 PGM- metal alloys catalysts

Studies have proved the Pt-M alloys on carbon support, where M= Fe, Co, Cu, Ni have higher activity then the pure platinum [52], [54]–[56]. The best performance was exhibited by the $Pt_{0.7}Ni_{0.3}$, $Pt_{0.6}Co_{0.4}$, $Pt_{0.5}Fe_{0.5}$ with current densities over 10, 15 and 20 times more than pure Pt [57]. One of the most convincing advantage of the alloying is that the catalyst stability is increased which help against the sintering as well as the dissolution of the Platinum catalyst which are a big problem for PEMFC catalyst stability and power loss issue as discussed earlier. The higher the oxidation potential of the metal, the higher will be the stabilization effect of the catalyst [18], [58], [59]. One factor that affects the ORR extensively is the binding energy of the Pt-based electrocatalyst. From the studies it is shown that the catalysts that bind oxygen molecule weakly, have more

expectancy to show better ORR activity during the enhanced removal of the oxygen-containing intermediates Figure 2.**5**.

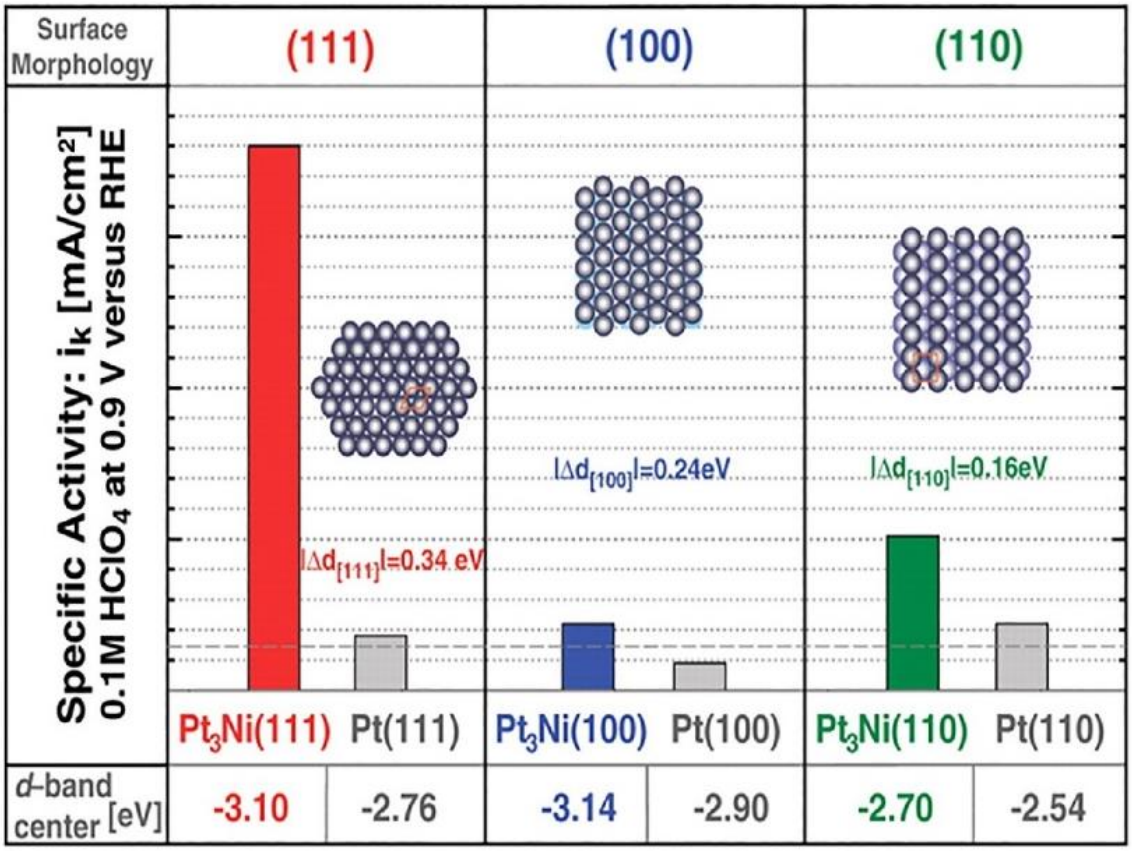

Figure 2.5 Trends in oxygen reduction activity plotted as function of oxygen binding energy. This figure was taken and used without any modification from reference [52]

Although metal alloying has its positive aspects towards the stability of the cell, but chemical leeching of base metals has a destructive effect on the fuel cell output potential. The cations released by the metals are hazardous for the membrane as they form the sulfonic groups rather than protons which causes the poisoning of the exchange sites of the membrane hindering the proton exchange [60]. This causes the increased resistance both in membrane and the catalyst layer with frequently decreasing oxygen diffusion layer and causing membrane to degrade faster with the loss of basic alloy structure of the metals. Studies conducted at room temperature revealed that with the dissolution of the base metals (Fe, Co, Ni, and Cu) they gave rise to the Pt skin within the monolayers of the surface, which later modified the basic electronic structure of the alloy surface which resulted in the increment of the

ORR activity. But problem still exists when PEMFC are operated at the standard temperature (>60 °C), causing the frequent dissolution of the metal resulting in reduced ORR activity of the system.

2.1.7 PGM-metal oxides catalysts

In the fuel cell the overall performance is attributed to the ORR. The thermodynamic reversibility potential of Pt for oxidation reaction is about 1.23 V. Studies reveal that using the Platinum with metal oxides base increases the activity of the catalyst. Various techniques are involved for the treatment of the catalyst including thermal treatments which increase the surface area of the catalyst by 26%. By using the Tin oxide and Titanium oxide based support catalyst with high surface area shows the high stability achievement [61], [62]. Pt-TiO_2 [62], Pt-NiO [63], Pt-V_2O_5, [64] Pt-RuO_2, Pt-WO_3 [65] shows the best performances and stability towards the ORR in the fuel cell [63]–[66].

2.1.8 PGM-metal nanoparticles alloy catalyst

The strategies for increasing the activity of the system includes the reduction of the size of the catalyst [67]. This strategy is helpful regarding the increment of the surface area that is a key requirement for the ORR but still the problem exist with the stability of the carbon structure. So, it was proposed to develop the nanoparticles of the catalyst by using the novel technologies [68]. However, these electrocatalyst suffer from the stability issues like detachment of small Pt particles and formation of agglomerates because of the Ostwald ripening effect under the standard operating condition of the cell [69].

a) Porous Pt-based nanomaterials

They have efficient structures due to their abundant exposed active, accessible and fluent mass transport. They've been a center of attraction since a very long time because of their porosity and Pt nanostructures for the catalytic activities. They don't only have active sites but they also have activity because of the inherited Pt conductivity which helps them to provide better transport activity for charge transfer [70]–[73].

b) Ultrathin Pt-based nanowires

Having better stability, improved electron transport and low number of defect sites, 1-D structures have been under consideration for ORR catalysis. In this technique, the structure is reduced to the diameter of a 1-D structure or few atomic layers, exposing the Pt active sites and surface atoms. Based on Pt-Ni, Pt-Co, Pt-Ni-Co, these nanowires showed best performances and stability attributes to the ORR [74]–[76].

c) Pt-based nanoframes

In the catalytic activity, the performance greatly relies on the topmost layer of the catalyst. The interconnected and highly open structures of the traditional catalyst are considered to be the good candidates for the ORR. They are highly active, with lesser susceptible to dissolution, sintering and detachment due to larger dimensions and enlarged interactions. It is therefore considered a good option to combine the nanoscale structures with the traditional structure for bringing out the best ORR activity. In the studies, the thermal surface etching was done for obtaining the nanohollow structure exhibiting the intrinsically higher activity for ORR with stability for over 10,000 cycles. This better activity is related to the less surface bonding strength materials promoting the easy detachment of the adsorbent molecule [77]–[79].

2.1.9 Cathode catalyst degradation

The cathode catalyst layer degradation is usually triggered due to electrochemical reduction in surface area of Pt or Pt-M alloys. This degradation is divided into three terms as per their causes: (i) Pt nanoparticles migration and agglomeration; (ii) Pt dissolution; (iii) carbon corrosion.

2.1.10 Pt nanoparticles migration

Pt particles that are supported on carbon are not stationary, in fact they can migrate across the carbon support and form agglomerates, which causes the loss of active pore sizes and surface area. This process decreases the surface tension which is the main cause for the inactivity of catalyst. A big factor for the instability of the catalyst is the interaction of Pt and the precursors with carbon and during the catalyst formation is severely crucial to the catalyst activity [80].

2.1.11 Pt dissolution:

A lot of work has been done and still underway for investigation of dissolution of the catalyst [47], [60], [81], [82]. It happens during the startup/shutdown of the cell when there is sudden demand for current at fuel cell stack causing the rapid reduction of Pt. This usually takes place at high potentials above 900mV. When it increases to 1.15V, a passivating oxides surface layer forms on Pt which leads to the saturation of platinum dissolution rate. However, in open circuit voltage (OCV), where voltage is about 1V, it is the highest potential to which cathode is exposed under normal conditions. Furthermore, during the cell operation, the current is withdrawn from the cell which causes the cell voltage to remain several hundred millivolts below the OCV. So there will be very less chances for optimal conditions for Platinum oxidation or reduction to reach during the normal cell operation [83], [84]. The reaction takes place as follows:

$$Pt + 2e^- \rightarrow Pt^{2+} \qquad (2.11)$$

$$PtO + 2H^+ \rightarrow Pt^{2+} + H_2O \qquad (2.12)$$

The dissolved Pt is flushed out of the system which usually takes place at higher potentials where water flow is comparably high from the cathode side. This loss of Pt^{2+} and redeposition on the larger crystallites causes the deficiency of activation sites which results in the loss of electrochemical surface area causing the decrease of the activity of the cell [85].

2.1.12 Carbon corrosion:

Although carbon is used extensively for the catalyst support for the PEMFC for a very long time but is actually thermodynamically unstable at standard conditions [86], [87]. This degradation reaction is so slow that it is considered as negligible under the standard operating conditions of the fuel cell. But when it comes for the automotive PEMFC where the cell undergoes a series of dynamic operating conditions with an estimate of around 300,000 voltage cycles for the total lifetime of the cell (5500 hr.), this degradation is very much accelerated at both the anode and the cathode posing damaging effects on the overall efficiency of the cell [88], [89].

$$C + 2H_2O \rightarrow CO_2 + 4H^+ + 4e^+ \qquad E = 0.207\ V$$

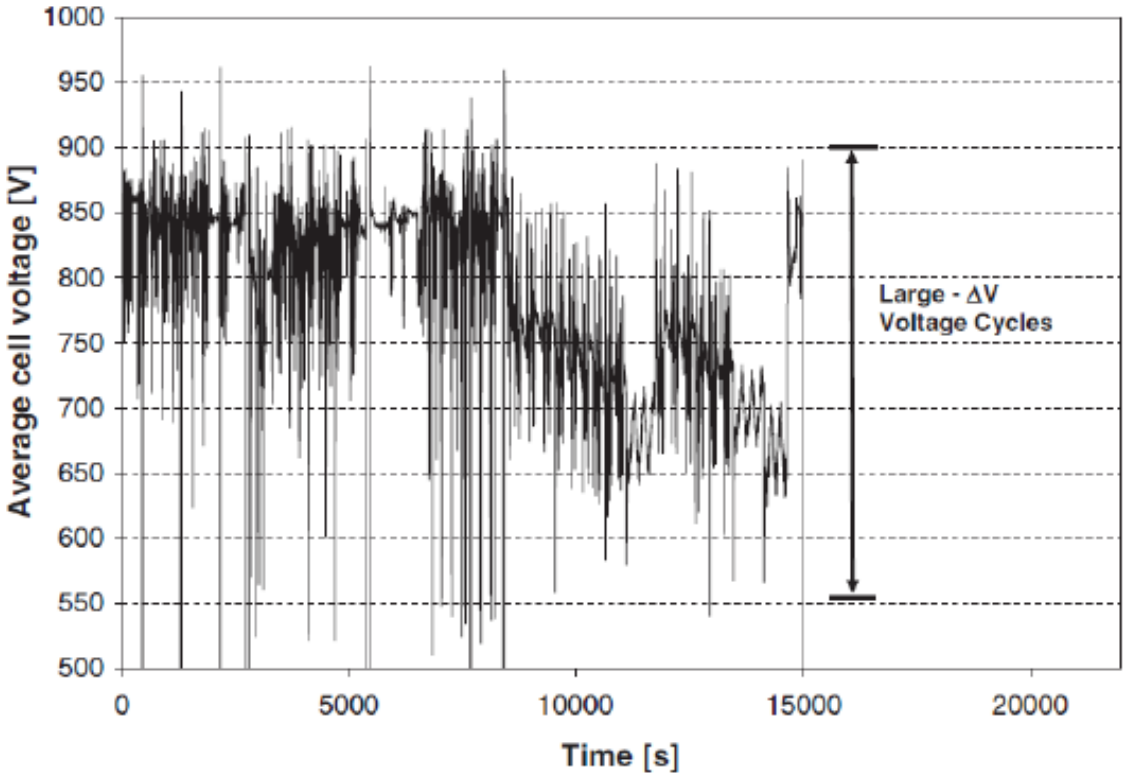

Figure 2.6 Overall lifetime cell voltage of automotive fuel cell w.r.t time. This figure was taken and used without any modification from reference [89]

By the corrosion of the carbon support, the Pt particles detach from the support and form the agglomerates reducing the electrochemical surface area and catalytic activity of the cell. In case of excessive corrosion, the total porous structure of the catalyst is destroyed which results in the increased mass transport resistance across the membrane causing the gas pathways blockage.

The solution of this issue, many research groups are working on developing a catalyst system that is corrosion resistant and more efficiently supports the system. For the reason, numerous ceramics or oxide supported catalyst have been introduced to the system including; ITO, CeO_2, WC, CeO_2-ZrO_2, SiC, TiN [64], [90]–[93]. Various other options are also under consideration including Carbon nanotubes (CNT), nanofibers (CNF), nanohorns (CNH), and nanocoils (CNC) [87],

[89], [94]–[96].the graphitic structure is also considered a better option in terms of the corrosion resistance but it has the limitation of having very low amount of the active sites where Pt can settle. But it is also a necessary point to keep the balance between the catalyst dispersion and the catalyst support to actually get a better fuel cell performance.

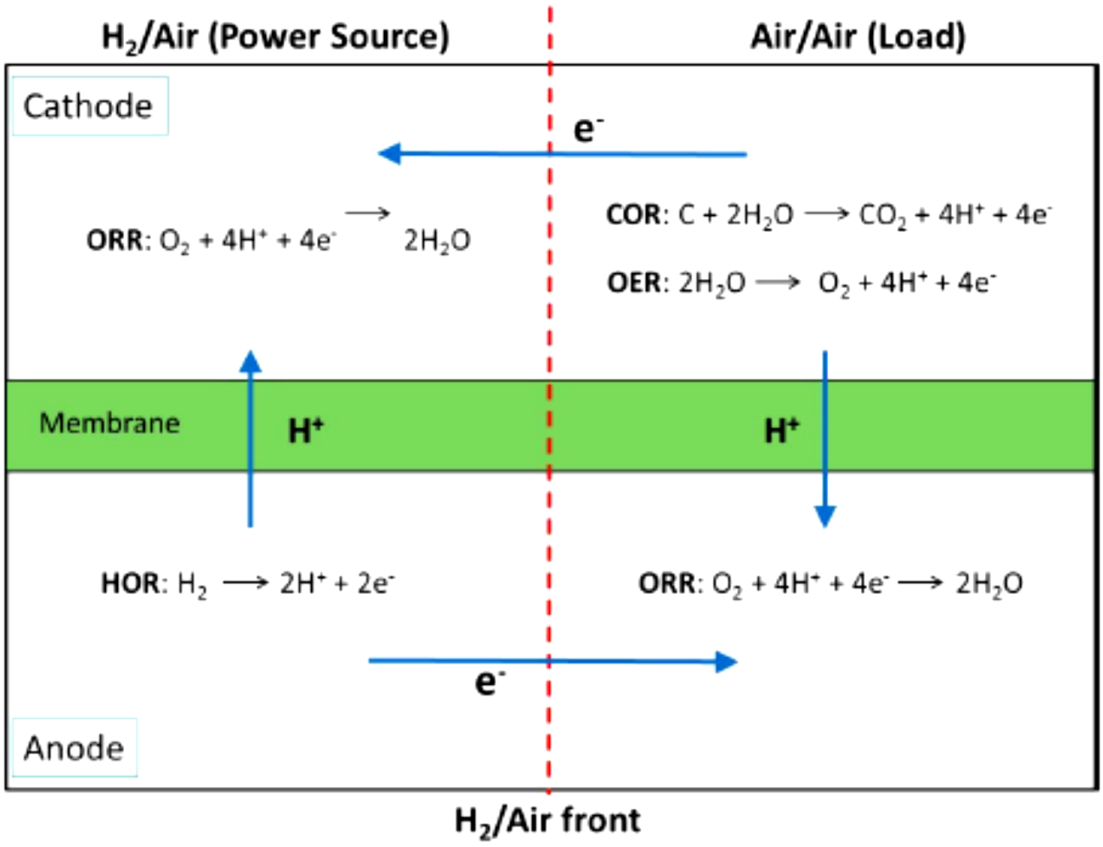

Figure 2.7 Overall sequence of startup/shutdown and electrochemical reactions in PEMFC. This figure was taken and used without any modification from reference [97]

2.1.13 Alternatives to Pt catalyst

As described earlier, catalyst layer adds an enormous amount to the overall price of the fuel cell. We can decrease the price by lowering the amount of the catalyst or to fully replace the catalyst by much active and stable catalyst. An approach was studied to use PGM metals as catalyst for the PEMFC but the extremely corrosive environment of the cell causes many problems for these non-noble metals. To overcome this problem, another approach towards the corrosion resistant materials was presented, introducing the metal organic frameworks (MOFs), chemical

organic frameworks (COFs). As the base for this research, metal organic frameworks will be discussed here.

2.1.14 Metal Organic Frameworks (MOF)

Metal organic frameworks have been considered as most versatile and adaptive materials for different applications including catalysis [97], gas and energy storage [98], drug storage [99] and energy conversion [8]. When compared to the conventional catalysts used in the fuel cells, MOFs have an advantage for having dynamic qualities as exceptionally high pore size, stability, corrosion resistance, uniform structure, tunable porosity, very high thermal stability and very wide range for the addition of the metal and functional groups for working structure of the MOFs [100], [101].

MOFs consists of open structure comprising of metallic centered secondary building unit (SBU) which are joined by several organic linkers forming a variety of 1-D, 2-D and 3-D structure. These structures are crystalline in nature and have long range order. They have exceptional pore size which is balanced by the solvent molecules or the solvent ions during the synthesis process. According to specific needs and desired applications, MOFs can be engineered, giving them an additional characteristic over the traditional zeolite or carbon frameworks where structure is difficult to alter [22], [23], [102].

2.1.15 Catalytic activity of MOFs

In catalysis, porosity, active surface area, adsorption properties are a key factor for the best catalysis results [103]. Having a wide range for metallic centers, organic linkers and organized structures puts them into a leading material to be considered for the catalysis [104]. MOFs are considered as heterogeneous catalysts. They are being used for the oxidation reduction reaction (ORR), oxidation evolution reaction (OER), hydrogen evolution reaction (HER), hydrogen oxidation reaction (HOR) and methanol oxidation reaction (MOR) [47], [53], [58], [98]. For obtaining better particle stability and uniform pore distribution, post synthetic modification (PSM) is carried out for combining the MOFs with nanoparticles for better catalysis.

2.1.16 Methods for enhancing current density

The current density is meant to be the major outcome of the catalyst in a reaction for which it is used. It is considered to be the most important factor for the efficiency of the catalyst as well as the system. There are several methods for enhancing the current density of the system by using an optimized catalyst.

$$i=io\{\exp(\beta nFRT\eta)-\exp(-[1-\beta]nFRT\eta)\} \qquad (2.13)$$

The equation is known as Butler-Volmer equation which consists *i* as current density for ORR, i_o as exchange current density. It consists of two parts. The first part consists of metallic dissolution/anodic reaction whereas the second part consists of metallic deposition /cathodic reaction. Keeping in view the above equation and electrochemical efficiency, the current density can be increased by following factors:

i. Increased number of electrons (low ohmic losses)
ii. Increased charge transfer (low transportation losses)
iii. Lower over-potential (yields higher current density)

When it comes to electrocatalyst to increase the reactions kinetics and increasing the overall potential of the system, following factors are responsible for achieving the higher current density.

i. Bimetallic alloy catalysts (increased no. of electrons)
ii. Increasing the catalyst active surface area
iii. Heat treatment of the catalyst
iv. Introducing CNTs for more better stability and performance
v. Optimizing the catalyst amount in the system

Current density can also be credited to the system and environment being used for the testing. There are several important factors that can be helpful for increasing the current density of the system.

i. Optimizing the molarity of electrolyte
ii. Increasing the working electrode area
iii. Amount of catalyst being deposited on the electrode surface
iv. Optimizing the distance between the electrodes

v. By variation of the scan rate

vi. Using rotation disk electrode for continuous replacement of product from electrode surface

2.1.17 Nickel-Cobalt based Metal Organic Framework (Ni/Co-ZIF):

Among the wide range of the metallic range and organic linkers in the metal organic framework family with different topology and activity properties, this work is based on combination of two MOFs i.e. ZIF-67 (Co based MOF) and bimetallic Ni/Co-ZIF. The work comprises of bimetallic center Ni-Co with imidazolate as organic linker having methanol as solvent. Nickel based MOFs are widely used in electro catalytic techniques[105], [106]. While Cobalt based MOFs are used in gas uptake enhancing factors, catalysis (OER), (ORR), (HOR) as well as gas capturing technologies [107]–[111]. With the increasing demand and technological upgrades in the PEMFC, the catalysis of the cell is also much focused. This work is based on the development of the ORR catalyst for the PEMFC and AFC.

ZIF-67 have been under consideration for its very porous and stable structure and activity for the applications. ZIF-67 carbon nanotubes (CNTs) with different metal doping (Pt, Cu, Ni, Zn) is considered as a good option for the catalyst as the catalyst gets its corrosion resistant support from the CNTs and the bimetallic doping provide extra activity and conduction towards the reactions [112]–[115]. When doped with Pt. the peak power density was obtained 630 & 560 mW cm^{-2} [112]. With doping Ni and Co, the onset potential was obtained 0.847V [113].

3. Characterization, Methodology and Experimentation

3.1 Physical Characterization

The purpose of physical characterization is to ensure that the material synthesized is accordingly the theoretically designed procedures and methods. Usually it comprises of many techniques but some of mainly used techniques are Scanning Electron Microscopy (SEM), Energy Dispersion Spectroscopy (EDS), X-Ray diffraction (XRD), Thermal Gravimetric Analysis (TGA), XPS, TEM, and ICP-MS which have been thoroughly discussed below.

3.1.1 Scanning Electron Microscopy (SEM)/ Energy Dispersion Spectroscopy (EDS)

A scanning electron microscopy is used to examine the topographical, morphological and composition analysis of things which are not examinable with simple microscope because electrons are used here to form image instead of a light source. In 1950, SEM was first time developed. It contains the following parts, Vacuum system, electron column, detectors, scanning system, display and electronic control system.

The main part of SEM is its electron column which consists of a gun source and two or more than two electromagnetic lenses (Figure 3.1). The gun source is usually called an electron gun which generates as well as accelerates electrons from 1-40KeV of energy. While the electromagnetic lenses are used to focus the electrons on specimen. Electron guns are of two types. First is thermionic gun which used a material to heat it up at a high temperature to emit electrons. Other is field emission in which a strong magnetic and electric field is used to draw electrons from metal (Tungsten) tip. Electric field of 2KV can be generated by help of an anode while second anode along with electromagnetic lenses is used to focus electrons beam forming a probe. Aperture draws the electrons as beam is passed through it and to avoid fluctuations, stigmators are used. Deflector coils are placed to send the beam

to collector where a special signal is generating relevant to each striking electrons to produce the final image. Secondary electron (SC) mode is used for SEM operation using both the backscattered and upper electron collector. Mixed collector is utilized to differentiate in different atomic number by introducing contrast. For example, Pt supported on carbon can be seen very clearly due to a contrast difference such as shown in Figure 3.1, where Pt metal is brighter than carbon support.

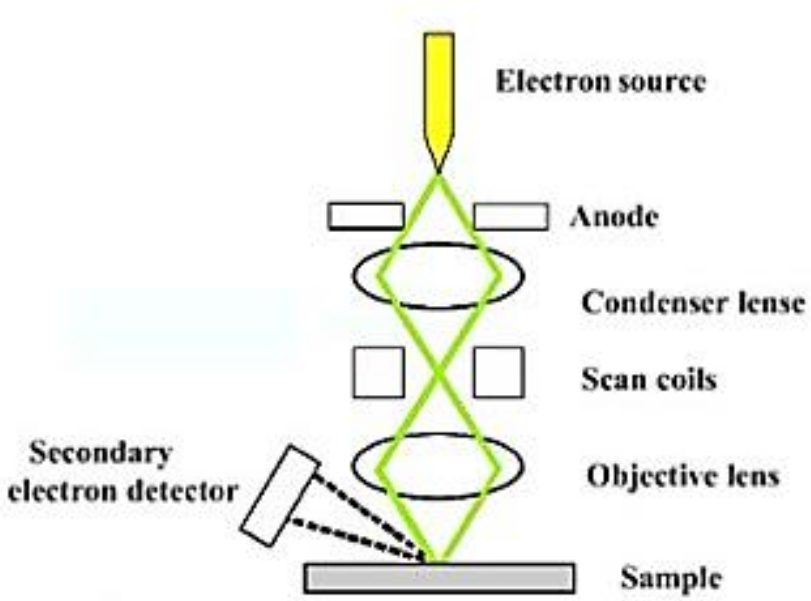

Figure 3.1 Schematic representation of basic SEM components

Field emission scanning electron microscopy (FESEM) is carried out for all samples by HITACHI S-4700 with 5-10 keV. Transmission electron microscopy (TEM) images were taken by CM200-FEG (Philips) at 200 keV. High Angle Annular Dark Field (HAADF) and energy dispersive spectroscopy (EDS) mapping were recorded by scanning transmission electron microscopy STEM (JEM-ARM200F) at 200 keV.

3.1.2 Thermal gravimetric analysis (TGA)

It is a thermal analysis technique of finding stability of a synthesized catalyst or sample over time in a given temperature range. The experiment is run on an equipment named as thermogravimetric analyzer shown in following (Figure 3.2).

A wide range of material can be tested in TGA such as composites, polymers, paints, fibers, fuels thermoplastic and thermosets etc. Basically, this technique gives the thermal degradability of tested material over a temperature change in an inert atmosphere to avoid any chemical reaction. There will be no mass change occur for those samples which are thermally stable. The result obtained from a TGA experiment are in graph form between initial mass (m) or percentage (%) at y-axis and temperature (T) change or time (t) on x-axis. Along with thermal decomposition, chemisorption, phase change, absorption/desorption and solid-gas reaction can also be determined by TGA.

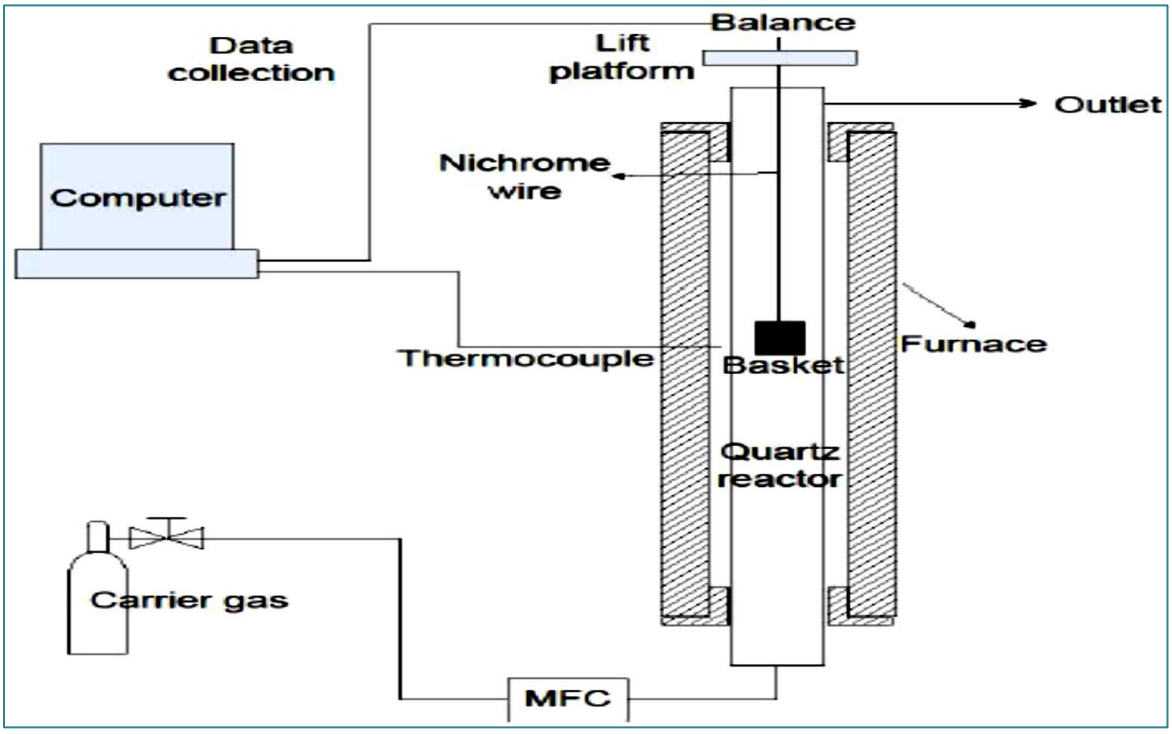

Figure 3.2 The basic design and working of a Thermogravimetric analyzer (TGA). This figure was taken and used without any modification from reference [134].

3.1.3 X-Ray Diffraction XRD

XRD is a type of characterization technique which is used to find the crystallographic planes of synthesized crystals by measuring its shift in phases due to X-ray light. XRD is a non-destructive technique which can find out the dimension

of unit cell, purity of a sample, crystal size, lattice parameters and other information related to a crystal.

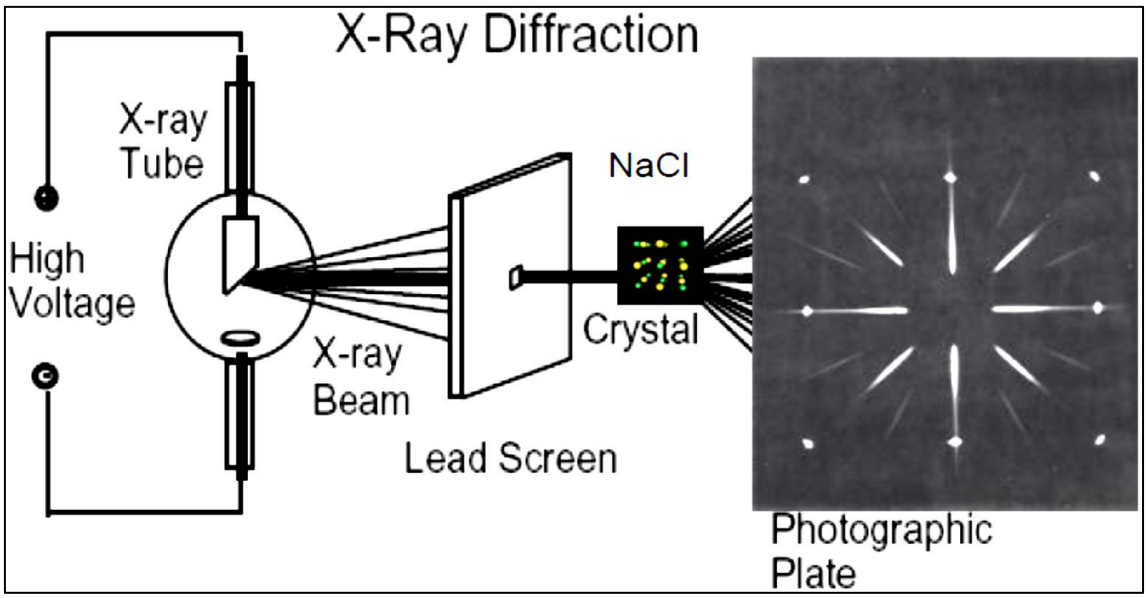

Figure 3.3 A schematic of how XRD works. This figure was taken and used without any modification from reference [132]

X-rays are produced by X-rays tube from where high energy electrons are targeted at a metal target. X-ray produced on screen are destructive interference of crystalline sample and monochromatic X-rays. XRD produced output in such a way that intensity is at y-axis while 2θ is at x-axis. θ is the incident angle of X-rays on sample. Due to presence of varying lattice spacing Figure 3.4 in material, phase shift in rays occur and particular peaks forms. It can be understand using Bragg's law;

$$2d \sin\theta = n\lambda \qquad (3.1)$$

Where;

d= is the interlayer distance

λ= is the wavelength

n= is total number of layer under observation

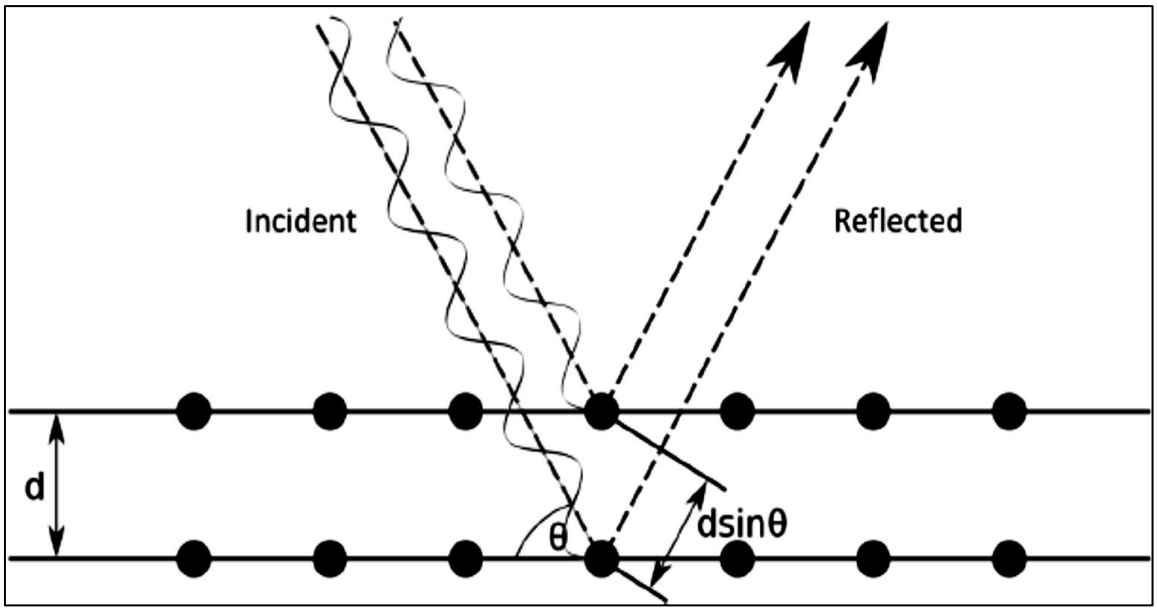

Figure 3.4 A view of X-ray incident and diffraction through a material of spacing (d). This figure was taken and used without any modification from reference [133]

Siemens D5000 Powder XRD (Co Kα 1.79 Å) was used to collect the XRD data. Data for ZIF samples was collected from 5 to 29 2θ degrees. For pyrolyzed ZIF samples, data was collected from 20 to 70 2θ degrees. This data was collected. Data for ZIF samples was collected from 5 to 29 2θ degrees. For pyrolyzed ZIF samples, data was collected from 20 to 70 2θ degrees.

3.1.4 Transmission Electron Microscopy (TEM)

In this technique, a beam of high-energy electrons (typically 100 – 400 keV) is collimated by magnetic lenses and allowed to pass through a specimen under high vacuum. Electric field of 2KV can be generated by help of an anode while second anode along with electromagnetic lenses is used to focus electrons beam forming a probe. Aperture draws the electrons as beam is passed through it and to avoid fluctuations, stigmators are used. Deflector coils are placed to send the beam to collector where a special signal is generating relevant to each striking electrons to produce the final image. Secondary electron (SC) mode is used for SEM operation

using both the backscattered and upper electron collector. Mixed collector is utilized to differentiate in different atomic number by introducing contrast.

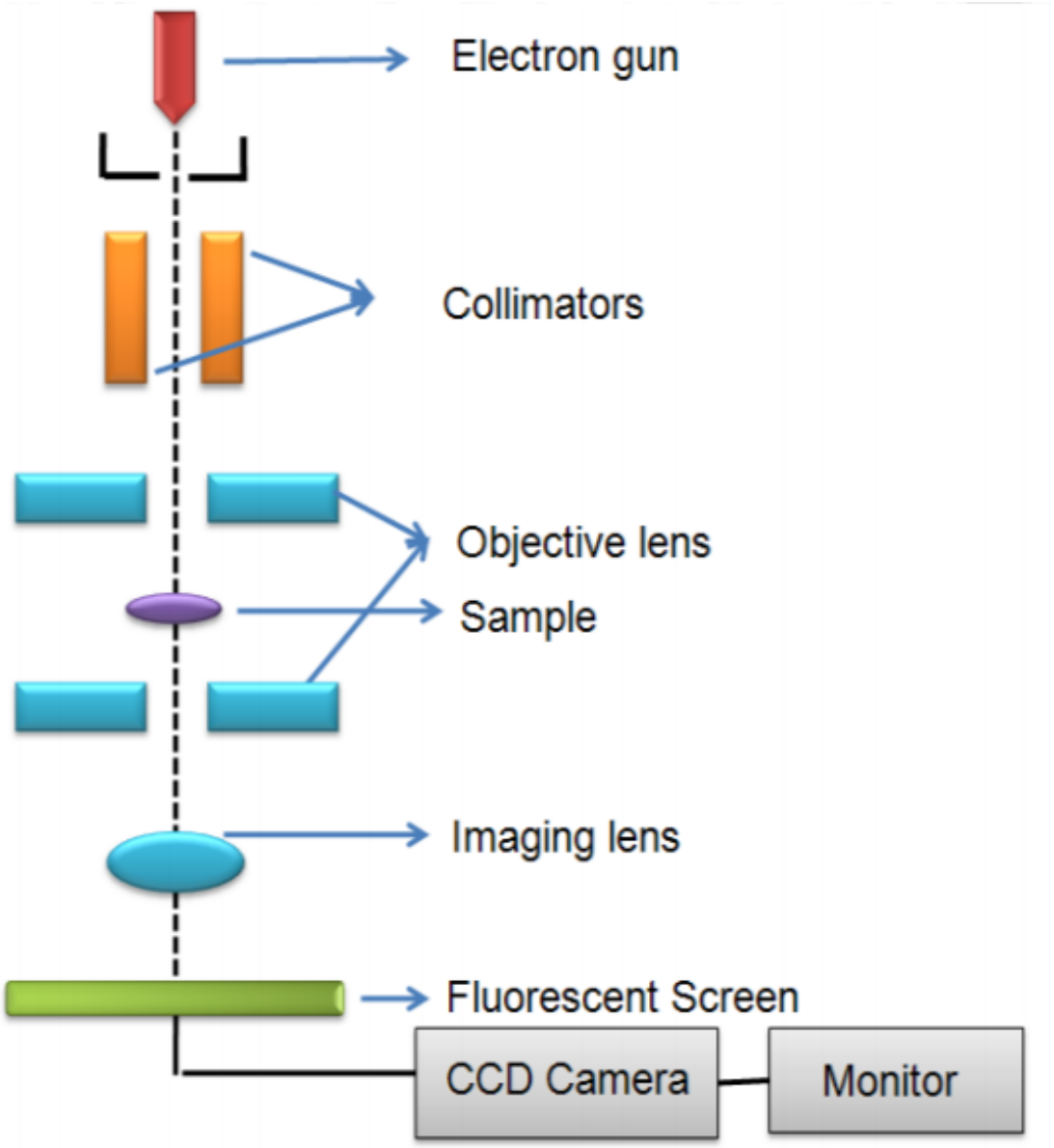

Figure 3.5 Functional diagram of TEM

3.1.5 X-ray photoelectron spectroscopy (XPS)

X-ray photoelectron spectroscopy, also known as electron spectroscopy for chemical analysis (ESCA), is a powerful surface-sensitive technique for the determination of chemical composition of materials. It is achieved by irradiating a sample with X-rays for the excitation of the material and energy analyzing of

emitted photoelectrons. The source used for the soft X-rays are generally MgKα (1253.6 eV) or AlKα (1486.6 eV).

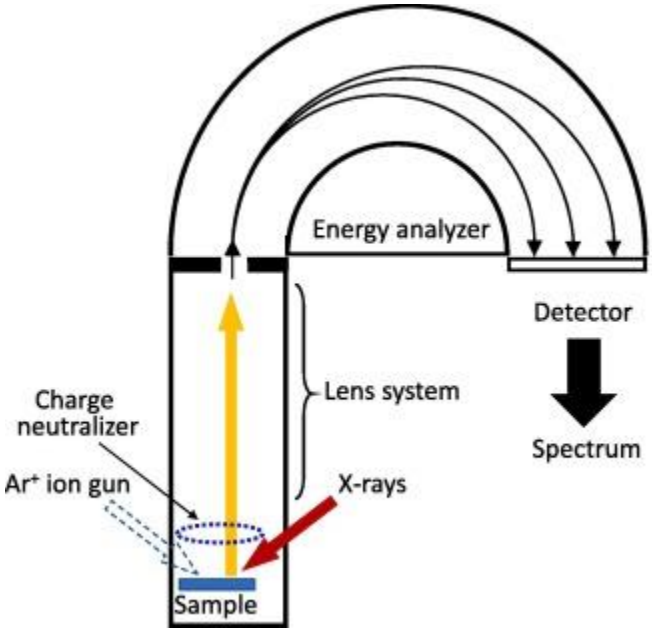

Figure 3. 1 The schematic view of the photoelectron spectrometer with a hemispherical electron energy analyzer. This figure was taken and used without any modification from reference [116].

3.2 Synthesis of ZIF-67

3.2.1 Solution Preparation

Classically, 1.97 g of 2-methylimidazole is dissolved in 20 mL of methanol. 1.746 g of $Co(NO_3)_2$.$6H_2O$ is dissolved in 60 mL of methanol. The above two solutions are then mixed under constant stirring for 30 s, and the final solution is kept for 24 h at room temperature.

The precipitates are then washed in methanol many times to remove the unreacted species and impurities from the mixture and vacuum dried at 80 ℃ [114]. The sample was grinded in mortar and pestle to obtain the finely grinded powder which was then dried in vacuum oven for 6 hours for activation by removing any solvent molecules trapped inside the MOF structure. The Co-ZIF is used to see the changes when compare to the NiCo-ZIF.

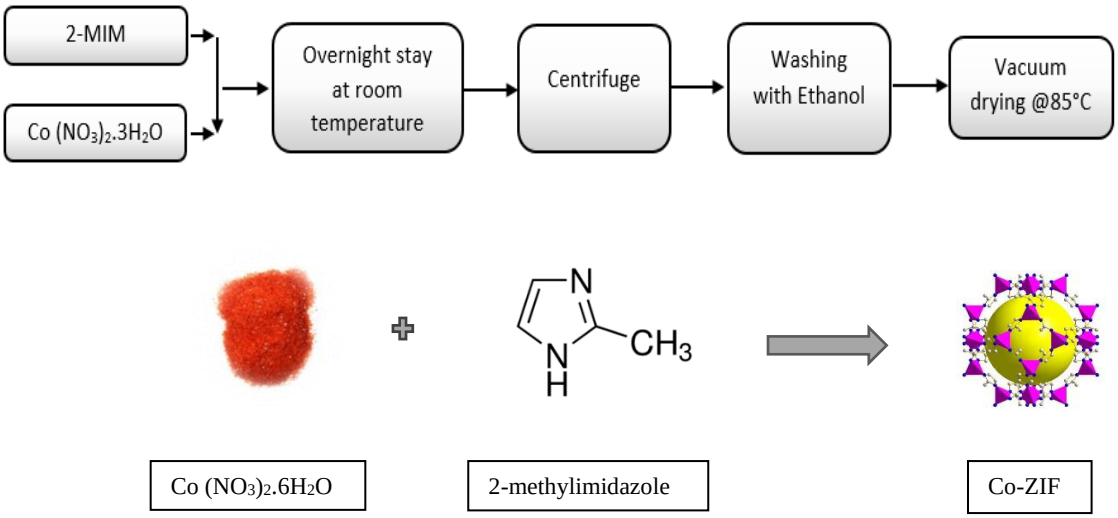

Figure 3.6 Synthesis scheme (our own work) for Co-ZIF

3.3 Synthesis of NiCo-ZIF

3.3.1 Solution preparation for NiCo-ZIF

Classically, weighed amount (1.97 g) of 2-methylimidazole is dissolved in 20 mL of methanol. Equal amount (872 mg) of $Co(NO_3)_2$.$6H_2O$ and 872 mg of $Ni(NO_3)_2$.$6H_2O$ are dissolved in 60 mL of methanol. Then above solutions mixed together with stirring for 30 min at rt for 24 h.

The obtained sample was cleansed with methanol until the clear solution was attained. The obtained material was heated in drying oven at 85 °C for 7 hours until the material was dried. The sample was grinded in mortar and pestle to obtain the finely grinded purple powder which was then dried in vacuum oven for 6 hours for activation by removing any solvent molecules trapped inside the MOF structure.

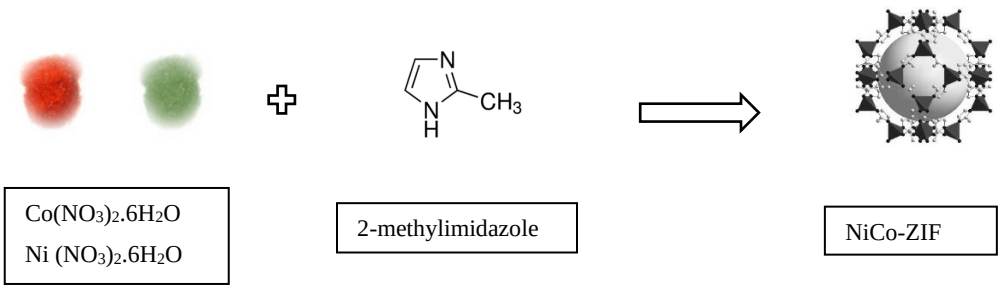

Figure 3.7 Synthesis scheme (our own work) for NiCo-ZIF.

3.3.2 Synthesis of PtNiCo/NC

The bimetallic ZIF sample is then mixed in chloroplatinic acid solution (5 wt. %) and dried at 80 ℃ for 3 hr. Afterwards powder is dispersed in a ceramic boat, heated to 350 ℃ and kept for 1.5 h in a tube furnace. The temperature in the furnace is further raised to 700 ℃ at a ramp rate of 2 ℃. min^{-1} and kept at that temperature for 3.5 h. The as-prepared black powder products are treated in 0.5M H_2SO_4 solution, stirred for 1 min and then allowed to sit for 6 h at 80 ℃. The resulting samples are collected by centrifugation, repeatedly washed with DI water, then dried at 80 ℃. The obtained sample was cleansed with methanol until the clear solution was attained. The obtained material was heated in drying oven at 85 °C for 7 hours until the material was dried. The sample was grinded in mortar and pestle to obtain the finely grinded purple powder which was then dried in vacuum oven for 6 hours for activation by removing any solvent molecules trapped inside the MOF structure.

3.3.3 Synthesis of NiCo NCNTs

The prepared samples were pyrolysed in tube furnace with a ramp rate of 10 °C per min from 50 °C to 350 °C, the sample was heated for 1.5 hr. and then it was pyrolysed from 350 °C to 700 °C with an increase of 2 °C per min. The sample was pyrolysed at 700 °C for 3.5 hr. under H_2/Ar atmosphere. After the process, the furnace was cooled down to room temperature with continuous flow of Ar to avoid any oxidation of the catalysts. The prepared samples were washed with 0.5M H_2SO_4

for removing the unreacted metal and other impurities to avoid the blockage of the active metal sites. After acid leeching, the sample was washed with plenty of water to normalize the pH of the sample. The obtained sample was dried and activated in vacuum oven at 90 °C for 6 hours.

3.3.4 Synthesis of Ni-MOF

Ni-MOF was synthesized according to the published literature. In 100 mL of DMF, terephthalic acid (0.41g) was dissolved by stirring. Then, few drops of triethyl amine were added in the solution. Nickel nitrate hexahydrate (0.61g) was added in the solution. The solution was stirred for 30 min. The prepared solution was poured into autoclave (Teflon lined) and heated at 120 ^{o}C for 24 hours in oven. The crystals of Ni-MOF were collected through filtration, repeatedly washed with DMF to washout extra organic materials followed by drying in vacuum oven at 80 ℃.

3.3.5 Synthesis of activated carbon

Activated carbon was prepared from the following procedure. Leaves of Lantana plant was collected from a nursery and washed thoroughly to remove all impurities. After proper drying, leaves were grinded to reduce its size until it can pass through mesh size of 200 micron. Then, powder sample was dispersed in a solution of diluted Phosphoric Acid (H_3PO_4) for 16 hours. It was then calcined at a temperature of 550 ˚C to activate it. Acid wash/neutralization was done with distilled water to remove any unreacted acid and neutralize the pH of solution up to 6-7. Resulting AC was then dried and collected for further use.

3.3.6 Synthesis of Ni-MOF @ AC composites

In 100 mL of DMF, terephthalic acid (0.41g) was dissolved by stirring. Then, few drops of triethyl amine were added in the solution. Nickel nitrate hexahydrate (0.61g) was added in the solution. The solution was stirred for 30 min. Activated carbon (2-10 wt%) was added into the solution and stirred for 2 hrs. The prepared solution was poured into autoclave (Teflon lined) and heated at 120 ^{o}C for 24 hrs in oven. The crystals of Ni/Co-MOF were collected through filtration, repeatedly washed with DMF to washout extra organic materials followed by drying in vacuum oven at 80 ℃.

3.4 Electrochemical Setup

The electrochemical setup was used for the stability and activity of the composites. For the reason, cyclic voltammetry (CV), linear sweep voltammetry (LSV), Electrochemical Impedance spectroscopy (EIS), Tafel plot, Chronoamperometry were used. 0.1M $HClO_4$ solution was prepared as supporting electrolyte for the testing. The ORR was performed in a three-electrode system comprising of glassy carbon electrode (GCE) as working electrode, Platinum coil as counter electrode and Ag/AgCl was used as reference electrode.

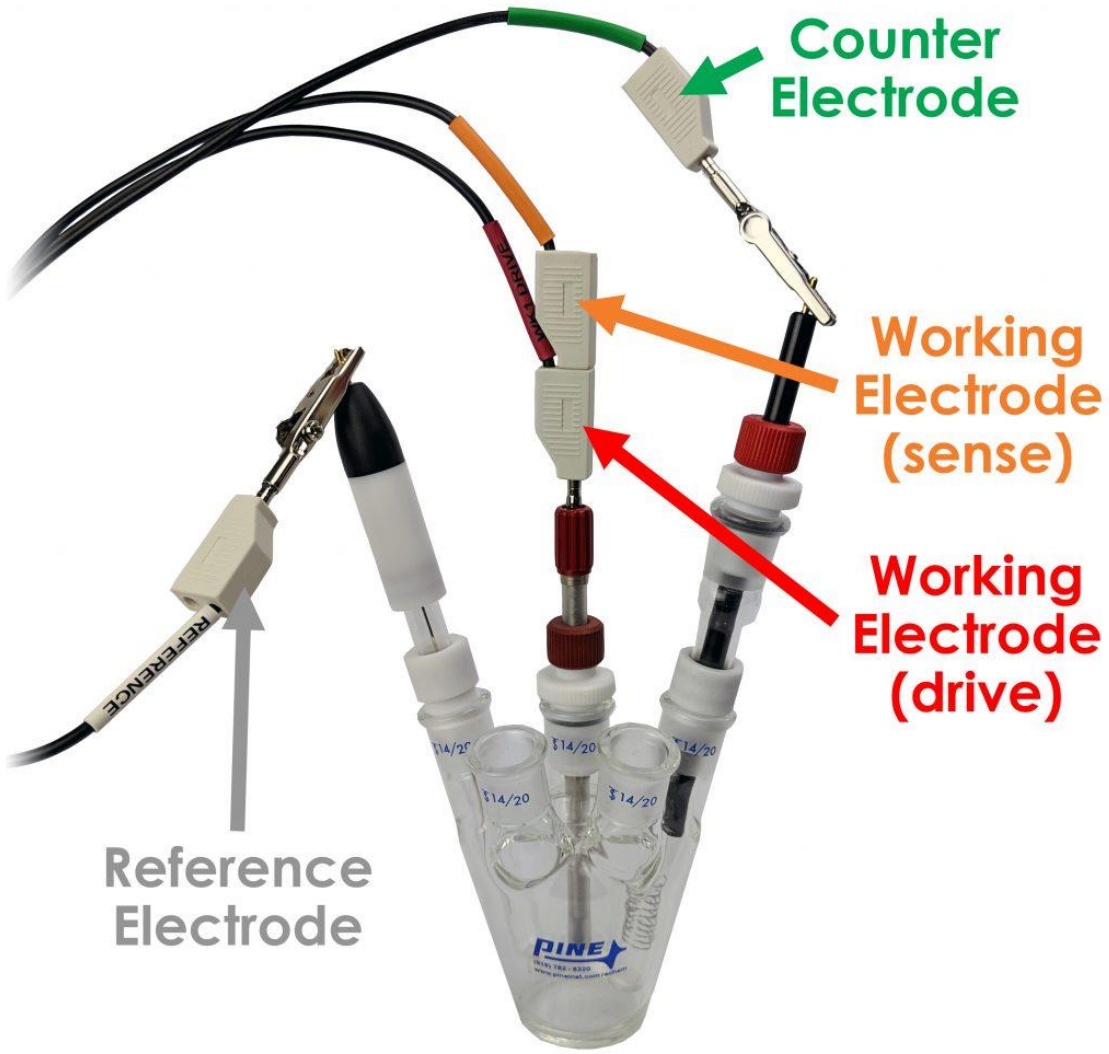

Figure 3.8 Three Electrode System

The testing was first done with the calibration of the setup following with the testing of the bare GCE electrode (without deposition of material) and afterwards, with the deposited material layers on the electrode.

3.4.1 Electrode fabrication for Electrochemical Evaluation in Acidic Medium

The ORR activity was measured by rotating disk electrode (RDE) with the PtNiCo/N-doped carbon (NC) and NiCo/NC materials electrodes. For comparison, commercial Pt/C (46.1 wt% from Tanaka Kikinzoku Kogyo, TEC10E50E) was also employed. The working electrodes were made by dropping required volume of catalyst inks on a glassy carbon working electrode (5 mm in diameter from Pine Research AFE5T050GC). The catalyst ink was made by dispersing 5 mg of carbon

catalysts in prepared solution. The solution contains 7.6 mL DI water, 2.4 mL IPA and 0.1 mL of a 5 wt. % Nafion (Ion power LQ-1105 - 1100 EW at 5% weight) solution. Approximately 25 μg_{Pt} cm^{-2} is applied when the sample contains Pt then dried in hot air with at 700 rpm to obtain a uniform thin film. For non-Pt catalysts, a 700-µg cm^{-2} were applied. The electrochemical performance was conducted in 0.1M $HClO_4$ solution with saturation of N_2 and O_2. The Pt wire as the counter electrode and the saturated calomel electrode (SCE) as reference electrode.

3.4.2 Electrochemical Evaluation on Rotating Disk Electrode in Acidic Medium

The scan rate for ORR activity was 20 mVs^{-1}. The ORR polarization curves were collected at 400, 800, 1200 and 1600 rpm. Long-term operation stability of PtNiCo/NC and commercial Pt/C catalyst was carried out at ambient conditions in 0.1M $HClO_4$ saturated with oxygen, by giving cyclic potential sweeps between 0.5 and 1.1V against reversible hydrogen electrode (RHE) at 200 mVs^{-1} for 5000 cycles.

3.4.3 Electrode fabrication for Electrochemical Evaluation in Alkaline Medium

Catalyst ink of NiCo/NCNTs was prepared by dispersing 2 mg of NCNTs in iso propanol (IPA), deionized (DI) water and nafion (1:3:0.016) Nafion (5 wt% Nafion in alcohol and water, 1100 EW, Sigma-Aldrich). The dispersion was sonicated for 30 min to obtain a uniform ink. A certain volume of ink was placed on the polished glassy carbon disk (GC) (5 mm, Pine Research AFE5T050GC) to obtain a thin film. It was then allowed to dry at 700 rpm for 15 min at 50 ^oC. For comparison, working electrode with commercial Pt/C (Tanaka TKK, Japan, TEC10E50E, 46.1 wt. % Pt) was also prepared. The loading of catalyst (NiCo/NCNTs) and Pt on working electrodes (Pt/C commercial catalyst) were ~0.2 mg/cm^2 and ~25 $\mu g_{Pt}/cm^2$, respectively.

3.4.4 Electrochemical Evaluation on Rotating Disk Electrode in Alkaline Medium

RDE experiments were conducted in electrolyte solution of 0.1M KOH with both N_2 and O_2 saturation. The values of background current from N_2 saturated solution were subtracted from O_2 saturated. Linear sweep voltammetry (LSV) measurements were performed from 1.0 to 0.0 V vs RHE at 20 $mV.s^{-1}$. Pt was used a counter electrode

and reference electrode of saturated calomel electrode (SCE) was used. PAR Bistat at different rpm, at ambient temperature was used for LSV measurements. For the evaluation of the stability of the catalyst films, LSV was performed between 0.1 and 1.1 V vs RHE with 1600 rpm in O_2 saturated 0.1 M KOH solution for 5000 cycles.

3.5 Fuel Cell Testing

3.5.1 Catalyst Coated Membranes for PEMFC Testing

The cathode and anode catalyst layers were directly coated on the Nafion 212 membrane with micro-spray method. Catalyst ink was prepared by dispersing in 5 wt. % Nafion dispersion and IPA. The Pt loadings on the anode (commercial Pt/C) and cathode sides are 0.12 and 0.12 $mg_{Pt}cm^{-2}$, respectively. Same amount of Pt loading was applied for the cathode for reference MEA with commercial Pt/C. For the non-Pt cathode, the I:C ratio was ~1:2 and the loading was ~ 3.5 mg. cm^{-2}.

3.5.2 Gas diffusion layer for PEMFC Testing

For the fabrication of GDL, graphitized non-woven carbon paper was used as a substrate. In 6.5 mL of DI water containing 120 mg of sodium dodecyl sulfate (SDS), 0.5 g of carbon powder (75 wt% Pure black carbon powder and 25 wt% VGCF) was first sonicated for 30 min and followed by stirring at 60 rpm for 60 min. Under gentle stirring, Teflon (30 wt%, Fuel Cell Earth) dispersion was added into the mixture. By using Easycoater equipment (EC26, Coatema) at 3 m min^{-1} speed, carbon slurry is coated on the non-woven carbon paper substrate (10 cm x 10 cm). They were desiccated at room temperature for 12 hours and then sintered at 350 ^oC for 30 min in air then immersed in DI water for 30 min to wash off SDS. The calculated carbon loading was ~3 mg cm^{-2} [117].

3.5.3 Membrane Electrode Assembly Fabrication for PEMFC Testing

Single fuel cell was made by stacking all the components with an active area of 5 cm^2. The single cell was evaluated on a fuel cell test station (G40 Test Station, Hydrogenics, Canada) at 75^oC with fully humidified gases. A flow of 0.2 and 0.3 normal liter per min were applied for anode and cathode, respectively. The stability test was similar to the activation process, except after reaching 0.2 V, the polarization

curve was collected. The program was cycled until it reached 100 h and the peak power densities were selected for plotting.

3.5.4 Catalyst Coated Membranes for AFC Testing

For AFC testing, the 5.0 cm^2 catalyst coated membranes (CCMs) were prepared according to the following procedure. The catalyst inks were made by adding 100 mg of commercial 46 wt% Pt/C (Tanaka TKK, Japan) or NiCo/NCNTs into a combination of 3 mL MeOH and 2.11 mL THF, trailed by addition of 0.16 mL Fumion FAA-3-10 solution (Br form). The mixture was sonicated 3 times for 10 min and strong agitation to get homogeneous ink. The catalyst coated membranes (CCMs) were prepared by spraying 0.12 mg_{Pt} cm^{-2} commercial Pt/C on the anode side and 4 mg cm^{-2} NiCo/NCNTs on the cathode side of the FAA-3-50 membrane (Br form, 50 mm, Fumatech), and dried in the hot air (~50 ^oC). The CCMs were kept at ambient temperature for membranes to regain moisture. The Pt and NiCo/NCNTs loadings were calculated by weight gain after spray coating. Membrane and ionomer were activated by dipping the prepared CCMs in 1 M KOH solution overnight at ambient temperature to substitute the Br^- counter ions with OH^- ions. After the activation of CCMs in KOH, they were washed with deionized water several times till the pH was ~7. For reference, a CCM with Pt/C as cathode and anode was also made [118]. The Pt loading on the anode was 0.2 $mg.cm^{-2}$ while on the cathode was 0.12 $mg.cm^{-2}$.

3.5.5 Gas diffusion layer for AFC Testing

For the fabrication of GDL, graphitized non-woven carbon paper was used as a substrate. In 6.5 mL of DI water containing 120 mg of sodium dodecyl sulfate (SDS), 0.5 g of carbon powder (containing 75 wt% of pure black carbon with 25 wt% of VGCF) was first sonicated for 30 min and followed by stirring at 60 rpm for 60 min. Under gentle stirring, Teflon (30 wt%, Fuel Cell Earth) dispersion was mixed. By using Easycoater equipment (EC26, Coatema) at 3 m min^{-1} speed, carbon slurry is coated on the non-woven carbon paper substrate (10 cm x 10 cm). They were desiccated at room temperature for 12 hours and then sintered at 350 ^oC for 30 min in air then immersed in DI water for 30 min to wash off SDS. The calculated carbon loading was ~3 mg cm^{-2}. The resultant slurry was coated on the carbon paper substrate

(10 cm x 10 cm) with Easycoater equipment (EC26, Coatema) at a speed of 3m min^{-1}. GDLs were first air dried overnight, sintered at 350 ^{o}C for 30 min and then immersed in deionized water for 30 min to remove SDS. The calculated carbon loading was ~3 mg cm^{-2} [117].

3.5.6 Membrane electrode assembly (MEA) for AFC Testing

The membrane electrode assembly (MEA) was prepared by placing CCM with the gas diffusion layers on both sides. Single stack test cell (Fuel Cell Technologies Inc., USA) was assembled using MEA and silicone coated fabric (Product # CF1007, Saint-Gobain Performance Plastics, USA) gasket. The cell was tightened with equal torque of 2.26 Nm on all of the eight bolts/nuts. Greenlight Test Station (G40 Test Station, Hydrogenics, Canada) was used to measure performance of single cell fuel cell at different temperatures with H_2/O_2 gases. The flow rates for anode and cathode were maintained at 0.2 and 0.3 normal liters per minute at ambient pressure, respectively. The relative humidity of the reactant gasses (H_2/O_2) was kept at 100%. The activation of MEA was performed by voltage was stepped down from initial voltage of 0.5 V to 0.2V with a rate of 20 mV per step per minute and stepped back up to initial voltage. Data was collected by galvanostatic polarization method until the progressive performance loss was seen [119].

4. Chapter 4 Results and Discussion

This chapter includes the characterization and electrochemical testing of prepared catalysts for PEMFC and AFC.

4.1 Electro-catalyst for Proton exchange membrane fuel cell (PEMFC)

The catalyst for PEMFC was prepared and characterized. The electrochemical performance was evaluated.

4.1.1 Crystal Structure and phase purity

Figure 4.1a displays the simulated Co-ZIF, as synthesized Co-ZIF and the bimetallic ZIF. The diffraction peaks of simulated pattern are matching with the peaks of the prepared Co-ZIF pattern, indicative of the well preparation of Co-ZIF. With the addition of Ni for the synthesis of bimetallic ZIF, the diffraction peaks remain identical except for the slight shift in all peaks towards the higher 2θ angle. The slight shift explains that nickel has replaced few Co ions in the imidazole framework resulting in reduced d-spacing thus shifting to the high 2θ angle. The diffraction angle of pure Ni metal (111) plane 51.8 is higher than the diffraction angle of pure Ni metal (111) plane 51.9. Figure 4.1b shows the XRD of NiCo/NC and PtNiCo/NC. All prepared catalysts have distinct graphite (002) peaks at ~30.7 2θ degrees. On the other hand, the prepared catalyst with Pt doping has sharp and narrow diffraction peaks indicating that carbon is more crystalline compared to the catalyst without Pt. The NiCo/NC contain a broad peak at ~ 52 2θ degrees due to the Co (111) at 51.8 (PDF#15-0806) and Ni (111) at 51.9 (PDF#65-0380). The alloy has been established for PtNiCo/NC by the broad

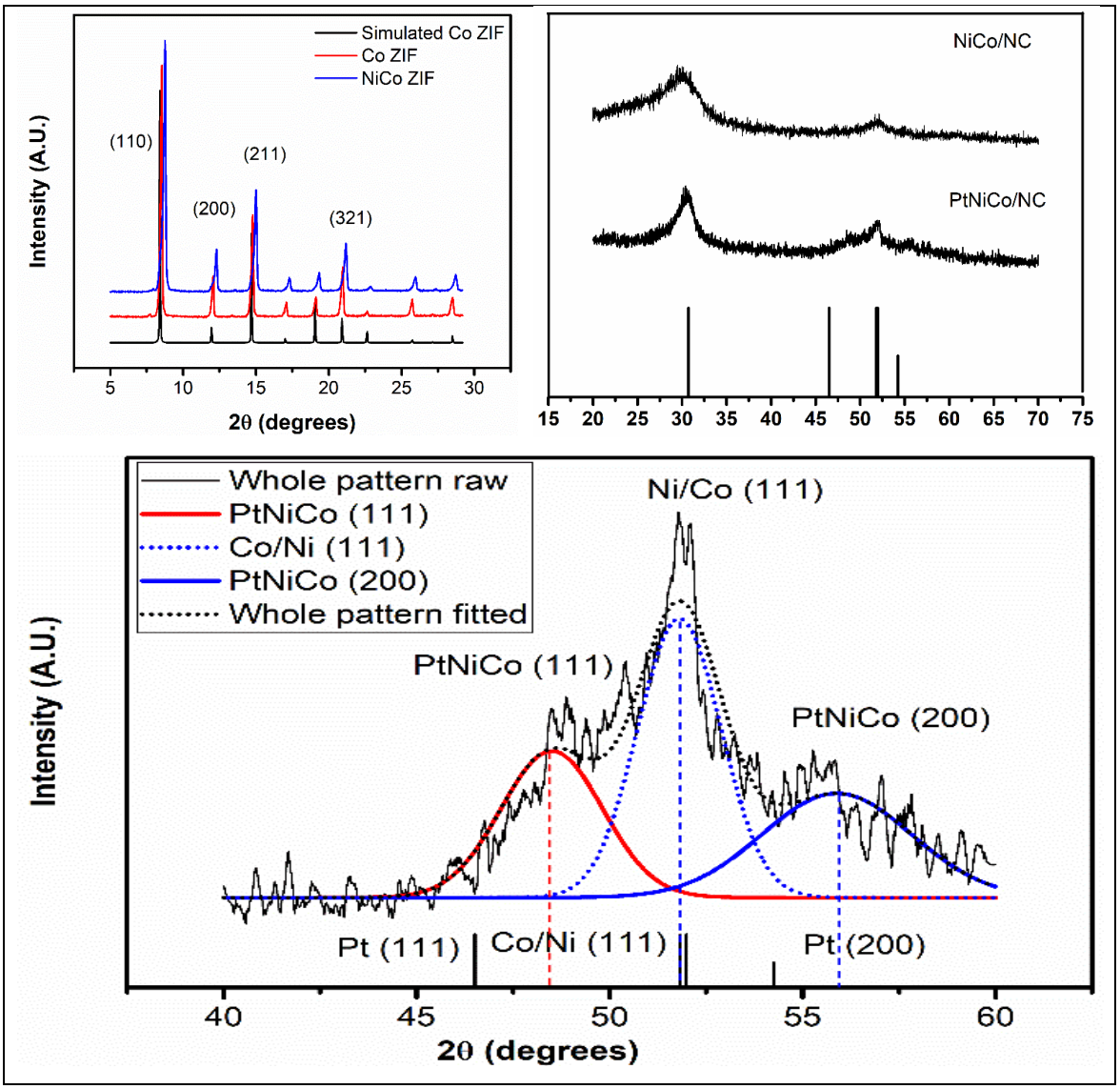

Figure 4.1 (a)XRD pattern of Co ZIF and NiCo ZIF with simulated pattern of Co ZIF (b) NiCo/NC and PtNiCo/NC, and (c) Pt, Ni, Co (111) regions with high resolution

diffraction peaks are shifting away from the Pt (111) at 46.5 (PDF#65-2868) 2θ degrees. Figure 4.1c is showing the magnifying diffraction pattern of PtNiCo/NC for PtNiCo (111), Ni/Co (111) and PtNiCo (200) at 48.4, 51.8 and 55.9, correspondingly. The $Pt_{2.45}$(Ni/Co) is assessed to be the formula of alloy. In PtNiCo/NC, there are also some (Ni/Co) particles which are unalloyed due to the Ni/Co (111) diffraction. The size of crystallite is estimated from the full width half maximum (FWHM) from the deconvolution of peaks. The size of PtNiCo and Ni/Co are estimated to be 3.1 and 3.5 nm. The diffraction peaks position, lattice

spacing, Pt:(Ni/Co) ratio and FWHM analysis of PtNiCo/NC is summarized in Table 4.1.

Table 4.1 The diffraction peaks position, lattice spacing, Pt:(Ni/Co) ratio and FWHM analysis of of Pt, Co, Ni, PtCo and PtNiCo

	Pt (111) PDF#65-2868	Co (111)/Ni (111) PDF#15-0806/ PDF#65-0380	PtNiCo (111)	Ni/Co (111)
Diffraction Angle (2θ degrees)	46.5	51.8/51.9	48.4	51.8
Lattice spacing (A)	2.27	2.05/2.04	2.18	2.05

4.1.2 Microporous structures and elemental analysis

The Figure 4.2a, b show SEM images of Co-ZIF and NiCo-ZIF. The size of NiCo-ZIF particles (~0.5 μm) is smaller than Co-ZIF particles (~2 μm). The Co-ZIF shows hexagonal based polyhedron while the NiCo-ZIF shows a cubic polyhedron. The difference after adding Ni precursor not only modified the shape of ZIF but also reduced the particle size during the solvothermal synthesis. After heat treatment of NiCo-ZIF and acid washing, the hollow structures is covered with

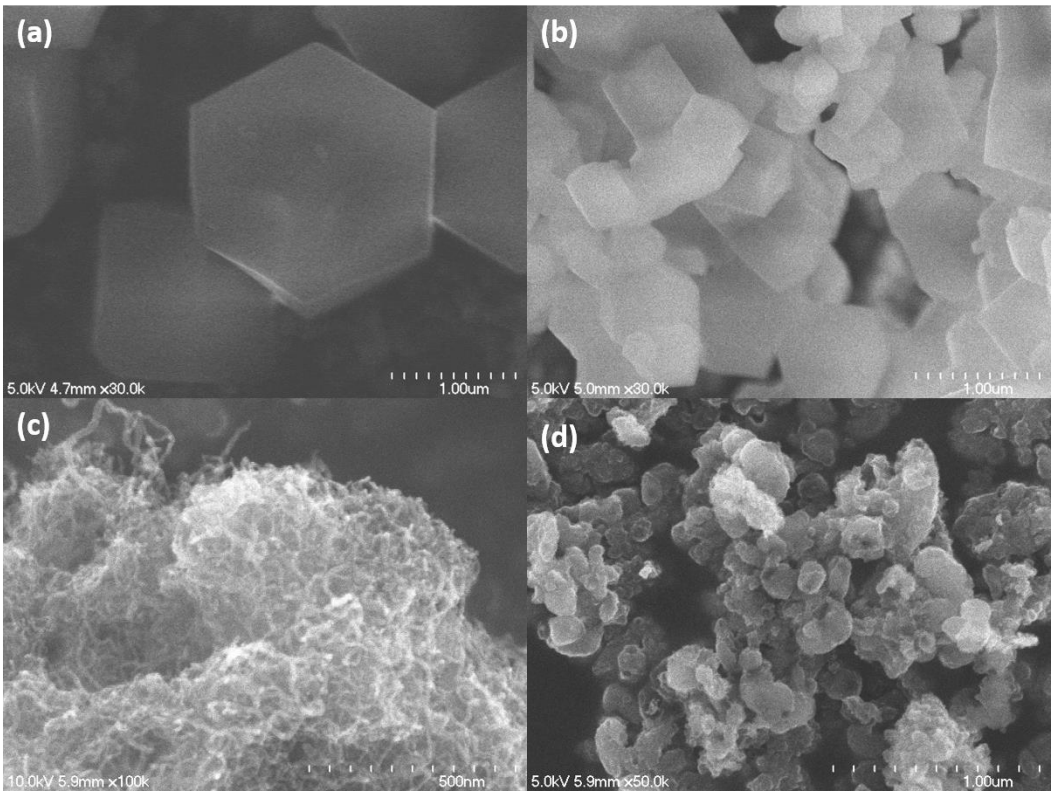

Figure 4.2 FESEM of (a) Co ZIF (ZIF-67) , (b) NiCo-ZIF crystals, (c) NiCo/NC, (d) PtNiCo/NC

interconnected carbon nanotubes (CNTs) showing in Figure 4.2c. Same observations are reported in reference [114], [120], [121]. Under Ar/H_2 environment, the Co/Ni ion are reduced by the hydrogen gas at high temperature, the Co/Ni metal will act as seed widely spread out in the carbon rich ZIF. In the meantime, the ZIF starts to decompose, evaporate the unstable organic groups, left mostly carbon in the sample. The heated carbon atoms start to move around under temperature, they are favorable to dissolve into heated seeds. When the seeds get saturated with carbon atoms, the bottom-up growing starts to begin [122]. The XRD showed broader peak for graphite (002) plane compared to the sample with Pt, this can conclude the CNTs only limited on the surface, the majority carbon is present as amorphous carbon inside the decomposed ZIF. Interestingly, no CNTs can be seen on the surface of the Pt loaded ZIF particles after the thermal treatment. The surface of the particles gets rougher and forms nano-porous carbon and the size is also shrunk under pyrolysis (Figure 4.2d). The possible reason for no CNTs is due

to the presence of Pt precursor, the reduced Pt atoms tends forming alloy with Ni/Co. The XRD showed more Pt compare to the Ni/Co, so the Ni/Co was buried into Pt then inhibited the forming of CNTs.

The HAADF image is showing in Figure 4.3a, the blueness is due to the thickness of the NiCo-ZIF. In the selected area in the green box, the EDS signal was collected. The element mapping is showing in the Figure 4.3b. C, N, Co and Ni are well dispersed into the ZIF material and the Ni mapping is relatively sparse in the structure. The well dispersed metal/metal alloy supported by the amorphous carbon with particle size ~2-3 nm can be viewed in the Figure 4.3c. The study shows that the Pt particle at around 2.2 nm is supposed to have the highest PEMFC activity [123]. The lattice spacing can be seen in Figure 4.3d at 0.21 nm attribute to Pt/Ni or Co alloy (111) plane. From the Table 4.1, the d-spacing of Pt and Ni/Co (111) plane are 0.227 and 0.204/0.205 nm, respectively. The contracting Pt (111) plane is also an indication for the formation of the alloy. Also, single atoms can be seen nearby the big island of atoms. The single atoms can be highly efficient for catalyzing reactions, due to (1) surface effects, the percentages of unsaturated bonds increases with particle downsizing and reach the max in single atom; (2) the energy level of single atom will increase due to quantum confinement and widen the Kubo gap and (3) the metal support interactions is stronger [124]. However, under harsh

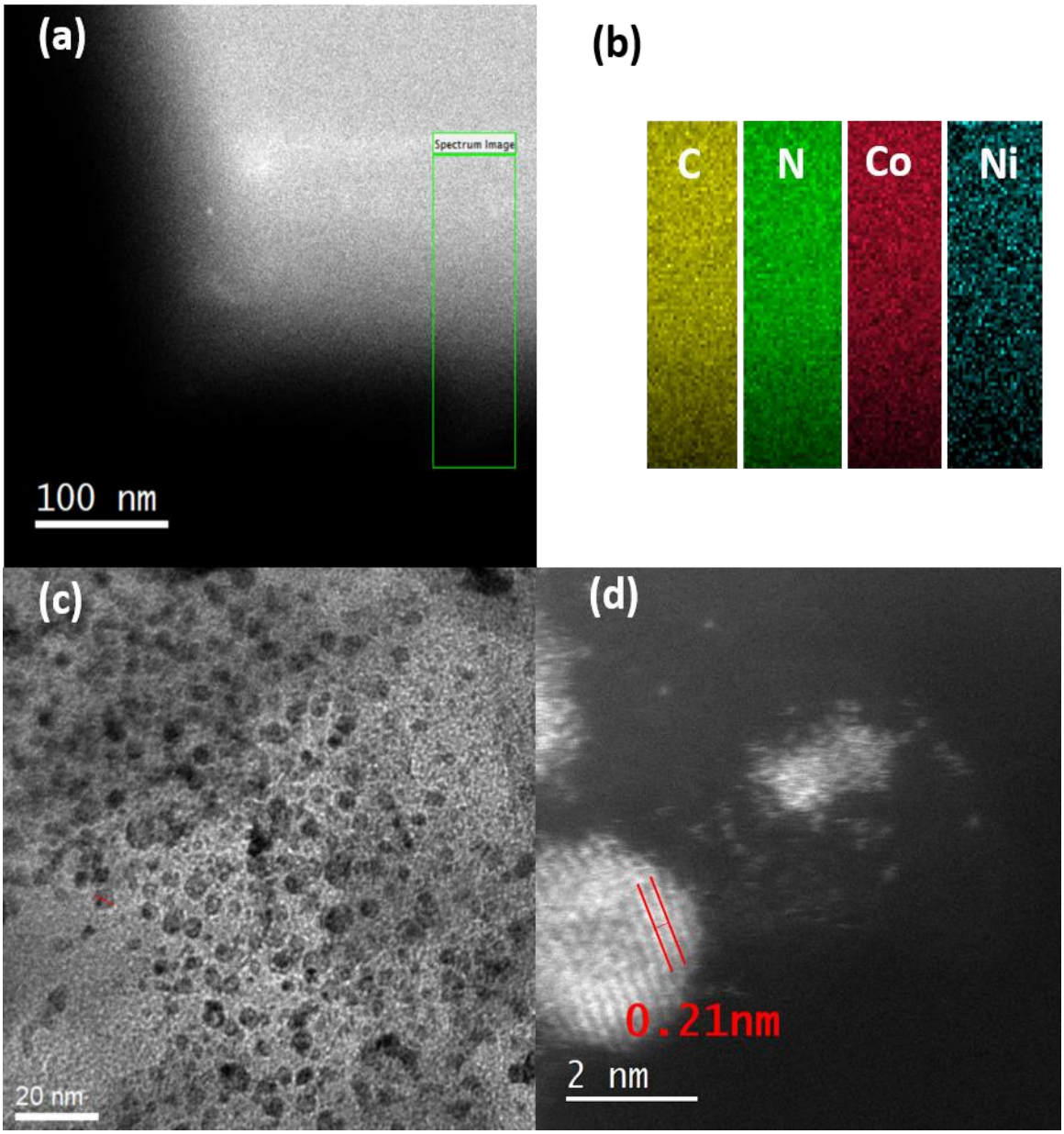

Figure 4.3 (a) The HAADF image of NiCo-ZIF, (b) EDS mapping of NiCo-ZIF (a), TEM (c), (d) STEM image of PtNiCo at different magnification

acidic medium in PEMFC, the lone platinum atoms will need anchorage sites in order to overcome the Ostwald ripening [82].

4.1.3 XPS Analysis

The Figure 4.4 shows the XPS data for PtNiCo/NC. The survey scan is displayed in Figure 4.4 a, from all the XPS peaks, there are 94.42, 0.72, 2.57, 2.11 and 0.18% of C, N, O, Pt and Co, respectively. The XPS didn't resolve Ni signal due to the at. %

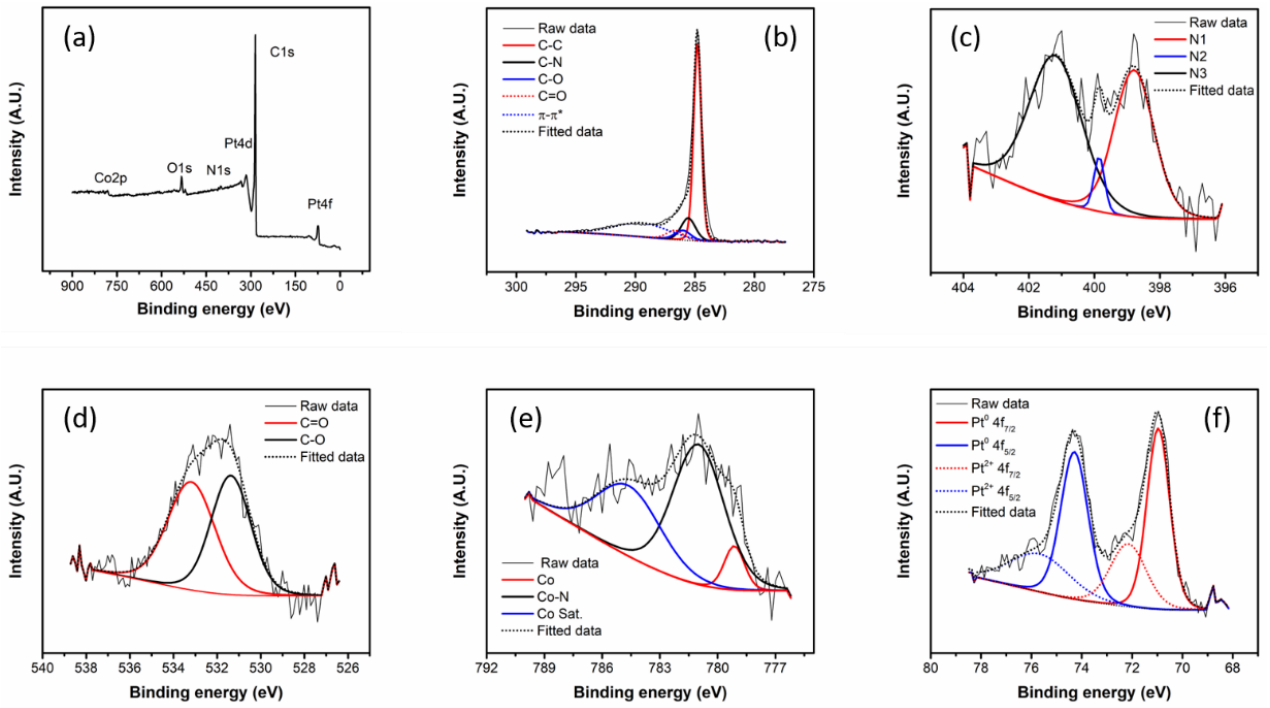

Figure 4.4 (a) XPS spectra of PtNiCo/NC (b)C1s, (c)N1s, (d) O1s, (e) Co2p and (f) Pt4f

of Ni is lesser than the detection range. The high resolution C1s scan is showing in Figure 4.4b for understanding the bonding pattern. Five C bonding, C-C , C-N , C-O , C=O and p-p* are resolved for our prepared catalyst [125], [126]. The N doping was also indicated in Figure 4.4c, N1 stand for pyridinic N (398.7 eV), N2 for-imine/ -amide/ -amine (399.8 eV) and N3 for pyrrolic N (400.3 eV) [127]. From XPS surface quantification analysis the values of atomic% for N1 43.14, N2 4.31 and N3 is 52.55. The presence of N1 and N3 are supposed to enhance the catalytic activity ORR [128], [129]. The form of N will determine the oxidation state of transition metal as well as platinum group metal [130]. O=C and O-C are deconvoluted in O1s XPS in Figure 4.4d, the small amount of oxygen content is due to oxidation during the pyrolysis. The defects rich carbon support is acting as anchor for Pt/Pt alloy particles even single Pt atoms [131], [132]. Figure 4.4e shows

the Co 2p XPS, three peaks are resolved, Co^0(779.1 eV), Co^{2+} (781.6 eV) and Co $2p_{3/2}$ (785.2 eV) shake up satellite peak. The Co^0 can be attributed to the Co and Pt alloy, the ionic Co belongs to Co-N coupling [125]. Co-N-C is also believed to act as an active site to catalyze the ORR in acidic media [133]. High resolution Pt 4f XPS is showing in Figure 4.4f, four distinct peaks are resolved of Pt^0 $4f_{7/2}$ (71.0 eV), Pt^{2+} $4f_{7/2}$ (72.3 eV), Pt^0 $4f_{5/2}$ (74.4 eV), Pt^{2+} $4f_{5/2}$ (75.6 eV) [134]. The ratio of Pt^0 to Pt^{2+} is around 4.17:1. From the XPS data provided in Figure 4.5. As shown in Table 4.2, the Pt^0 is 51 and 64 atomic % for commercial Pt/C and PtNiCo/NC, respectively [135]. Although, the commercial Pt/C depicted the occurence of Pt^{2+} and Pt^{4+}, the PtNiCo/NC catalyst judt displayed Pt^{2+} signals. The presence of Ni and Co decreases the oxophilicity of Pt resulting in increased fuel cell activity [136], [137]. The Table 4.2 also reviews the data from XPS.

Table 4.2 Composition of elements in the PtNiCo/NC

Element	**Total (Atomic %)**	**Atomic % for each component**				
C	94.42	52.2 (C-C)	11.7 (C-N)	5.35 (C-O)	5.2 (C=O)	26.8 (π–π*)
N	0.72	43.14 (N1)	4.31 (N2)	52.55 (N3)		
Pt (PtNiCo/NC)	2.11	32.62 (Pt^0 $4f_{7/2}$)	17.76 (Pt^{2+} $4f_{7/2}$)	31.65 (Pt^0 $4f_{5/2}$)	17.97 (Pt^{2+} $4f_{5/2}$)	

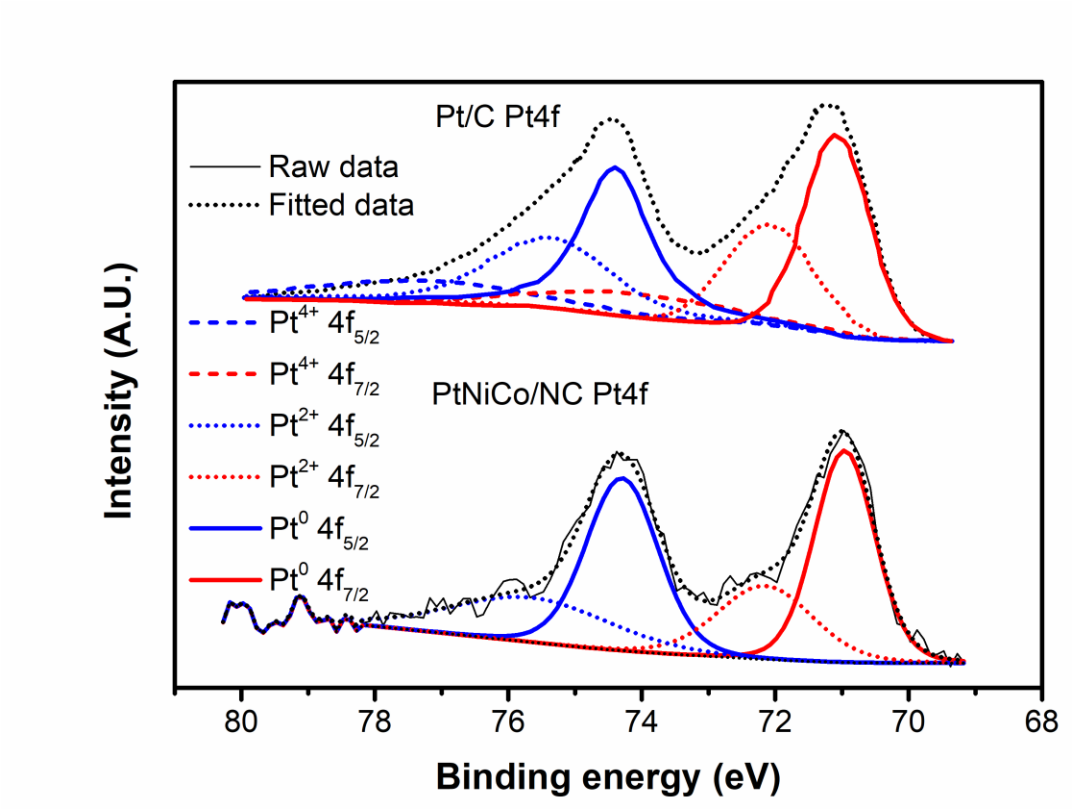

Figure 4.5 Pt4f XPS comparison of PtNiCo/NC and Pt/C

4.1.4 Electrochemical Characterization

4.1.5 Electrochemical Evaluation on Rotating Disk Electrode

The electrocatalytic activity of the PtNiCo/NC is measured by CV. As depicted in Figure 4.6a when the perchloric acid soln. is bubbled with N_2, no redox peak is seen. On the other hand, when the solution is saturated with O_2, a

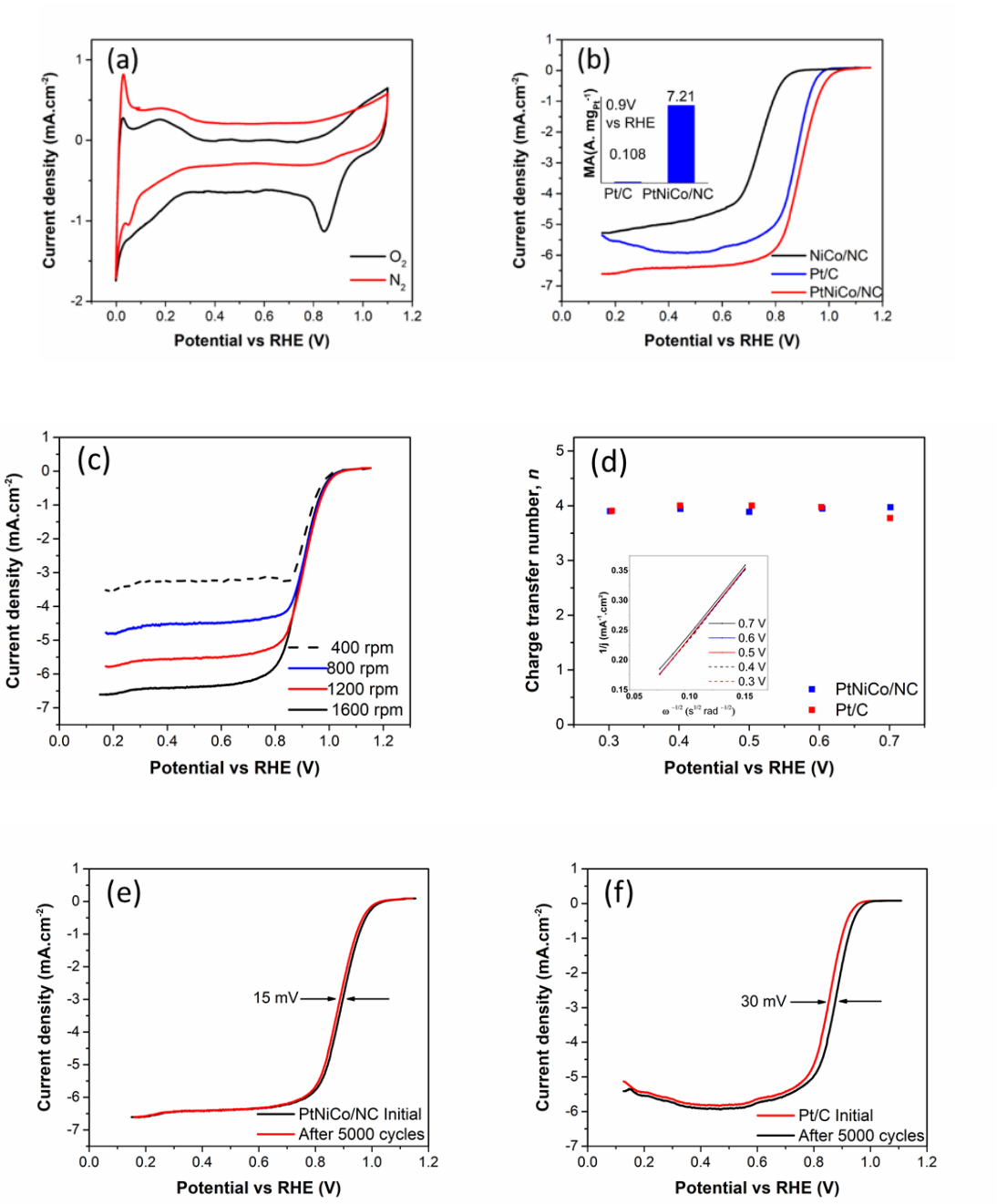

Figure 4.6 Electrochemical oxygen reduction on PtNiCo/NC (a) CV profiles (red and black curves indicate CV curves recorded in N_2 and O_2 saturated 0.1M $HClO_4$ solution, respectively). (b) LSV curves of different samples at O_2-saturated 0.1M $HClO_4$ solution at 1600 rpm. Insert, The comparison of MAs at 0.85 V versus RHE (c) LSV curves at different rotation rates (rpm) for PtNiCo/NC (d) Charge transfer number (n). Insert, K–L plots, ω is the angular rotation speed. (e) Durability Test: ORR polarization curves (1600 rpm) of PtNiCo/NC before and after 5000 cycles. (f) Durability Test: ORR polarization curves (1600 rpm) of Pt/C before and after 5000 cycles.

clear cathodic peak is seen because of oxygen reduction. Linear sweep voltammetry (LSV) at several rpm are then carried out with a rotating disk electrode (RDE) system.. NiCo/NC displays good activity at 1600 rpm as represented by the onset potential value of 0.86 V vs. RHE and current density value of 5.55 mA. cm^{-2}. With the addition of Pt in the catalysts, the ORR performance is further improved. The PtNiCo/NC catalyst exhibited the finest catalytic performance for the ORR by onset potential value at 1600 rpm (Figure 4.6b). At 1600 rpm PtNiCo/NC gives an onset potential value of 1.03 V. While the onset potential of Pt/C is 0.98 V. With the addition of Pt in the catalysts, the ORR performance is further improved. The PtNiCo/NC catalyst exhibited the finest catalytic performance for the ORR by the onset potential value at 1600 rpm (Figure 4.6b). [138] [139] [140] [141] (Figure 4.6c). The Koutecky-Levich equation (K-L equation) was employed to study kinetic parameters.

$$\frac{1}{i} = \frac{1}{ik} + \frac{1}{id} = \frac{1}{nFAkCo} + \frac{1}{B\omega^{\frac{1}{2}}} \qquad \text{(Equation 4.1)}$$

$$B = 0.62nFACoDo^{2/3}V^{-1/6} \qquad \text{(Equation 4.2)}$$

where, i, i_k and i_d and represent measured, kinetic and diffusion-limiting current, respectively.

The fast reaction kinetics is represented by linear K-L plots in dissolved O_2 from 0.7 to 0.3V potential range and the reaction is diffusion controlled [141], [142]. The value of n is between ~3.97-3.98 (Figure 4.6d) [143]. Table 4.3 shows the different parameters of the activity of the prepared catalyst and commercial Pt/C in RDE.

CV test is also carried out for the PtNiCo/NC catalyst to assess the stability of the electrocatalyst in acidic madium. After 5000 CV sets the electrocatalyst shows insignificant loss in activity evaluated by the LSV curve. Figure 4.6e, f. A contrast of Pt catalyst reported by other authors is provided in Table 4.4.

Table 4.3 Performance comparison of different prepared catalyst with commercial Pt/C

Electrocatalysts	**Onset Potential[a]**	**Half wave Potential**	**Loading**	**Limiting current density at 0.1V vs. RHE**

	(V vs RHE)	(V vs. RHE)		$mA.cm^{-2}$
PtC	0.98	0.87	25 $\mu g_{Pt}/cm^2$	5.50
PtNiCo/NC	1.03	0.91	25 $\mu g_{Pt}/cm^2$	6.51

Table 4.4 Performance comparison of different Pt based catalysts for ORR in acidic media (ORR test conditions: 1600 rpm and 0.1M $HClO_4$)

Electrocatalysts	**Onset Potential V vs RHE**	**Halfwave Potential V vs RHE**	**Loading $\mu g_{Pt}/cm^2$**	**Limiting current density at 0.1V vs. RHE $mA.cm^{-2}$**	**Scan rate mV/s**	**Reference**
Pt_1-N/BP	0.94	0.76	24	4.8	5	[139]
Pt/Zr–C 3	0.90	-	40	5.7	10	[144]
$Pt_{0.61}$Ni/C	-	0.85	24	5.2	5	[145]
PtNi@Pt	0.95	-	12	6.0	10	[146]
PtNiCo/NC	1.05	0.91	25	6.5	20	This work

4.1.6 Membrane Electrode Assembly and Fuel Cell Performance Evaluation

4.1.7 PEM Fuel Cell Evaluation

The figure 4.7a displays the PEM fuel cell performance of MEA with PtNiCo/NC as cathode catalyst and commercial Pt/C as anode catalyst with H_2 and O_2 at different temperatures up to 70 ^oC. For the performance comparison commercial Pt/C was also evaluated. The value of open circuit voltages for PtNiCo/NC is 1.1V, comparable to that of commercial Pt/C. The activation losses in the low current density region are lowest at 70 ^oC. In high current density region, MEA with

PtNiCo/NC as cathode showed the best performance. The peak performance is a factor of activation losses and concentration losses. Hence, PtNiCo/NC showed the highest peak power of 740 $mW.cm^{-2}$ at 70 ^{o}C with H_2 and O_2 gases at ambient pressure and 100 % RH. As given in Figure 4.7b, the peak power density is only ~ 630 $mW.cm^{-2}$ for Pt/C and ~ 100 $mW.cm^{-2}$ for NiCo/NC at identical test conditions. The high OCV and peak current density values compared to Pt/C show great potential of PtNiCo/NC catalyst for replacing commercial Pt/C in PEMFC. The comparatively higher PEMFC performance of the PtNiCo/NC electrocatalyst could be attributed mostly to the synergistic effect of nitrogen doped CNTs, Co/Ni active sites dispersed evenly in the NCNTs conducting framework and the Pt alloy. The Pt-NiCo/NC cathode catalyst based MEA assessed for 100 h at 100 % RH using H_2 and O_2 at ambient pressure exhibited exceptional stability. As shown in Figure 4.7c, the peak power density values did not show any loss in performance, signifying that the Pt nanoparticles and its alloy are having a good anchorage on the carbon support.

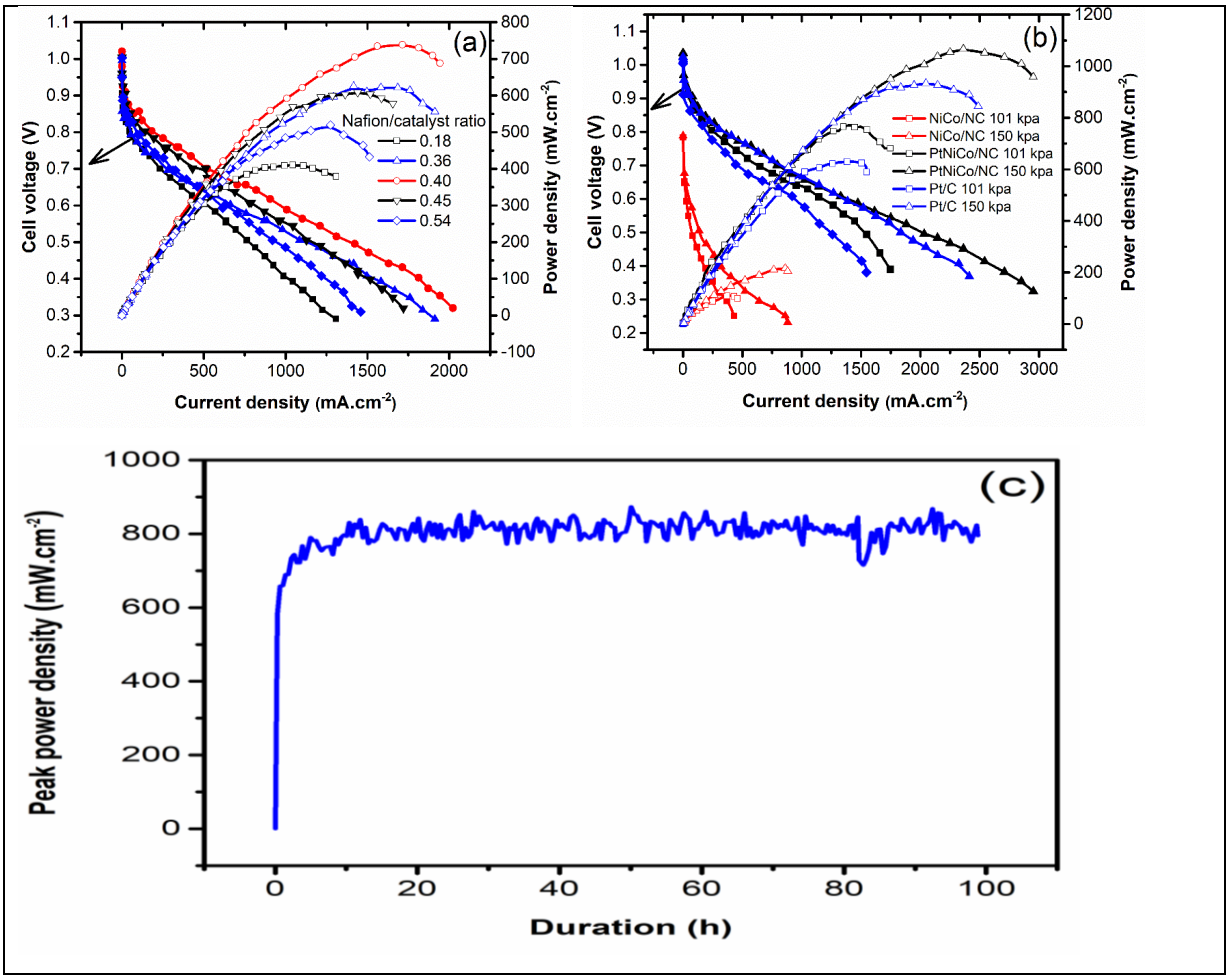

Figure 4.7 The acidic fuel cell activity of (a) effect of Nafion:catalyst ratio on PtNiCo/NC performance, (b) Fuel cell performamnce with PtNiCo/NC, NiCo/NC and Pt/C with and without back pressure, (c) 100 h stability test for PtNiCo/NC catalyst at ambient pressure. (Measurements were taken at 70℃, 100% relative humidity with H_2 and O_2 at 0.2 and 0.3 NLPM with Nafion212 membrane**)**

4.2 Electrocatalyst for alkaline fuel cell (AFC)

4.2.1 Crystal Structure and phase purity

The X-Ray diffraction (XRD) was carried out using Bruker X-ray diffractometer linked with a computer interface having Cu Kα at λ=1.5418 Å. All the samples (ZIF-67, NiCoZIF, NiCo/NCNTs (1:1), NiCo/NCNTs (1:4) and NiCo/NCNTs (4:1)) were placed in X-ray beam of angle 2θ ranging from 5-70° while step size was set as 4°/s. X-ray diffraction (XRD) pattern of the as prepared Co-ZIF matches with the simulated one, indicating successful synthesis of porous crystalline

framework. When NiCo-ZIF (1:1) is prepared by adding Ni precursor, all characteristic peaks of Co-ZIF are retained. This indicates that the structure of the parent ZIF remain intact after metal loading [147]. The diffraction pattern, however, is shifted to the higher 2θ angle. This shifting explains that Ni replaced some of the Co ion in the imidazole framework and shifted to the higher 2θ angle. The diffraction angle of pure Ni metal (111) plane 51.8 is higher than the diffraction angle of pure Ni metal (111) plane 51.9 (figure 4.8a). Figure 4.8b shows the XRD of Co-ZIF and NiCo-ZIFs after the heat treatment. All samples have distinct graphite (002) diffraction peaks at ~26.3 2θ degrees. All samples with different Ni/Co ratios have broad diffraction peaks at ~ 45 2θ degrees indicating the presence of Co-Ni alloy nanoparticles as no single metal peak can be observed from the XRD patterns of alloy catalyst [148][149]. All NiCo/NCNTs have broad peaks at ~ 45 2θ degrees due to the Co (111) and Ni (111) diffraction at 44.2 (PDF#15-0806) and 44.5 (PDF#04-0850) 2θ degrees.

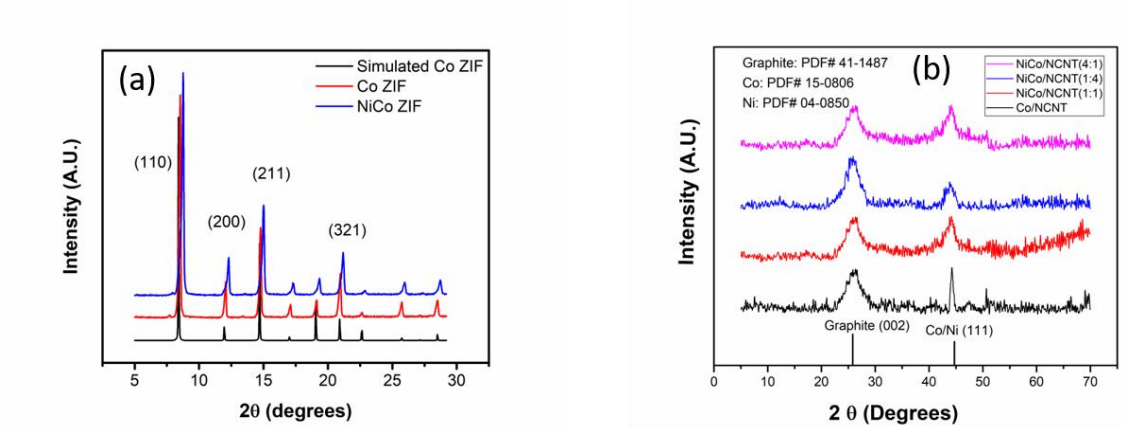

Figure 4.8 XRD pattern of (a) Co ZIF, NiCo ZIF and simulated Co ZIF, (b) Co/NCNT, NiCo/NCNT (1:1), NiCo/NCNT (1:4), and NiCo/NCNT (4:1)

The diffraction peaks position, lattice spacing, (Ni/Co) ratio and FWHM analysis of Ni/Co is summarized in Table 4.5.

Table 4.5 The diffraction peaks position, lattice spacing, (Ni/Co) ratio and FWHM analysis of Ni/Co

	Co (111)/Ni (111)	Ni/Co

	PDF#15-0806/ PDF#04-0850	(111)
Diffraction Angle (2θ degrees)	44.2/44.5	44.2
Lattice spacing (A)	2.05/2.03	2.05
FWHM estimation	-	5.25

4.2.2 Microporous structures and elemental analysis

Figure 4.9a shows SEM image of NiCo-ZIF. There is change in size and shape of ZIF particles with the addition of Ni. The particle size of NiCo-ZIF (**~0.5 µm)**, is smaller than particle size of Co-ZIF (**~2 µm**). The Co-ZIF displays hexagonal polyhedron while the NiCo-ZIF exhibits cubic structure. After heat treatment of ZIFs and subsequent acid washing, the hollow structures are covered with numerous interconnected carbon nanotubes (CNTs) to deliver a conducting catalyst support [114] [120] .

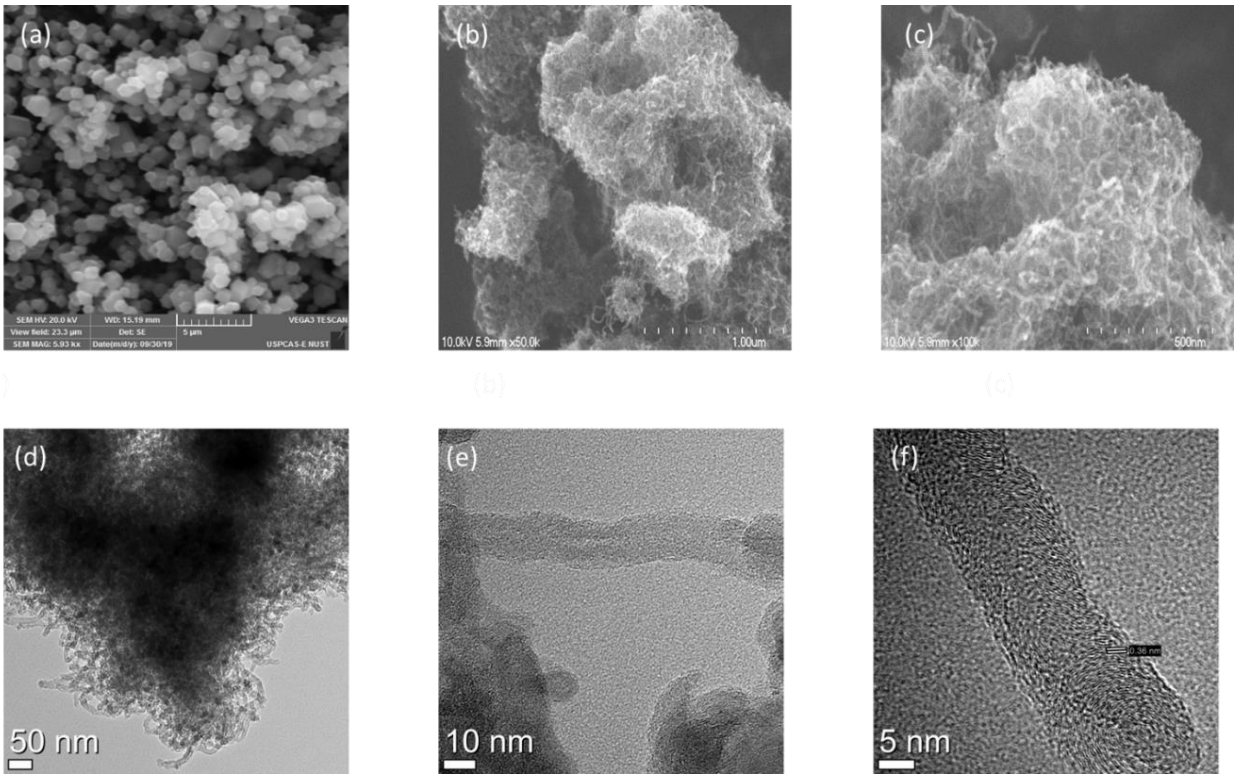

Figure 4.9 Morphology and structural analysis by a-c) FESEM. a) NiCo-ZIF, b,c) NiCo/NCNTs, d-f) HRTEM

The surface of the particles gets rougher and the size is also shrunk after pyrolysis (Figure-4.9c). During the heat treatment under the reducing environment provided by hydrogen, the Co and Ni ions are reduced at inceased temperatures. The reduced Co and Ni metals are distributed in the carbon rich ZIF. After decomposition of ZIF particles at high temperature, unstable organic groups are evaporated and what is left is carbon rich framework [121] [122]. The microstructure is further investigated by HRTEM. Figure 4.9d confirms the presence of CNTs on the surface of hollow carbon shells. The HRTEM images also reveal the Co/Ni nanoparticles encapsulated by the carbon layers. Moreover, it shows that these thick multiwalled CNTs are crystalline and the lattice fringes with an inter-planar distance of 0.36nm correspond to the C (002) plane (Fig. 4.9 e,f).

4.2.3 XPS of NiCo/NCNTs electrocatalyst

The XPS data for NiCo/NCNTs is shown in figure 4.10. The atomic percentage of C, N, O and Co from the survey scan is 91.48, 4.28, 3.45 and 0.8 % (figure 4.10a). The atomic percentage of Ni being less than the detecting limit of XPS was not

obtained [150]. There is some oxygen also which is because of the oxidation. C1s high resolution scan is shown in figure 4.10b. Total five C bondings are resolved [125]. The N doping was also confirmed in Figure 4.10c. Pyridinic N (398.7 ± 0.3 eV) and pyrrolic N (400.3 ± 0.2 eV) are resolved from N1s scan. The nitrogen doping of carbon enhances the catalytic activity towards ORR [129]. Figure 4.10d shows the Co 2p XPS, for which three peaks are resolved, Co^0(779.1 eV), Co^{2+} (781.6 eV) and Co $2p_{1/2}$ (795.2 eV). The Co $2p_{1/2}$ can be attributed to N-coordinated Co2+ (Co−N) [151].

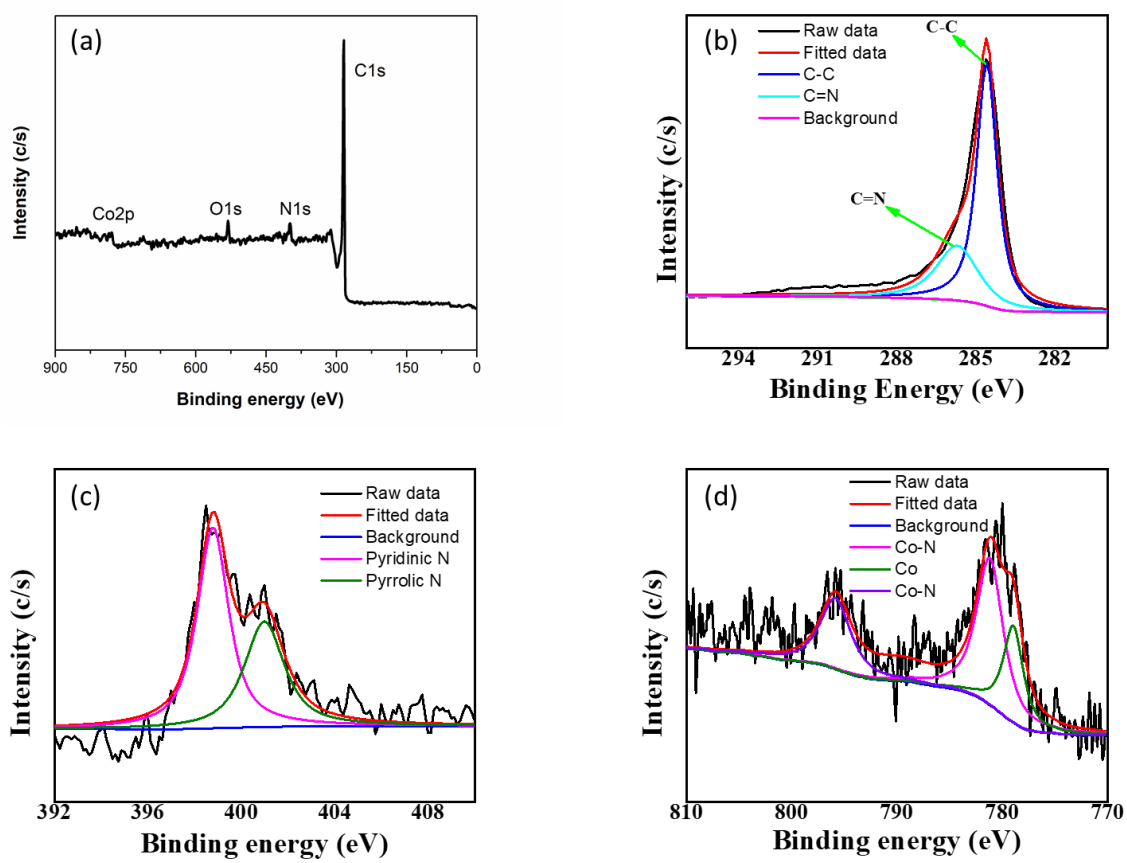

Figure 4.10 (a) The XPS survey scan and the deconvoluted HR XPS scan of (b)C1s, (c)N1s and (d) Co2p

4.2.4 Electrocatalytic performance of NiCo/NCNTs

4.2.5 CV and LSV

The electrocatalytic performance of the as prepared NiCo/NCNTs was studied using RDE in a three-electrode system. Linear sweep voltammetry was carried out to investigate the ORR performance in 0.1M KOH. For comparison, the electrocatalytic performance with LSV of Co/NCNTs and commercial Pt/C were also measured in similar conditions. Figure 4.11a shows the ORR performance of NiCo/NCNTs, Co/NCNTs and Pt/C in O_2 saturated system at 1600 rpm. All values of current density are after subtracting N_2 current. The NiCo/NCNTs (1:1) showed the best performance for ORR with respect to onset potential and current density. At 1600 rpm, it showed limiting current density of -5.6 $mA.cm^{-2}$ and onset potential of 0.98 V vs RHE. However, the commercial Pt/C in O_2 saturated electrolyte system exhibited -5.3 $mA.cm^{-2}$ and onset potential of 0.95 V vs RHE with a Pt loading of 25 $\mu g.cm^{-2}$ under matching conditions. The better activity can be credited to the synergistic effect of Ni-Co active sites and the nitrogen doped CNTs framework. Figure 4.11b displays the LSV data for the NiCo/NCNTs (1:1) in O_2 saturated electrolyte system at different rpm. With the rise in rpm, the limiting current increase. The kinetic parameters are analysed by the Koutecky-Levich (K-L) equation. The linearity of the K-L plots indicates the first-order reaction kinetics regarding the concentration of dissolved oxygen. The K-L plot presented in Figure 4.11c was attained from RDE data at different rpm (400, 800, 1200, 1600 rpm) in O_2 saturated electrolyte. Figure 4.11d shows the calculated electron-transfer numbers (n) derived from the K-L plot at various potentials from 0.3 to 0.7 V vs. RHE.

The kinetic parameters are analysed by the Koutecky-Levich (K-L) equation. The linearity of the K-L plots indicates the first-order reaction kinetics regarding the concentration of dissolved oxygen. The K-L plot presented in Figure 4.11c was attained from RDE data at different rpm (400, 800, 1200, 1600 rpm) in O_2 saturated electrolyte. Figure 4.11d shows the calculated electron-transfer numbers (n) derived from the K-L plot at various potentials from 0.3 to 0.7 V vs. RHE.

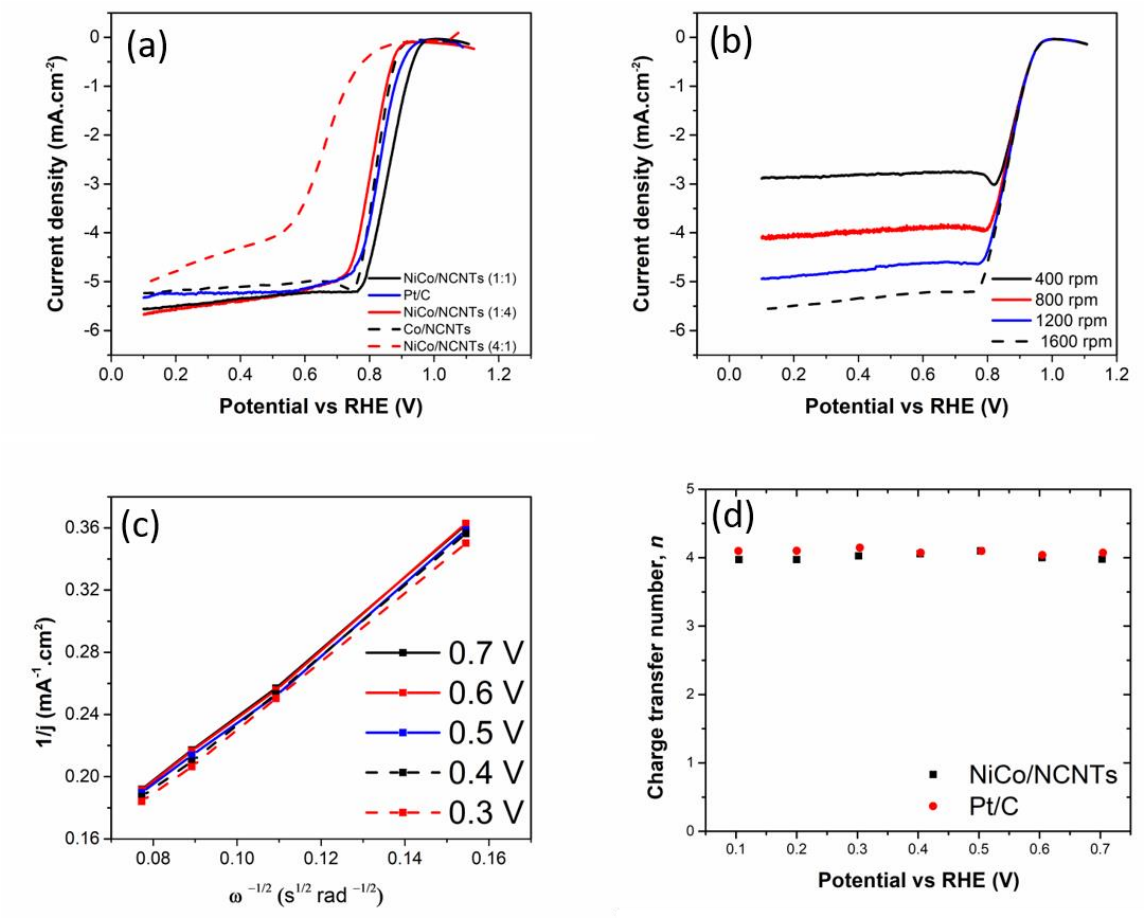

Figure 4.11 Electrochemical oxygen reduction on NiCo/NCNTs a, LSV curves of different samples at O2-saturated 0.1M KOH solution at 1600 rpm. b, LSV curves at different rotation rates (rpm) for NiCo/NCNT (1:1). c, K–L plots, ω is the angular rotation speed. d, Charge transfer number (n)

The better ORR activity of the NiCo/NCNTs is further confirmed by a smaller Tafel slope (81mVdecade^{-1} versus 96mVdecade^{-1} for Pt/C) (figure 4.12 a). The electrocatalyst was subjected to CV cycles to assess its stability in KOH. In O_2 saturated electrolyte, after 5000 CV cycles from 1.1 and 0.5 V vs RHE, there is negligible loss in performance for NiCo/NCNTs. There is a negative shift of 15 mV in terms of half wave potential after 5000 cycles (Figure 4.12b). Under identical test conditions for Pt/C, there is a negative shift of 40 mV in terms of half wave potential after 5000 cycles (Figure 4.12c). In addition, NiCo/NCNTs and Pt/C catalysts are subjected to chronoamperometric response at 0.6V for 100,000 s in O_2-saturated 0.1M KOH solution with a rotation rate of 1,600 r.p.m. to investigate their stability (Fig.

4.12d). During the period, about 95% of the original current density is retained for the NiCo/NCNTs, whereas the Pt/C shows a much higher current loss of 31%. This further confirms the superior stability of the as-prepared catalyst.

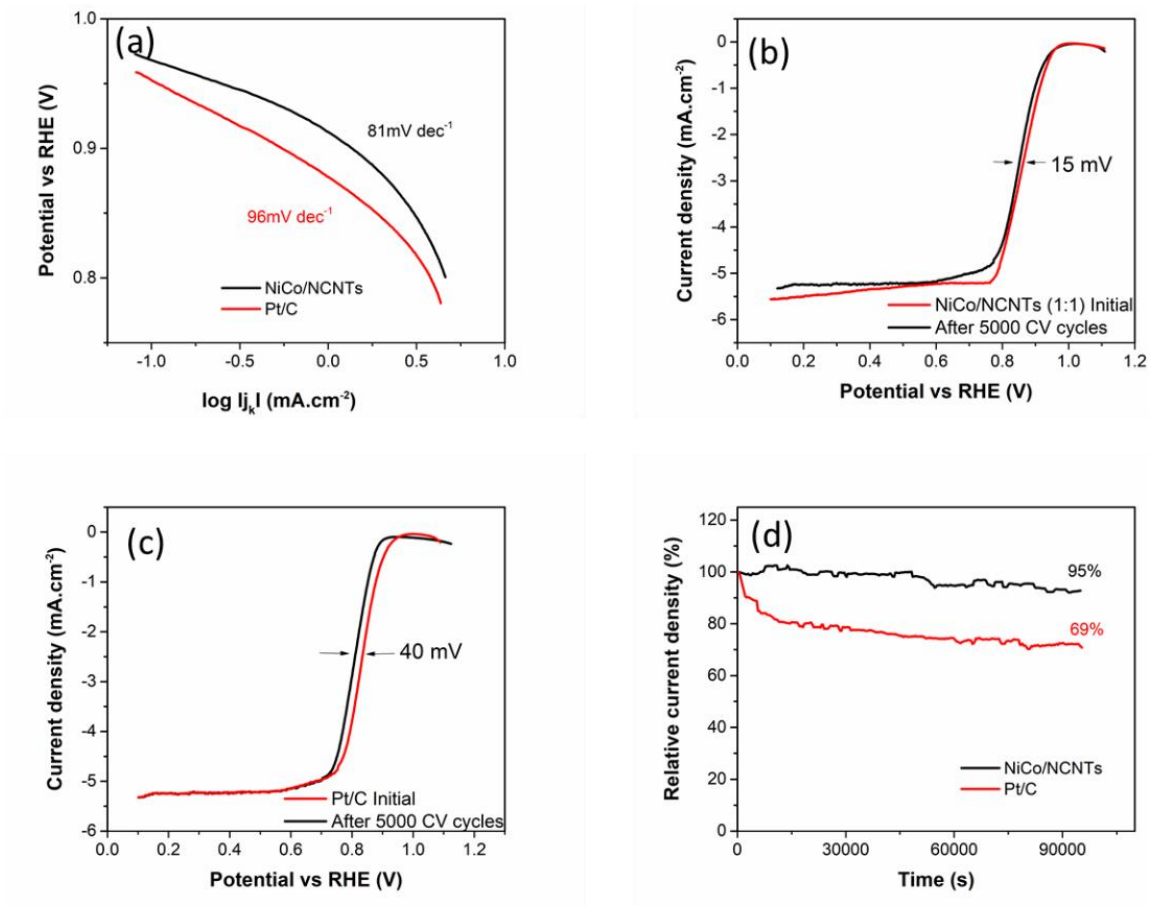

Figure 4.12 a, Tafel plots of Pt/C and NiCo/NCNTs derived from Figure 3a. b, Durability Test: ORR polarization curves (1600 rpm) of NiCo/NCNTs (1:1) before and after 5000 cycles. c, Durability Test: ORR polarization curves (1600 rpm) of Pt/C before and after 5000 cycles. d, Chronoamperometric response at 0.6V

A comparison of ZIF derived catalysts from recent studies is displayed in Table 4.6.

Table 4.6 Performance comparison of reported ZIF based catalysts for ORR in alkaline media (ORR test conditions: 1600 RPM, 0.1M KOH).

Electrocatalysts	**Onset Potential V vs RHE**	**Halfwave Potential V vs RHE**	**Loading mg/cm^2**	**Limiting current density at 0.1V vs. RHE mA.cm^{-2}**	**Scan rate mV/s**	**Reference**
N-CNTFs	0.97	0.87	0.2	5.2	10	[114]
Co/N-carbon fibres	0.95	-	0.3	-	10	[152]
ZIF-Co_3O_4/NCF	-	0.81	0.89	5.2	5	[153]
Fe@NMC-1	1.0	0.88	-	5.5	10	[154]
NiCo/NCNT	0.98	0.88	0.2	5.6	20	This work

4.2.6 Electrode Fabrication and Alkaline Fuel Cell Performance

4.2.7 Single Fuel Cell Performance

Figure 4.13a displays the AEM fuel cell performance of MEA with NiCo/NCNT (1:1) as cathode catalyst and commercial Pt/C as anode catalyst with H_2 and O_2 at different temperatures up to 50 ^oC. After 50 ^oC, membrane becomes unstable and gets degraded. For the performance comparison commercial Pt/C was also evaluated. The value of open circuit voltages for NiCo/NCNTs is 0.96V, comparable to that of commercial Pt/C. The activation losses in the low current density region are lowest at 50 ^oC. In high current density region, MEA with NiCo/NCNTs as cathode showed the best performance. The peak performance is a factor of activation losses and concentration losses. Hence, NiCo/NCNTs showed the highest peak power of 65 mW.cm^{-2} at 50 ^oC with H_2 and O_2 gases at ambient

pressure and 100 % RH. As given in Figure 4.13b, the peak power density is only ~ 60 mW.cm^{-2} for Pt/C and ~ 55 mW.cm^{-2} for Co/NCNTs at identical test conditions. The high OCV and peak current density values compared to Pt/C show great potential of NiCo/NCNTs catalyst for replacing Pt in AFC. The comparatively higher AFC performance of the NiCo/NCNTs electrocatalyst could be attributed mostly to the synergistic effect of nitrogen doped CNTs and Co/Ni active sites dispersed evenly in the NCNTs conducting framework.

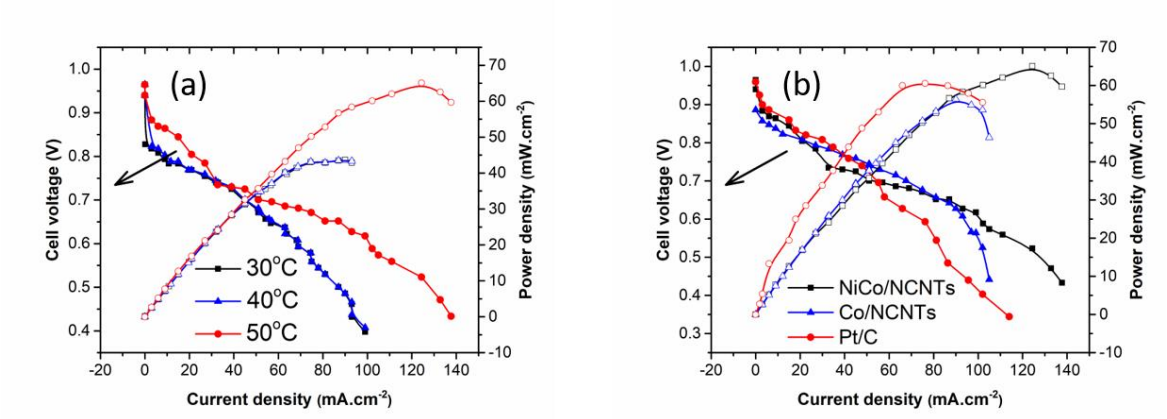

Figure 4.13 The electrochemical performance evaluations in fuel cell. a, The voltages and power densities of H_2/O_2 fuel cells with NiCo/NCNTs as cathode (4 mg cm-2) at different temperatures. b, Comparison of NiCo/NCNTs, CoNCNTs and commercial Pt/C as cathode (0.12 mg$_{Pt}$ cm^{-2}) (membrane: FAA-3-50, anode: 0.12 mg$_{Pt}$ cm^{-2} back pressure: 0 atm, 50^{o}C) fuel cells with H_2 and O_2 in 100% RH

It is to be noted here that low peak power in AFC is a factor of membrane thickness, resistance and stability. To improve the AFC performance, optimization of membrane and MEA operating conditions needs to be done [155].

5. Conclusions and recommendations

5.1 Conclusions

In a nutshell, we have prepared very active and durable PtNiCo/NC catalyst, from NiCo-ZIF towards ORR. Series of NiCo-ZIF were prepared by hydrothermal method. After the pyrolysis at 700 °C in Ar/H_2 environment, porous, conducting framework of nitrogen doped CNTs was synthesized. . XRD depicted that with the addition of the Pt into the bimetallic ZIF, carbon is more crystalline is attained, to offer a more conducting carbon matrix. The Pt doped NiCo/NCs elecro-catalysts were investigated for ORR in acidic medium. These electro-catalysts exhibited exceptional performance for ORR as revealed by the values of onset potential, current density and durability. The synthesized catalysts demonstrate appreciable performance in PEMFC, with the advantage of it contains less amount of noble metals synthesized via facile and cost-effective method. The MEA with PtNiCo/NC catalyst as cathode exhibited superior PEMFC actvity with a peak power density of 1070 $mW.cm^{-2}$ which is 15% more than the commercial Pt/C catalyst by utilizing nafion membrane at 70 ^oC with H_2 and O_2 gases. A 100 hr stability test displayed no activity loss with PtNiCo/NC MEA.

In summary, series of NiCo-ZIF were prepared by hydrothermal method. After the pyrolysis at 700 °C in Ar/H_2 environment, porous, conducting framework of nitrogen doped CNTs was synthesized. The NiCo/NCNTs elecro-catalysts were investigated for ORR in alkaline medium. These electro-catalysts exhibited exceptional performance for ORR as revealed by the values of onset potential, current density and durability. The synthesized catalysts demonstrate appreciable performance in AFC, with the advantage of it contains only non-noble metals synthesized via facile and cost-effective method. The MEA with NiCo/NCNTs catalyst as cathode exhibited higher AFC performance with a peak power density of 65 $mW.cm^{-2}$ compared to 60 $mW.cm^{-2}$ by the commercial Pt/C catalyst using FAA-3-50 membrane at 50 ^oC with H_2 and O_2 gases.

Remaining hurdles include more reduction of Pt loading while sustaining synergistic interaction at different fuel cell voltages and better humidity measures to guarantee

effective proton and peroxide transfers over the catalyst surface, as well as enhanced operation with air.

5.2 Future Recommendations

The PEMFC catalyst layers are facing many challenges for the development of new sustainable catalysts. Different Pt based catalysts have been reported and a cheaper way to synthesis and alternatives have been proposed as per studies. The studies are still underway to develop new and better catalysts. Catalysts degradation and different catalysts along with metal alloys and alternatives are discussed in detail. Where carbon corrosion is highlighted as a main failure and degradation factor towards the loss of active surface area with performance of the cell. It is obvious from the discussion that there is a lot of space for work to be done for the balance between the cost, durability and activity of the catalysts and the cell performance.

Since the work was based on finding a better and more environment friendly alternative for the clean energy using fuel cells with better performing catalysts. Thus, this work can be expanded making more environment friendly MOFs with introduction of other active materials like Graphene oxide to further decrease the platinum loading and/or eliminate the Pt.

During the testing of the materials, for having better activity it was seen that with the addition of Pt in the catalyst, the activity can be fairly increased. This addition can be kept as under the proposed percentage by US. DOE. Further activity enhancements can be done by addition of GO in the materials as GO is attributed to having the best activity as well as best stability standard for the MOFs under highly energy intensive operations.

In a nutshell, as this viewpoint specifies, the fast progress of carbon-based nanomaterials from the heat treatment of MOFs offers several novel prospects for efficient catalysis. This innovative method should help to have a simple and more tunable way to develop advanced carbon-based catalysts for fuel cell applications. Although the use of MOF-derived carbon-based nanohybrids for catalysis is still in the laboratory scale, the advances and sustained research efforts in this field will

trigger interest in scaling up their catalysis applications in industry. Hence, MOF-derived carbon-based nanomaterials, undoubtedly, will remain at the heart of research in the field of nanomaterials and catalysis in future.

REFERENCES

[1] M. M. Rafique and S. Rehman, “National energy scenario of Pakistan – Current status, future alternatives, and institutional infrastructure: An overview,” *Renew. Sustain. Energy Rev.*, vol. 69, no. November 2016, pp. 156–167, 2017.

[2] A. Ahmed, A. Q. Al-Amin, A. F. Ambrose, and R. Saidur, “Hydrogen fuel and transport system: A sustainable and environmental future,” *Int. J. Hydrogen Energy*, vol. 41, no. 3, pp. 1369–1380, 2016.

[3] S. R. Shakeel, J. Takala, and W. Shakeel, “Renewable energy sources in power generation in Pakistan,” *Renew. Sustain. Energy Rev.*, vol. 64, pp. 421–434, 2016.

[4] M. Asif, “Sustainable energy options for Pakistan,” *Renew. Sustain. Energy Rev.*, vol. 13, no. 4, pp. 903–909, 2009.

[5] M. Wakeel, B. Chen, and S. Jahangir, “Overview of energy portfolio in Pakistan,” *Energy Procedia*, vol. 88, pp. 71–75, 2016.

[6] H. Zameer and Y. Wang, “Energy production system optimization: Evidence from Pakistan,” *Renew. Sustain. Energy Rev.*, vol. 82, no. March 2016, pp. 886–893, 2018.

[7] O. Z. Sharaf and M. F. Orhan, “An overview of fuel cell technology: Fundamentals and applications,” *Renew. Sustain. Energy Rev.*, vol. 32, pp. 810–853, 2014.

[8] U. Lucia, “Overview on fuel cells,” *Renew. Sustain. Energy Rev.*, vol. 30, pp. 164–169, 2014.

[9] N. Matulić, G. Radica, F. Barbir, and S. Nižetić, “Commercial vehicle auxiliary loads powered by PEM fuel cell,” *Int. J. Hydrogen Energy*, no. xxxx, 2019.

[10] F. Ning *et al.*, “Flexible and Lightweight Fuel Cell with High Specific Power Density,” *ACS Nano*, vol. 11, no. 6, pp. 5982–5991, Jun. 2017.

[11] N. Djilali, G. F. Mclean, T. Niet, S. Prince-Richard, and N. Djilali, “An assessment of alkaline fuel cell technology Hydrogen peroxide detection in PEM Fuel cells View project Transportation Futures for British Columbia View project An

assessment of alkaline fuel cell technology," *Artic. Int. J. Hydrog. Energy*, vol. 27, pp. 507–526, 2002.

[12] N. Sammes, R. Bove, and K. Stahl, "Phosphoric acid fuel cells: Fundamentals and applications," *Curr. Opin. Solid State Mater. Sci.*, vol. 8, no. 5, pp. 372–378, 2004.

[13] L. Carrette and K. A. Friedrich, "Fuel Cells: Principles, Types, Fuels, and Applications," *ChemPhysChem*, vol. 1, no. 4, pp. 162–193, 2000.

[14] W. C. O'Hayre Ryan P. Suk-Won Cha, F.B. Prinz, "Fuel Cell Fundamentals." John Wiley & Sons.

[15] A. Choudhury, H. Chandra, and A. Arora, "Application of solid oxide fuel cell technology for power generation - A review," *Renew. Sustain. Energy Rev.*, vol. 20, pp. 430–442, 2013.

[16] S. P. S. Badwal, S. Giddey, C. Munnings, and A. Kulkarni, "Review of progress in high temperature solid oxide fuel cells," *J. Aust. Ceram. Soc.*, vol. 50, no. 1, pp. 23–37, 2014.

[17] K. Epping Martin, J. P. Kopasz, and K. W. McMurphy, "Status of Fuel Cells and the Challenges Facing Fuel Cell Technology Today making further progress in eliminating cost, durability, and performance challenges that remain for fuel cell technology," *Fuel Cell Chem. Oper. ACS Symp. Ser.*, pp. 1–13, 2010.

[18] O. T. Holton and J. W. Stevenson, "The Role of Platinum in Proton Exchange Membrane Fuel Cells Evaluation of platinum's unique properties for use in both the anode and cathode of a proton exchange membrane fuel cell," *@BULLETPlatinum Met. Rev*, vol. 57, no. 4, pp. 259–271, 2013.

[19] J. Marcinkoski, J. Spendelow, A. Wilson, and D. Papageorgopoulos, "DOE Hydrogen and Fuel Cells Program Record - Fuel Cell System Cost - 2015," *J. Mech. Robot.*, vol. 9, no. 4, pp. 1–9, 2017.

[20] O. M. Yagui, M. O'Keeffe, M. Eddaoudi, and H. Li, "Design and synthesis of an exceptionally stable and highly," *Nature*, vol. 402, no. November, pp. 276–279, 1999.

[21] M. H. Yap, K. L. Fow, and G. Z. Chen, “Synthesis and applications of MOF-derived porous nanostructures,” *Green Energy Environ.*, vol. 2, no. 3, pp. 218–245, 2017.

[22] P. Kumar, A. Pournara, K. H. Kim, V. Bansal, S. Rapti, and M. J. Manos, *Metal-organic frameworks: Challenges and opportunities for ion-exchange/sorption applications*, vol. 86. 2017.

[23] D. Farrusseng, S. Aguado, and C. Pinel, “Metal-organic frameworks: Opportunities for catalysis,” *Angew. Chemie - Int. Ed.*, vol. 48, no. 41, pp. 7502–7513, 2009.

[24] R. I. D, “Electrode assembly for use in a solid polymer electrolyte fuel cell,” no. 13, pp. 201–203, 1989.

[25] S. Litster and G. McLean, “PEM fuel cell electrodes,” *J. Power Sources*, vol. 130, no. 1–2, pp. 61–76, 2004.

[26] J. Hu, K. A. Kuttiyiel, K. Sasaki, C. Zhang, and R. R. Adzic, “Determination of Hydrogen Oxidation Reaction Mechanism Based on Pt−H $_{ad}$ Energetics in Alkaline Electrolyte,” *J. Electrochem. Soc.*, vol. 165, no. 15, pp. J3355–J3362, 2018.

[27] K. Ojha, S. Saha, P. Dagar, and A. K. Ganguli, “Nanocatalysts for hydrogen evolution reactions,” *Phys. Chem. Chem. Phys.*, vol. 20, no. 10, pp. 6777–6799, 2018.

[28] J. Durst, A. Siebel, C. Simon, F. Hasché, J. Herranz, and H. A. Gasteiger, “New insights into the electrochemical hydrogen oxidation and evolution reaction mechanism,” *Energy Environ. Sci.*, vol. 7, no. 7, pp. 2255–2260, 2014.

[29] D. Strmcnik *et al.*, “Improving the hydrogen oxidation reaction rate by promotion of hydroxyl adsorption,” *Nat. Chem.*, vol. 5, no. 4, pp. 300–306, 2013.

[30] H. A. Gasteiger, J. E. Panels, and S. G. Yan, “Dependence of PEM fuel cell performance on catalyst loading,” *J. Power Sources*, vol. 127, no. 1–2, pp. 162–171, 2004.

[31] C. Merlet *et al.*, “Highly confined ions store charge more efficiently in supercapacitors,” *Nat. Commun.*, vol. 4, no. May, pp. 2–7, 2013.

[32] W. Sheng, Z. Zhuang, M. Gao, J. Zheng, J. G. Chen, and Y. Yan, “Correlating hydrogen oxidation and evolution activity on platinum at different pH with measured hydrogen binding energy,” *Nat. Commun.*, vol. 6, pp. 1–6, 2015.

[33] J. Wei *et al.*, “Heterostructured Electrocatalysts for Hydrogen Evolution Reaction Under Alkaline Conditions,” *Nano-Micro Lett.*, vol. 10, no. 4, p. 75, 2018.

[34] O. Savadogo and H. Lavoie, “Hydrogen evolution reaction in an alkaline medium on cobalt electrodeposited with heteropolyacids,” *Int. J. Hydrogen Energy*, vol. 17, no. 7, pp. 473–477, 1992.

[35] B. Hammer and J. K. Nørskov, “Electronic factors determining the reactivity of metal surfaces,” *Surf. Sci.*, vol. 343, no. 3, pp. 211–220, 1995.

[36] A. Nilsson, L. G. M. Pettersson, B. Hammer, T. Bligaard, C. H. Christensen, and J. K. Nørskov, “The electronic structure effect in heterogeneous catalysis,” *Catal. Letters*, vol. 100, no. 3–4, pp. 111–114, 2005.

[37] J. K. Norskov, F. Abild-Pedersen, F. Studt, and T. Bligaard, “Density functional theory in surface chemistry and catalysis,” *Proc. Natl. Acad. Sci.*, vol. 108, no. 3, pp. 937–943, 2011.

[38] T. Tingelof, *Polymer Electrolyte Fuel Cells in Reformate Power Generators*, no. december. 2010.

[39] S. S. Mahapatra and J. Datta, “Characterization of Pt-Pd/C Electrocatalyst for Methanol Oxidation in Alkaline Medium,” *Int. J. Electrochem.*, vol. 2011, pp. 1–16, 2011.

[40] A. Hassan and E. A. Ticianelli, “Activity and stability of dispersed multi metallic Pt-based catalysts for CO Tolerance in proton exchange membrane fuel cell anodes,” *An. Acad. Bras. Cienc.*, vol. 90, no. 1, pp. 697–718, 2018.

[41] C. Qin, J. Wang, D. Yang, B. Li, and C. Zhang, “Proton Exchange Membrane Fuel Cell Reversal: A Review,” *Catalysts*, vol. 6, no. 12, p. 197, 2016.

[42] P. Mandal, B. K. Hong, J. G. Oh, and S. Litster, “Understanding the voltage reversal

behavior of automotive fuel cells," *J. Power Sources*, vol. 397, no. June, pp. 397–404, 2018.

[43] H. Chen, X. Zhao, T. Zhang, and P. Pei, "The reactant starvation of the proton exchange membrane fuel cells for vehicular applications: A review," *Energy Convers. Manag.*, vol. 182, no. September 2018, pp. 282–298, 2019.

[44] Y. Siju, "ANODE CATALYST COMPOSITIONS FOR A VOLTAGE REVERSAL TOLERANT FUEL CELL," vol. 1, no. 19, 2013.

[45] C. Y. Chen, C. C. Chen, S. W. Hsu, M. P. Lai, W. H. Lai, and W. M. Yang, "Behavior of a proton exchange membrane fuel cell in reformate gas," *Energy Procedia*, vol. 29, pp. 64–71, 2012.

[46] S. Jiménez, J. Soler, R. X. Valenzuela, and L. Daza, "Assessment of the performance of a PEMFC in the presence of CO," *J. Power Sources*, vol. 151, no. 1–2, pp. 69–73, 2005.

[47] H. A. Gasteiger *et al.*, "Electrocatalysis and Catalyst Degradation Challenges in Proton Exchange Membrane Fuel Cells," *Hydrog. Fuel Cells Fundam. Appl.*, pp. 3–16, 2010.

[48] A. Engström, "Determination of acceptable contaminant levels for PEM fuel cell stacks and poisoning mitigation strategies," pp. 1–61, 2014.

[49] T. J. Schmidt, V. Stamenkovic, P. N. Ross, and N. M. Markovic, "Oxygen Reduction Reaction on Pt and Pt Bimetallic Surfaces A Selective Review.pdf," no. 2, pp. 105–116, 2001.

[50] M. Sun *et al.*, "CO-tolerant PtRu@h-BN/C core–shell electrocatalysts for proton exchange membrane fuel cells," *Appl. Surf. Sci.*, vol. 450, pp. 244–250, 2018.

[51] J. S. Spendelow, P. K. Babu, and A. Wieckowski, "Electrocatalytic oxidation of carbon monoxide and methanol on platinum surfaces decorated with ruthenium," *Curr. Opin. Solid State Mater. Sci.*, vol. 9, no. 1–2, pp. 37–48, 2005.

[52] and L. L. J. K. Nørskov,* J. Rossmeisl, A. Logadottir, "Origin of the Overpotential

for Oxygen Reduction at a Fuel-Cell Cathode," *Proc. 14th Sci. Meet. Int. Soc. Magn. Reson. Med.*, p. 3493, 2006.

[53] N. Markovic, "Surface science studies of model fuel cell electrocatalysts," *Surf. Sci. Rep.*, vol. 45, no. 4–6, pp. 117–229, 2002.

[54] M. Kim, C. Lee, S. M. Ko, and J. M. Nam, "Metal alloy hybrid nanoparticles with enhanced catalytic activities in fuel cell applications," *J. Solid State Chem.*, vol. 270, no. October 2018, pp. 295–303, 2019.

[55] A. Stassi *et al.*, "Electrocatalytic behaviour for oxygen reduction reaction of small nanostructured crystalline bimetallic Pt-M supported catalysts," *J. Appl. Electrochem.*, vol. 36, no. 10, pp. 1143–1149, 2006.

[56] C. V. Boone and G. Maia, "Pt–Pd and Pt–Pd–(Cu or Fe or Co)/graphene nanoribbon nanocomposites as efficient catalysts toward the oxygen reduction reaction," *Electrochim. Acta*, vol. 247, pp. 19–29, 2017.

[57] M. P. Ralph, T.R.; Hogarth, "Catalysis for Low Temperature Fuel Cells," *Platin. Met. Rev.*, vol. 46, no. l, pp. 3–14, 2002.

[58] Q. Yu, S. Yin, J. Zhang, and H. Yin, "Structure dependent activity and durability towards oxygen reduction reaction on Pt modified nanoporous gold," *Electrochim. Acta*, vol. 298, pp. 599–608, 2019.

[59] R. V. Hull, L. Li, Y. Xing, and C. C. Chusuei, "Pt nanoparticle binding on functionalized multiwalled carbon nanotubes," *Chem. Mater.*, vol. 18, no. 7, pp. 1780–1788, 2006.

[60] J. Zhang, K. Sasaki, E. Sutter, and R. R. Adzic, "Stabilization of platinum oxygen-reduction electrocatalysts using gold clusters," *Science (80-.).*, vol. 315, no. 5809, pp. 220–222, 2007.

[61] A. Kumar and V. Ramani, "Ta 0 . 3 Ti 0 . 7 O 2 Electrocatalyst Supports Exhibit Exceptional Electrochemical Stability," *J. Electrochem. Soc.*, vol. 160, no. 11, pp. 1207–1215, 2013.

[62] F. Takasaki *et al.*, “Carbon-Free Pt Electrocatalysts Supported on SnO 2 for Polymer Electrolyte Fuel Cells : Electrocatalytic Activity and Durability Carbon-Free Pt Electrocatalysts Supported on SnO 2 for Polymer Electrolyte Fuel Cells : Electrocatalytic Activity and Durabili,” *J. Electrochem. Soc.*, vol. 158, no. 10, pp. 1270–1275, 2011.

[63] V. Di Noto E. Negro, “Pt–Fe and Pt–Ni Carbon Nitride-Based ‘Core–Shell’ ORR Electrocatalysts for Polymer Electrolyte Membrane Fuel Cells.pdf,” *Fuel Cells*, vol. 10, no. 2, 2010.

[64] S. Sun, G. Zhang, X. Sun, M. Cai, and M. Ruthkosky, “Highly Stable and Active Pt / Nb-TiO 2 Carbon-Free Electrocatalyst for Proton Exchange Membrane Fuel Cells,” vol. 2012, pp. 13–15, 2012.

[65] C.-J. Z. L. M. M. H. N. K. He, “Core-shell synthesis of carbon-supported alloy nanoparticle catalysts,” 2006.

[66] M. G. Hosseini and P. Zardari, “Applied Surface Science Electrocatalytical study of carbon supported Pt , Ru and bimetallic Pt – Ru nanoparticles for oxygen reduction reaction in alkaline media,” *Appl. Surf. Sci.*, vol. 345, pp. 223–231, 2015.

[67] C. Li *et al.*, “Emerging Pt-based electrocatalysts with highly open nanoarchitectures for boosting oxygen reduction reaction,” *Nano Today*, vol. 21, pp. 91–105, 2018.

[68] D. I. K. D. S. C. D. A. R. Z. D. K. J. J. Mayrhofer, “Oxygen Electrochemistry as a Cornerstone for Sustainable Energy Conversion Angewandte,” *Angew. Chemie - Int. Ed.*, vol. 53, no. 1, pp. 102–121, 2014.

[69] Y. Cong, B. Yi, and Y. Song, “Hydrogen oxidation reaction in alkaline media: From mechanism to recent electrocatalysts,” *Nano Energy*, vol. 44, no. December 2017, pp. 288–303, 2018.

[70] X. Huang *et al.*, “A Facile Strategy to Pt 3 Ni Nanocrystals with Highly Porous Features as an Enhanced Oxygen Reduction Reaction Catalyst,” *Adv. Mater.*, vol. 25, no. 21, pp. 2974–2979, 2013.

[71] S. Chen, H. Su, Y. Wang, W. Wu, and J. Zeng, “Size-Controlled Synthesis of

Platinum – Copper Hierarchical Trigonal Bipyramid Nanoframes," *Angew. Chemie - Int. Ed.*, vol. 54, no. 1, pp. 108–113, 2015.

[72] B. Jiang, C. Li, V. Malgras, and Y. Yamauchi, "Synthesis of ternary PtPdCu spheres with three- dimensional nanoporous architectures toward superior electrocatalysts †," *J. Mater. Chem. A Mater. energy Sustain.*, vol. 3, no. 35, pp. 18053–18058, 2015.

[73] C. Li, B. Jiang, M. Imura, V. Malgras, and Y. Yamauchi, "Mesoporous Pt hollow cubes with controlled shell thicknesses and investigation of their electrocatalytic performace," *Chem. Commun.*, vol. 50, no. 97, pp. 15337–15340, 2014.

[74] S. Guo, S. Zhang, D. Su, and S. Sun, "Seed-Mediated Synthesis of Core / Shell FePtM / FePt (M = Pd , Au) Nanowires and Their Electrocatalysis for Oxygen Reduction Reaction," *Am. Chem. Soc.*, vol. 37, no. 135, pp. 13879–13884, 2013.

[75] H. Li *et al.*, "Ultrathin PtPdTe Nanowires as Superior Catalysts for Methanol Electrooxidation," *Angew. Chemie - Int. Ed.*, vol. 52, no. 29, pp. 7472–7476, 2013.

[76] B. Y. Xia, H. Bin Wu, Y. Yan, X. Wen, D. Lou, and X. Wang, "Ultrathin and Ultralong Single-crystal Pt Nanowire Assemblies with Highly Stable Electrocatalytic Activity Ultrathin and Ultralong Single-crystal Pt Nanowire Assemblies with Highly Stable Electrocatalytic Activity," *J. Am. Chem. Soc.*, vol. 25, no. 135, pp. 9480–9485, 2013.

[77] J. F. and S. Z. Jun Zhang, Hongzhou Yang, "Synthesis and Oxygen Reduction Activity of Shape-Controlled Pt3Ni Nanopolyhedra," *nano Lett.*, vol. 2, no. 10, pp. 638–644, 2010.

[78] J. Wu, J. Zhang, Z. Peng, S. Yang, and F. T. Wagner, "Truncated Octahedral Pt 3 Ni Oxygen Reduction Reaction Electrocatalysts," *J. Am. Chem. Soc.*, vol. 14, no. 132, pp. 4984–4985, 2010.

[79] C. Wang *et al.*, "Synthesis of Homogeneous Pt-Bimetallic Nanoparticles as Highly Efficient Electrocatalysts," *ACS Catal.*, vol. 10, no. 1, pp. 1355–1359, 2011.

[80] X. Yu and S. Ye, "Recent advances in activity and durability enhancement of Pt/C catalytic cathode in PEMFC. Part II: Degradation mechanism and durability

enhancement of carbon supported platinum catalyst," *J. Power Sources*, vol. 172, no. 1, pp. 145–154, 2007.

[81] F. Ettingshausen, J. Kleemann, A. Marcu, G. Toth, H. Fuess, and C. Roth, "Dissolution and migration of platinum in PEMFCs investigated for start/stop cycling and high potential degradation," *Fuel Cells*, vol. 11, no. 2, pp. 238–245, 2011.

[82] P. J. Ferreira, Y. Shao-Horn, D. Morgan, E. F. Holby, W. C. Sheng, and S. Chen, "Instability of Supported Platinum Nanoparticles in Low-Temperature Fuel Cells," *Top. Catal.*, vol. 46, no. 3–4, pp. 285–305, 2007.

[83] R. Kou *et al.*, "Enhanced activity and stability of Pt catalysts on functionalized graphene sheets for electrocatalytic oxygen reduction," *Electrochem. commun.*, vol. 11, no. 5, pp. 954–957, 2009.

[84] V. I. Birss, M. Chang, and J. Segal, "Platinum oxide film formation-reduction: an in-situ mass measurement study," *J. Electroanal. Chem.*, vol. 355, no. 1–2, pp. 181–191, 1993.

[85] M. J. N. Pourbaix, J. Van Muylder, and N. de Zoubov, "Electrochemical Properties of the Platinum Metals," *Platin. Met. Rev.*, vol. 3, no. 3, pp. 100–106, 1959.

[86] A. P. Young, J. Stumper, and E. Gyenge, "Characterizing the Structural Degradation in a PEMFC Cathode Catalyst Layer: Carbon Corrosion," *J. Electrochem. Soc.*, vol. 156, no. 8, p. B913, 2009.

[87] L. Dubau *et al.*, "Carbon corrosion induced by membrane failure: The weak link of PEMFC long-term performance," *Int. J. Hydrogen Energy*, vol. 39, no. 36, 2014.

[88] E. S. Lett, P. A-a, L. M. Roen, C. H. Paik, and T. D. Jarvi, "Electrocatalytic Corrosion of Carbon Support in PEMFC Cathodes service Electrocatalytic Corrosion of Carbon Support in PEMFC Cathodes," vol. 7, no. 1, pp. 8–12, 2004.

[89] P. T. Yu, W. Gu, J. Zhang, R. Makharia, F. T. Wagner, and H. A. Gasteiger, "Carbon-Support Requirements for Highly Durable Fuel Cell Operation."

[90] B. Avasarala, T. Murray, W. Li, and P. Haldar, “Titanium nitride nanoparticles based electrocatalysts for proton exchange membrane fuel cells †,” no. Cv, pp. 1803–1805, 2009.

[91] and A. M. E. Klito C. Petallidou, Kyriaki Polychronopoulou, Soghomon Boghosian, Sergio Garcia-Rodriguez, “Water–Gas Shift Reaction on PtCe1–xTixO2−δ The Effect of CeTi Ratio.pdf,” *Phys. Chem. Chem. Phys.*, vol. 48, no. 117, pp. 25467–25477, 2013.

[92] H. Chhina, S. Campbell, and O. Kesler, “An oxidation-resistant indium tin oxide catalyst support for proton exchange membrane fuel cells,” vol. 161, pp. 893–900, 2006.

[93] J. Rajeswari and B. Viswanathan, “Tungsten trioxide nanorods as supports for platinum in methanol oxidation,” vol. 106, pp. 168–174, 2007.

[94] M. Yaldagard, M. Jahanshahi, N. Seghatoleslami, and E. T. Al, “Carbonaceous Nanostructured Support Materials for Low Temperature Fuel Cell Electrocatalysts — A Review,” vol. 2013, no. December, pp. 121–153, 2013.

[95] Z. Zhang, S. Han, C. Wang, J. Li, and G. Xu, “Single-Walled Carbon Nanohorns for Energy Applications,” *nanomaterials*, vol. 5, pp. 1732–1755, 2015.

[96] Taeghwan Hyeon Prof. Dr. Sangjin Han Yung-Eun Sung Prof. Dr. Kyung-Won Park Young-Woon Kim Prof. Dr., “High-Performance Direct Methanol Fuel Cell Electrodes using Solid-Phase-Synthesized Carbon Nanocoils.pdf,” *Angew. Chemie - Int. Ed.*, vol. 42, no. 36, 2013.

[97] S. Noro, “Metal-Organic Frameworks,” *Compr. Inorg. Chem. II (Second Ed. From Elem. to Appl.*, vol. 5, pp. 45–71, 2013.

[98] Z. Li *et al.*, “Directed Growth of Metal-Organic Frameworks and Their Derived Carbon-Based Network for Efficient Electrocatalytic Oxygen Reduction,” *Adv. Mater.*, vol. 28, no. 12, pp. 2337–2344, 2016.

[99] X. Wang *et al.*, “Highly dispersible and stable copper terephthalate metal-organic framework-graphene oxide nanocomposite for an electrochemical sensing

application," *ACS Appl. Mater. Interfaces*, vol. 6, no. 14, pp. 11573–11580, 2014.

[100] B. Zornoza *et al.*, "Functionalized flexible MOFs as fillers in mixed matrix membranes for highly selective separation of CO2 from CH4 at elevated pressures," *Chem. Commun.*, vol. 47, no. 33, pp. 9522–9524, 2011.

[101] K. Shen, X. Chen, J. Chen, and Y. Li, "Development of MOF-Derived Carbon-Based Nanomaterials for Efficient Catalysis," *ACS Catal.*, vol. 6, no. 9, pp. 5887–5903, 2016.

[102] L. Zou and H. C. Zhou, "Hydrogen storage in metal-organic frameworks," *Nanostructured Mater. Next-Generation Energy Storage Convers. Hydrog. Prod. Storage, Util.*, pp. 143–170, 2017.

[103] M. Wang *et al.*, "Metal-organic frameworks (ZIF-67) as efficient cocatalysts for photocatalytic reduction of CO2: The role of the morphology effect," *J. Mater. Chem. A*, vol. 6, no. 11, pp. 4768–4775, 2018.

[104] E. Environ, A. Morozan, B. Jousselme, and S. Palacin, "Energy & Environmental Science Low-platinum and platinum-free catalysts for the oxygen reduction reaction at fuel cell cathodes," pp. 1238–1254, 2011.

[105] L. Yan *et al.*, "Metal-Organic Frameworks Derived Nanotube of Nickel–Cobalt Bimetal Phosphides as Highly Efficient Electrocatalysts for Overall Water Splitting," *Adv. Funct. Mater.*, vol. 27, no. 40, 2017.

[106] Y. Han *et al.*, "Zinc/Nickel-Doped Hollow Core-Shell Co_3O_4 Derived from a Metal-Organic Framework with High Capacity, Stability, and Rate Performance in Lithium/Sodium-Ion Batteries," *Chem. - A Eur. J.*, vol. 67, pp. 1651–1656, 2018.

[107] Y. Bai *et al.*, "A high performance non-noble metal electrocatalyst for the oxygen reduction reaction derived from a metal organic framework," *Cuihua Xuebao/Chinese J. Catal.*, vol. 37, no. 7, pp. 1127–1133, 2016.

[108] X. Wang *et al.*, "MOF derived catalysts for electrochemical oxygen reduction," *J. Mater. Chem. A*, vol. 2, no. 34, pp. 14064–14070, 2014.

[109] A. Zanon, S. Chaemchuen, B. Mousavi, and F. Verpoort, “1 Zn-doped ZIF-67 as catalyst for the CO2 fixation into cyclic carbonates,” *J. CO2 Util.*, vol. 20, no. January, pp. 282–291, 2017.

[110] H. Yang, X. W. He, F. Wang, Y. Kang, and J. Zhang, “Doping copper into ZIF-67 for enhancing gas uptake capacity and visible-light-driven photocatalytic degradation of organic dye,” *J. Mater. Chem.*, vol. 22, no. 41, pp. 21849–21851, 2012.

[111] P. Zhang, F. Sun, Z. Xiang, Z. Shen, J. Yun, and D. Cao, “ZIF-derived in situ nitrogen-doped porous carbons as efficient metal-free electrocatalysts for oxygen reduction reaction,” *Energy Environ. Sci.*, vol. 7, no. 1, pp. 442–450, 2014.

[112] X. Shi, N. Iqbal, S. S. Kunwar, G. Wahab, H. A. Kasat, and A. M. Kannan, “Pt–Co@NCNTs cathode catalyst using ZIF-67 for proton exchange membrane fuel cell,” *Int. J. Hydrogen Energy*, vol. 43, no. 6, pp. 3520–3526, 2018.

[113] L. Li, W. Xie, J. Chen, and J. Yang, “ZIF-67 derived P/Ni/Co/NC nanoparticles as highly efficient electrocatalyst for oxygen reduction reaction (ORR),” *J. Solid State Chem.*, vol. 264, no. April, pp. 1–5, 2018.

[114] B. Y. Xia, Y. Yan, N. Li, H. Bin Wu, X. W. D. Lou, and X. Wang, “A metal-organic framework-derived bifunctional oxygen electrocatalyst,” *Nat. Energy*, vol. 1, no. 1, 2016.

[115] Z. Chen, D. Higgins, A. Yu, L. Zhang, and J. Zhang, “A review on non-precious metal electrocatalysts for PEM fuel cells,” *Energy Environ. Sci.*, vol. 4, no. 9, pp. 3167–3192, 2011.

[116] G. Greczynski and L. Hultman, “Progress in Materials Science X-ray photoelectron spectroscopy : Towards reliable binding energy referencing,” *Prog. Mater. Sci.*, vol. 107, no. July 2019, p. 100591, 2020.

[117] X. Liu *et al.*, “Development of gas diffusion layer using water based carbon slurry for proton exchange membrane fuel cells,” *Electrochim. Acta*, vol. 56, no. 3, pp. 1591–1596, 2010.

[118] B. Britton and S. Holdcroft, “The Control and Effect of Pore Size Distribution in AEMFC Catalyst Layers,” *J. Electrochem. Soc.*, vol. 163, no. 5, pp. F353–F358, 2016.

[119] M. Carmo, G. Doubek, R. C. Sekol, M. Linardi, and A. D. Taylor, “Development and electrochemical studies of membrane electrode assemblies for polymer electrolyte alkaline fuel cells using FAA membrane and ionomer,” *J. Power Sources*, vol. 230, pp. 169–175, 2013.

[120] M. Hu *et al.*, “Direct carbonization of Al-based porous coordination polymer for synthesis of nanoporous carbon,” *J. Am. Chem. Soc.*, vol. 134, no. 6, pp. 2864–2867, 2012.

[121] J. K. Sun and Q. Xu, “Functional materials derived from open framework templates/precursors: Synthesis and applications,” *Energy Environ. Sci.*, vol. 7, no. 7, pp. 2071–2100, 2014.

[122] J. Keun, H. Jung, J. Lee, S. Yong, J. Jin, and W. Seok, “Metal-free CNTs grown on glass substrate by microwave PECVD,” vol. 10, pp. 447–450, 2010.

[123] M. Shao, A. Peles, and K. Shoemaker, “Electrocatalysis on Platinum Nanoparticles : Particle Size Effect on,” pp. 3714–3719, 2011.

[124] J. Liu, “Catalysis by Supported Single Metal Atoms,” *ACS Catal.*, vol. 7, no. 1, pp. 34–59, 2017.

[125] C. Su, H. Cheng, W. Li, Z. Liu, N. Li, and Z. Hou, “Atomic Modulation of FeCo – Nitrogen – Carbon Bifunctional Oxygen Electrodes for Rechargeable and Flexible All-Solid-State Zinc – Air Battery,” vol. 201602420, pp. 1–12, 2017.

[126] A. Shchukarev and D. Korolkov, “XPS study of group IA carbonates,” *Open Chem.*, vol. 2, no. 2, pp. 347–362, 2004.

[127] R. Pietrzak, “XPS study and physico-chemical properties of nitrogen-enriched microporous activated carbon from high volatile bituminous coal,” vol. 88, pp. 1871–1877, 2009.

[128] E. Luo, M. Xiao, J. Ge, C. Liu, and W. Xing, “into a 3D porous carbon matrix through template- activity towards the oxygen reduction reaction †,” pp. 21709–21714, 2017.

[129] J. Liu, P. Song, and W. Xu, “Structure-activity relationship of doped-nitrogen (N)-based metal-free active sites on carbon for oxygen reduction reaction,” *Carbon N. Y.*, vol. 115, pp. 763–772, 2017.

[130] A. Ejaz and S. Jeon, “ScienceDirect The individual role of pyrrolic , pyridinic and graphitic nitrogen in the growth kinetics of Pd NPs on N-rGO followed by a comprehensive study on,” *Int. J. Hydrogen Energy*, vol. 43, no. 11, pp. 5690–5702, 2018.

[131] P. Chandran, A. Ghosh, and S. Ramaprabhu, “High-performance Platinum-free oxygen reduction reaction and hydrogen oxidation reaction catalyst in polymer electrolyte membrane fuel cell,” *Sci. Rep.*, vol. 8, no. 1, p. 3591, 2018.

[132] Y. Zhou, R. Pasquarelli, T. Holme, J. Berry, D. Ginley, and R. O’Hayre, “Improving PEM fuel cell catalyst activity and durability using nitrogen-doped carbon supports: observations from model Pt/HOPG systems,” *J. Mater. Chem.*, vol. 19, no. 42, p. 7830, 2009.

[133] A. Zitolo *et al.*, “carbon materials for the oxygen reduction reaction,” *Nat. Commun.*, vol. 2017, no. OCT, pp. 1–10.

[134] V. A. Online, “1 Introduction,” pp. 5109–5118, 2013.

[135] W. S. Jung and B. N. Popov, “Effect of Pretreatment on Durability of fct-Structured Pt-Based Alloy Catalyst for the Oxygen Reduction Reaction under Operating Conditions in Polymer Electrolyte Membrane Fuel Cells,” *ACS Sustain. Chem. Eng.*, vol. 5, no. 11, pp. 9809–9817, 2017.

[136] J. Zeng and J. Y. Lee, “Effects of preparation conditions on performance of carbon-supported nanosize Pt-Co catalysts for methanol electro-oxidation under acidic conditions,” *J. Power Sources*, vol. 140, no. 2, pp. 268–273, 2005.

[137] J. Xu, X. Liu, Y. Chen, Y. Zhou, T. Lu, and Y. Tang, “Platinum–cobalt alloy

networks for methanol oxidation electrocatalysis," *J. Mater. Chem.*, vol. 22, no. 44, pp. 23659–23667, 2012.

[138] L. Dubau *et al.*, "Tuning the Performance and the Stability of Porous Hollow PtNi/C Nanostructures for the Oxygen Reduction Reaction," *ACS Catal.*, vol. 5, no. 9, pp. 5333–5341, 2015.

[139] J. Liu *et al.*, "High performance platinum single atom electrocatalyst for oxygen reduction reaction," *Nat. Commun.*, vol. 8, no. May, pp. 1–9, 2017.

[140] P. Mani, R. Srivastava, and P. Strasser, "Dealloyed binary PtM3 (M = Cu, Co, Ni) and ternary PtNi 3M (M = Cu, Co, Fe, Cr) electrocatalysts for the oxygen reduction reaction: Performance in polymer electrolyte membrane fuel cells," *J. Power Sources*, vol. 196, no. 2, pp. 666–673, 2011.

[141] X. X. Wang *et al.*, "Nitrogen-Coordinated Single Cobalt Atom Catalysts for Oxygen Reduction in Proton Exchange Membrane Fuel Cells," vol. 1706758, pp. 1–11, 2018.

[142] C. C. L. McCrory, S. Jung, J. C. Peters, and T. F. Jaramillo, "Benchmarking heterogeneous electrocatalysts for the oxygen evolution reaction," *J. Am. Chem. Soc.*, vol. 135, no. 45, pp. 16977–16987, 2013.

[143] L. Lin, Q. Zhu, and A. W. Xu, "Noble-metal-free Fe-N/C catalyst for highly efficient oxygen reduction reaction under both alkaline and acidic conditions," *J. Am. Chem. Soc.*, vol. 136, no. 31, pp. 11027–11033, 2014.

[144] P. Dhanasekaran, S. R. Williams, D. Kalpana, and S. D. Bhat, "Boosting efficiency and stability using zirconia nanosphere-held carbon for proton exchange membrane fuel cells," *RSC Adv.*, vol. 8, no. 1, pp. 472–480, 2018.

[145] J. Liu *et al.*, "Pt0.61Ni/C for High-Efficiency Cathode of Fuel Cells with Superhigh Platinum Utilization," *J. Phys. Chem. C*, vol. 122, no. 26, pp. 14691–14697, 2018.

[146] J. Choi *et al.*, "Gram-scale synthesis of highly active and durable octahedral PtNi nanoparticle catalysts for proton exchange membrane fuel cell," *Appl. Catal. B Environ.*, vol. 225, no. July 2017, pp. 530–537, 2018.

[147] H. Tang *et al.*, “Metal-organic-framework-derived dual metal-and nitrogen-doped carbon as efficient and robust oxygen reduction reaction catalysts for microbial fuel cells,” *Adv. Sci.*, vol. 3, no. 2, pp. 1–8, 2015.

[148] J. Long, R. Li, and X. Gou, “Well-organized Co-Ni@NC material derived from hetero-dinuclear MOFs as efficient electrocatalysts for oxygen reduction,” *Catal. Commun.*, vol. 95, no. 3, pp. 31–35, 2017.

[149] J. Hu, J. Chen, H. Lin, R. Liu, and X. Yang, “MOF derived Ni/Co/NC catalysts with enhanced properties for oxygen evolution reaction,” *J. Solid State Chem.*, vol. 259, no. October 2017, pp. 1–4, 2018.

[150] S. Hanif, X. Shi, N. Iqbal, T. Noor, R. Anwar, and A. M. Kannan, “ZIF derived PtNiCo/NC Cathode Catalyst for Proton Exchange Membrane Fuel Cell,” *"Applied Catal. B, Environ.*, p. 117947, 2019.

[151] J. Li, S. Lu, H. Huang, D. Liu, Z. Zhuang, and C. Zhong, “ZIF-67 as Continuous Self-Sacrifice Template Derived NiCo2O4/Co,N-CNTs Nanocages as Efficient Bifunctional Electrocatalysts for Rechargeable Zn-air Batteries,” *ACS Sustain. Chem. Eng.*, 2018.

[152] S. Wang, Z. Cui, and M. Cao, “A Template-Free Method for Preparation of Cobalt Nanoparticles Embedded in N-Doped Carbon Nanofibers with a Hierarchical Pore Structure for Oxygen Reduction,” pp. 1–9, 2014.

[153] L. Song, J. Tang, T. Wang, C. Wu, Y. Ide, and J. He, “Self-Supported ZIF-Derived Co 3 O 4 Nanoparticles-Decorated Porous N-Doped Carbon Fibers as Oxygen Reduction Catalyst,” pp. 6807–6813, 2019.

[154] X. Chen, N. Wang, K. Shen, Y. Xie, Y. Tan, and Y. Li, “MOF-Derived Isolated Fe Atoms Implanted in N - Doped 3D Hierarchical Carbon as an E ffi cient ORR Electrocatalyst in Both Alkaline and Acidic Media,” *ACS Appl. Mater. Interfaces*, vol. 11, pp. 25976–25985, 2019.

[155] Y. Leng, L. Wang, M. A. Hickner, and C. Wang, “Electrochimica Acta Alkaline membrane fuel cells with in-situ cross-linked ionomers,” *Electrochim. Acta*, vol.

152, pp. 93–100, 2015.